(2)

WT-1668 (EX)
EXTRACTED VERSION

OPERATION ARGUS

SATELLITE MEASUREMENTS

Defense Atomic Support Agency
Washington, D. C.

April 8, 1960

NOTICE

This is an extract of WT-1668, which remains classified SECRET/RESTRICTED DATA as of this date.

Extract version prepared for:

Director

DEFENSE NUCLEAR AGENCY

Washington, D. C. 20305

31 August 1984

Approved for public release;
distribution unlimited.

REPORT DOCUMENTATION PAGE

READ INSTRUCTIONS BEFORE COMPLETING FORM

1. REPORT NUMBER: WT-1668 (EX)
2. GOVT ACCESSION NO.:
3. RECIPIENT'S CATALOG NUMBER:

4. TITLE (and Subtitle): OPERATION ARGUS - SATELLITE MEASUREMENTS
5. TYPE OF REPORT & PERIOD COVERED:
6. PERFORMING ORG. REPORT NUMBER: WT-1668 (EX)

7. AUTHOR(s):
P. C. Kostoff, Capt, USA, Project Officer
Ernst Stuhlinger
H. W. Kampneier, Josef Boehm

8. CONTRACT OR GRANT NUMBER(s):

9. PERFORMING ORGANIZATION NAME AND ADDRESS:
Army Ballistic Missile Agency
Redstone Arsenal, Alabama

10. PROGRAM ELEMENT, PROJECT, TASK AREA & WORK UNIT NUMBERS:

11. CONTROLLING OFFICE NAME AND ADDRESS:
Defense Atomic Support Agency
Washington, D. C.

12. REPORT DATE: April 8, 1960
13. NUMBER OF PAGES:

14. MONITORING AGENCY NAME & ADDRESS(if different from Controlling Office):

15. SECURITY CLASS. (of this report): UNCLASSIFIED
15a. DECLASSIFICATION/DOWNGRADING SCHEDULE:

16. DISTRIBUTION STATEMENT (of this Report)
Approved for public release; unlimited distribution.

17. DISTRIBUTION STATEMENT (of the abstract entered in Block 20, if different from Report)

18. SUPPLEMENTARY NOTES
This report has had the classified information removed and has been republished in unclassified form for public release. This work was performed by Kaman Tempo under contract DNA001-83-C-0286 with the close cooperation of the Classification Management Division of the Defense Nuclear Agency.

19. KEY WORDS (Continue on reverse side if necessary and identify by block number)
Operation ARGUS
Satellite Measurements
Radiation Instrumentation
Radiation Measurements
Electron Plasma

20. ABSTRACT (Continue on reverse side if necessary and identify by block number)
This report describes the Argus Satellite Project, the broad theory of the Christofilos effect, the measurements of the background radiation, and the measurement of the effect itself. After each Argus nuclear detonation, the instrumented satellite reported a new and well-defined radiation belt that persisted for many hours.

FOREWORD

This report has had classified material removed in order to make the information available on an unclassified, open publication basis, to any interested parties. This effort to declassify this report has been accomplished specifically to support the Department of Defense Nuclear Test Personnel Review (NTPR) Program. The objective is to facilitate studies of the low levels of radiation received by some individuals during the atmospheric nuclear test program by making as much information as possible available to all interested parties.

The material which has been deleted is all currently classified as Restricted Data or Formerly Restricted Data under the provision of the Atomic Energy Act of 1954, (as amended) or is National Security Information.

This report has been reproduced directly from available copies of the original material. The locations from which material has been deleted is generally obvious by the spacings and "holes" in the text. Thus the context of the material deleted is identified to assist the reader in the determination of whether the deleted information is germane to his study.

It is the belief of the individuals who have participated in preparing this report by deleting the classified material and of the Defense Nuclear Agency that the report accurately portrays the contents of the original and that the deleted material is of little or no significance to studies into the amounts or types of radiation received by any individuals during the atmospheric nuclear test program.

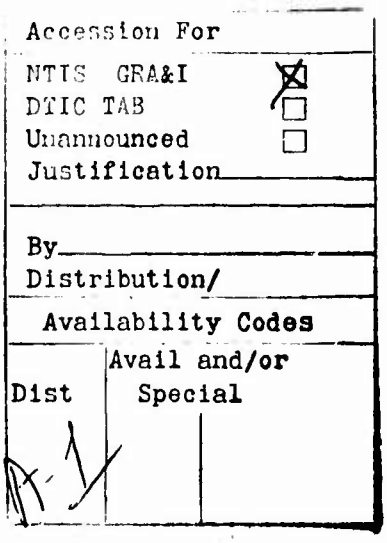

PREFACE

Following a theory on the trapping of electrons from nuclear explosions by the magnetic field of the earth, the Department of Defense initiated Operation Argus in May 1958 to provide an experimental check of the theory. Nuclear devices were detonated at great altitudes, and the ensuing effects were measured by instrumented satellites, rocket probes, and land and sea observation stations in various parts of the world.

This report describes the Argus Satellite Project, the broad theory of the Christofilos effect, the measurements of the background radiation, and the measurement of the effect itself. After each Argus nuclear detonation, the instrumented satellite reported a new and well-defined radiation belt that persisted for many hours.

After considerable data had been processed, the various participating agencies sent representatives to the Lawrence Radiation Laboratory to evaluate the Argus experiments. The principal results of this meeting and some of the data later made public are presented in this report. Further detailed analyses of specialized problems associated with the experiments remain to be completed.

This report presents the work of the members of many organizations, as described in Section 1.3, Project Initiation and Project Organization.

By directive of AFSWP, the report in its present form was compiled and edited by the Research Projects Laboratory, Development Operations Division, Army Ballistic Missile Agency, Army Ordnance Missile Command, with contributions from: Dr. A. Weber, Dr. C.A. Lundquist, Dr. R. Shelton, Mr. A. Thompson, Mr. G. Bucher, and Mr. R. Naumann.

CONTENTS

Chapter I
BACKGROUND and HISTORY

Early in 1958, N.C. Christofilos prepared a classified report (Reference 1) in which he developed the theory of an effect, which (for security reasons) came to be called the "Argus effect" but will be referred to later in this report as the "Christofilos effect". According to electromagnetic theory, high-energy electrons introduced several hundred miles above the surface of the earth would be trapped by the earth's magnetic field. The electrons would follow spiral paths, with the center lines of the spirals following the field lines of the earth's magnetic field. The increase of the magnetic field strength in the vicinity of the magnetic poles would compress the windings of the spirals until the electrons were reflected into the opposite direction, a variation of the well-known magnetic-mirror effect. An electron would continue to oscillate back and forth between the poles until removed by collisions with the residual air molecules, possibly for months or even years.

If a sufficiently powerful source of electrons were employed, such as a nuclear bomb of several megatons yield, the conjecture was made that the density of electrons trapped in such oscillating orbits might be great enough to produce effects having military applications: (1) The electromagnetic radiation emitted by the spiraling electrons might produce a noise level high enough to black out world-wide radio and radar operations in the 50- to 200-Mc band. (2) The arming and fuzing systems of intercontinental ballistic missiles might be damaged lethally by the high-intensity radiation. (3) An artificial radiation belt might make manned flight at certain altitudes impossible.

These potential implications quickly aroused military interest in the Christofilos effect. In March, the Department of Defense initiated plans for an experimental verification of the effect. The advanced Research Projects Agency (ARPA), together with the Armed Forces Special Weapons Project (AFSWP), decided to detonate several nuclear devices of small yields at suitably high altitudes and to have the radiation effects measured by instrumented satellites, rocket probes, and ground equipment. The Army Ballistic Missile Agency (ABMA) was directed to submit a proposal for two instrumented satellites to be launched in the summer of 1958.

In the meantime, Explorers I and III revealed the presence of an intense natural radiation belt at altitudes above about 1,000 km. Quite obviously, the same trapping mechanism by the earth's magnetic field described in Christofilos' theory is responsible for the existence of this region of intense natural radiation. The significance of the Christofilos effect was greatly enhanced by this discovery.

In support of Project Argus, the joint capabilities of ABMA and the Jet Propulsion Laboratory (JPL) to launch two satellites were presented to representatives of ARPA in April. The satellites were to be instrumented by the State University of Iowa (SUI), which had successfully instrumented Explorers I and III.

On 2 May, the Department of the Army directed ABMA to participate in the Argus test as proposed. Overall project direction for the construction, instrumentation, checkout, and launching of the satellites; for tracking, orbit computation, and ground station organization; and finally, for the collection of all the measured data, was assigned to ABMA.

The first of the two satellites, Explorer IV, was launched on 26 July 1958 by the Jupiter-C vehicle and is shown in Figure 1.1. It measured the natural background radiation effects from

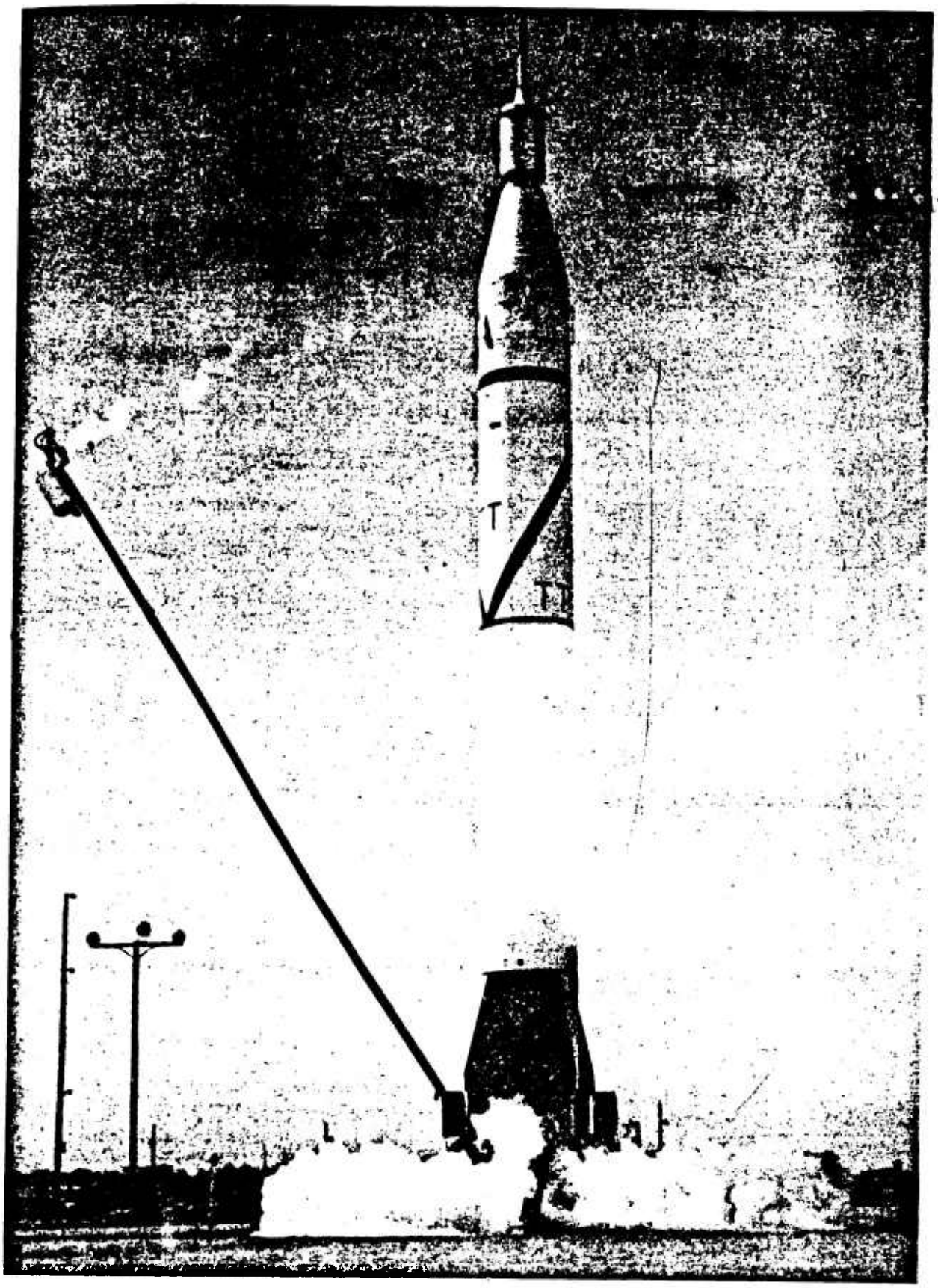

Figure 1.1 Jupiter-C vehicle launching Explorer IV.

the two Hardtack missiles fired on 31 July and 11 August, and effects from the three Argus firings on 27 August, 30 August, and 6 September 1958.

The second satellite launching was attempted on 24 August 1958. Shortly after separation of the booster from the forward portion of the four-stage vehicle, the booster collided with the rear end of the instrument compartment and disturbed its orientation. The satellite, Explorer V, subsequently failed to go into orbit.

Preparation, testing, and launching of two complex satellite missiles like Explorers IV and V requires a major effort of the agency to which the project is assigned. In the present case, the situation was aggravated by three facts: first, the total time between inception of the project and launching of Explorer IV was only four months; second, the Argus project was permitted to cause only small slippages in the Redstone, Jupiter, and Pershing Projects; and third, the agency was at that time already engaged in another special project, the Hardtack firings from Johnston Island, which occupied considerable parts of ABMA during 1958. The greatest shares of the burden had to be carried by the Missile Firing Laboratory, the Guidance and Control Laboratory, and the Aeroballistics Laboratory. A postponement of Argus was not possible, because the timing of the first satellite launching had to be such that the satellite would first measure the natural background radiation; then, during the period from 31 July until the middle of August, the Hardtack effects; and finally, between late August and early September, the Argus effects. The launching of Explorer IV, therefore, had to be accomplished on 26 July, with a possible variation of not more than plus or minus 2 days. This condition was met, and the purpose of the Argus project was fully accomplished.

1.1 THE CHRISTOFILOS EFFECT

As stated above, Christofilos developed a detailed theory for the high altitude entrapment of electrons upon the magnetic flux density lines of the earth, using as the basic model a single electron moving in a magnetic-mirror machine. This simple single-particle model was then extrapolated to the high-altitude situation. The main features of this analysis were: first, the development of a lune of electrons (because of the north-south spiraling of the electrons), and second, the extension of the lune (because of an eastward drift velocity caused by the gradient and curvature of the field) into a shell of electrons extending completely around the earth over the middle latitudes.

Christofilos calculated: (1) the electron density and flux of the relativistic electrons artificially injected into the earth's magnetic field at high altitudes by nuclear bursts; (2) the eastward drift velocity of the electrons within the shell (about 6 mi/sec for 1-Mev electrons); and (3) the trapped lifetime of the electrons. The calculations of these quantities include evaluations or estimates of all important variables. The essentials of the theory are presented in Chapter 2.

The Argus effect is concerned with an artificial production of a shell of electrons. Hence, to check the theory of this effect by experiment, it is necessary that the artificial effect be greater than any existing natural effect. Prior to the Argus experiments, Van Allen had shown the existence of a radiation belt of high intensity, beginning at about 1,000 km altitude and extending with increasing intensity to the highest altitudes (about 2,000 km) of Explorers I and III (Reference 2). From these satellite measurements, he found normal cosmic ray intensities up to about 1,000 km. Above this altitude, unexpectedly high intensities, increasing rapidly with increasing altitude, were found. This new effect was rather strongly dependent upon latitude and, to a lesser degree, longitude. The evidence indicated that the primary radiation of this high-altitude belt consisted of charged particles constrained to the altitude and latitude pattern by the earth's magnetic field. Thus, there exists a natural region of charged particles similar to the shell of electrons that Christofilos wished to establish artificially.

The radiation detected by Explorer IV confirmed entirely the general features of the natural-radiation belt just described (Reference 3). Surfaces of constant count rate were mapped out in the space around the earth, providing an indication of the natural-radiation intensities.

Still later, Pioneers III and IV launched by ABMA and JPL carried radiation detectors supplied by SUI to extreme distances from the earth. Van Allen has reported from the results of these flights the existence of two belts of natural radiation (Reference 4).

1.2 OBJECTIVES OF THE ARGUS EXPERIMENTS

The objective of the Argus experiments was to test the theoretical predictions concerning particle injection by a nuclear device and the particle density, flux, trapping lifetime, and eastward-drift revolution time of the artificially injected electrons. The trapping lifetimes would determine also the duration time of the electron shell around the earth. Finally, the detection of artifically injected particles would have to be made in the presence of the naturally existing and constantly maintained Van Allen radiation zone. For test purposes, a nuclear burst of modest size for artificial particle injection was dictated by every military and scientific precaution. The existence of the natural radiation zone means that the Argus electrons would have to be injected and detected at altitudes high enough to avoid excessive loss of trapped particles by interactions with atmospheric particles near the mirror points and at a position in space such that the artificial belt would not be obscured by the natural radiation.

Explorer IV contained radiation detectors of considerably greater dynamic range than those of Explorers I and III. This instrumentation permitted the detailed measurement of the natural background radiation encountered at all satellite altitudes and the several aspects of the Christofilos effect.

The origin and nature of the natural (Van Allen) effect are not yet completely understood. Presumably, the particles are electrons, protons, or both. At least two mechanisms have been suggested: (1) plasmas of electrons and ions ejected from the sun into the earth's magnetic field and (2) neutron decay particles injected at high altitudes by outward-moving neutrons from cosmic-ray interactions with the earth's atmosphere.

In Chapter 2, the theoretical estimates of electron particle density, flux, and corresponding radiation-detector counting rates are presented for beta-decay electrons resulting from a high-altitude nuclear burst. It is shown that a counting rate of between 20 and 10^6 times the natural background (at altitudes below the intense Van Allen radiation belts) is expected. By observing the radiation intensity of the trapped electrons in later revolutions, when the satellite returns to almost the same position relative to the earth, it is possible to obtain the lifetime of the artificial electron shell. Special attention to the position of the satellite, at the time of the nuclear burst, provides data for determining the eastward-drift revolution time.

The radiation detectors provided in Explorer IV had wide dynamic range and crude energy discrimination. The detection package contained: (1) a scintillation counter designed to reject the high-intensity, low-energy radiation assumed to be present from the Explorer I and III results; (2) a shielded Geiger-Mueller counter sensitive to particles in the expected Argus range; (3) an unshielded G-M counter for low-energy radiation count; and (4) a total-radiation-energy detector for integrating radiations of all energies. This compact instrument package provided overall energy discrimination for the analysis of the natural background radiation and the detection of the Christofilos effect above the background.

The physical properties of the Explorer IV satellite are given in Figure 1.2, taken from Page 2 of Reference 5.

1.3 EXECUTION OF SATELLITE PROJECT

1.3.1 Project Initiation. The original report by Christofilos was distributed as a classified document in January, 1958. On 13 March, ABMA received a teletype from the Department of the Army, which pointed out that the Department of Defense was actively planning for a nuclear-weapon test in support of broad plans by ARPA to verify experimentally the theory of Christofilos. On 19 March, ABMA was asked by DA to formulate a preliminary concept for its participation in this project, including a cost estimate. ABMA's answer was given to DA on 24 March and submitted to AFSWP on 27 March. A meeting was held at ARPA on 2 April, during which the detailed

requirements for an Argus test were discussed by representatives of Lawrence Radiation Laboratory (Livermore, California), DA, ABMA, JPL, and several other organizations. The proposals and capabilities of ABMA were presented at this meeting. A number of subsequent meetings and discussions were held, and on 2 May, the Department of Defense approved the participation of ABMA. On 27 June, ABMA received final detailed written authorization from AFSWP to proceed with the project as proposed. Project costs were to be carried by AFSWP. The DA then directed ABMA to launch two satellites in support of Operation Argus.

The AFSWP was given prime responsibility for Operation Argus. Mission assignments are shown in Table 1.1. The ABMA was assigned responsibility for the satellite portion, which included construction, instrumentation, checkout, launching, data collection, tracking, and orbit determination of two satellites of the Explorer type, and was directed to launch the first satellite as early as possible so that the natural background radiation could be measured in detail before the detonation at high altitudes of the first nuclear device.

During the week following the 2 May directive, Jupiter-C Missiles 44 and 47, which had been planned for high-visibility inflatable sphere satellites, were scheduled to carry satellites instru-

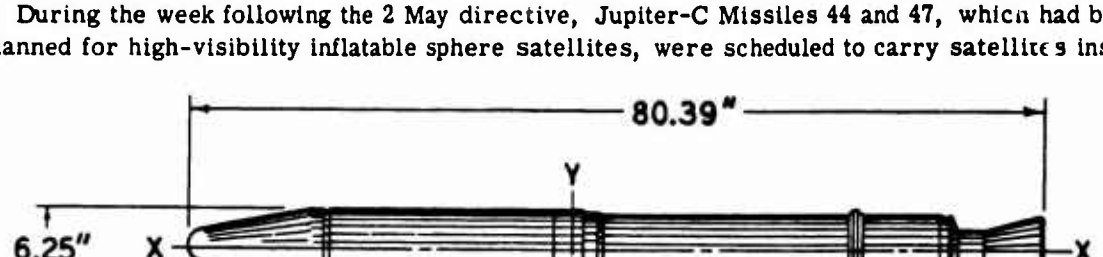

DATA

Total Weight	36.8 lb
Payload Weight	25.8 lb
Location of C.G. from Rear	45 in
Moment of Inertia around X-X Axis	0.50 in-lb-sec^2
Y-Y Axis	42.0 in-lb-sec^2
Spin Rate at Second Stage Separation	750 rpm

Figure 1.2 Physical properties of Explorer IV.

mented to measure the Christofilos effect. Work on Juno II lunar-probe vehicles was postponed in favor of the more urgent work on the Argus vehicles. Full support with the upper stages, satellite shells, and some components of the instrumentation was offered by JPL. A high priority program to develop, test, and fabricate detectors for the expected radiation was initiated by SUI. Negotiations with the Smithsonian Astrophysical Observatory (SAO), the Signal Corps (O Sig O), the Ballistic Research Laboratory (BRL), Naval Ordnance Test Station (NOTS), Stanford Research Institute (SRI), and other organizations were begun to obtain support in the areas of tracking, orbit determination, and data collection. On 10 May, an organizational meeting was held at SUI during which detailed plans for the Argus satellite project evolved. In that meeting, test schedules and final delivery were established and responsibilities assigned. The crash program was then underway.

1.3.2 Satellite Project Organization. The Argus satellite project involved six major areas of effort: (1) fabrication, checkout, and launching of the carrier vehicles; (2) design, fabrication, and environmental testing of the satellites; (3) development, design, fabrication, environmental testing, and calibration of the radiation detectors; (4) fabrication and operation of the data transmission system; (5) computation of ephemerides; and (6) collection of data and evaluation of results.

For the launching vehicles, ABMA provided the booster, the spin launchers, and the guidance and control equipment, and JPL furnished the solid propellant motors for the upper stages and

TABLE 1.1 ARGUS PROJECT MISSIONS (AS ORIGINALLY ASSIGNED)

Armed Forces Special Weapons Project (AFSWP)

Conduct this special test.

Coordinate activities of all participating agencies and provide funds to agencies involved.

Army Ordnance Missile Command - Army Ballistic Missile Agency

Provide two satellite missiles (one as back-up) and satellite instrumentation and ground receivers.

Office of Naval Research (ONR)

Provide warhead missile (X-17).

Air Force Special Weapons Center (AFSWC)

Provide counter instrumentation to be used on Atlas research and development flights, if permissible, and provide sounding rockets.

Air Force Cambridge Research Center (AFCRC)

Provide instrumentation for ground stations.

The Army Ballistic Missile Agency, as a prime participant, was aided by the following installations:

State University of Iowa (SUI)

Supplied satellite instrumentation, consisting of two scintillation counters and two Geiger-Muller counters for each package.

Calibrated radiation detectors.

Received raw telemeter data on tape from ground station, reduced and evaluated data.

Jet Propulsion Laboratory (JPL)

Supplied satellite payload shells and low power 108.00-Mc Microlock transmitter with power supply and subcarrier oscillators for satellite instrumentation package. Manned and operated Microlock ground stations at Cape Canaveral Missile Test Annex, Florida, and Camp Irwin, California.

Naval Research Laboratory (NRL)

Supplied AM circuitry and transmitters, frequency 108.03 Mc. Operated Minitrack ground station network at times requested.

U.S. Army Signal Research and Development Laboratory (USASRDL)

Supplied battery packs for high power transmitter to SUI and operated the Deal ground station at Ft Monmouth.

Office of the Chief Signal Officer, U.S. Army (OC Sig O)

Manned and operated ground tracking station in Van Buren, Maine.

Smithsonian Astrophysical Observatory (SAO)

Operated optical tracking stations and produced final ephemerides.

Army Map Service (AMS)

Provided tracking data from stations located in Pacific (code name: Betty Stations).

Ballistic Research Laboratory (BRL)

Provided tracking data.

Army Security Agency (ASA)

Provided sufficient telemetering data prior to Argus shots for background calibration, and provided some three days' telemetering data following the nuclear burst.

the steel shells for the satellites. Satellite engineering, packaging of all the instruments, environmental and spin testing, antenna measurements, passive temperature control, and checkout was done by ABMA. Development, fabrication, calibration, and testing of the radiation detectors was the responsibility of SUI.

Two independent transmitters, both used for tracking and telemetry, were employed: (1) a phase-modulated Microlock transmitter from JPL and (2) an amplitude-modulated Minitrack transmitter from NRL. Subcarrier oscillators were furnished by JPL. The Signal Corps provided the battery package for detector and transmitter operation. The final wiring of the satellite was done at ABMA. The proper surface treatment for passive temperature control was designed and applied by ABMA.

In order to save weight and electric power, no tape recorders or other data-storage systems were used on the Argus satellites. Data were transmitted continuously and received by a system of more than forty ground stations, which covered a major part of the globe. These ground stations were operated by NRL (normal Minitrack stations), JPL (some of the Microlock stations), ABMA, NOTS, WSMR, O Sig O and its subcontractors, and by some universities under U. S. Government contracts, such as Johannesburg, in South Africa, and Heidelberg and Bonn, in Germany. The O Sig O established and maintained communications with those stations which were not previously included in the normal Minitrack or Microlock networks.

The first quick evaluation of tracking data and subsequent establishment of preliminary orbit parameters was carried out at ABMA; NRL carried out a continuing orbit determination and made pass predictions for all stations; SAO, on the basis of its optical observations and NRL Minitrack data, produced ephemerides of high precision.

Each of the ground stations recorded the received signals on tape and shipped them to SUI, where they were played back and reduced to counting rates as functions of time, altitude, and geographical and magnetic latitude and longitude.

The telemetry records from the ABMA station at Redstone Arsenal were reduced at once by ABMA personnel, who made a preliminary analysis of the results after each Argus shot. Such preliminary results were transmitted to AFSWP within hours after each of the three detonations.

A detailed evaluation of the telemetered data prior to the Argus nuclear detonations, providing a comprehensive picture of the background radiation, has been made by SUI (Appendix A). Telemetry records containing the Christofilos effect were reduced to counting rates above background as a function of time after detonation and geographic and magnetic location (Appendix B). This data provides the basis for an evaluation of the several essential details of the theory.

1.3.3 Data Collection and Processing. The satellite carried two radio beacons, which transmitted identical information continuously. The transmitters were modulated by the first five RDB telemetry channels. The low-power beacon transmitted on 108.00 Mc with 10 mw power and was phase-modulated; the high-power transmitter operated at 108.03 Mc with 30 mw power and was amplitude-modulated. The predicted lifetime of the power supply for both transmitters was 2 months.

An extensive system of ground stations participated in tracking and receiving telemetry from the satellite. A list of these stations, the operating organization, tracking equipment, and telemetry capability are given in Table 1.2. The ABMA was responsible for coordinating efforts of the network. A communications center was established by ABMA at Huntsville, Alabama, for the purpose of alerting all stations prior to the satellite launching.

The initial determination of the orbital parameters was made immediately after the launch by ABMA. Doppler stations at Cape Canaveral, Huntsville, Fort Monmouth, Aberdeen Proving Ground, and at Van Buren, Maine tracked the satellite during launch. The Doppler data were evaluated and the performance of Stages 2, 3, and 4 of the Juno I vehicle and the injection point of the satellite into its orbit were determined. This procedure is reported in detail by Speer on Page 8 of Reference 5.

After the initial orbit determination, tracking data from ground stations were channeled as shown in the block diagram in Figure 1.3.

The ephemerides produced by the Smithsonian Astrophysical Observatory, with participation by the Computation Laboratory of ABMA in some areas, was a tabulation of satellite positions at 1-minute intervals. The printed ephemerides extended from launch until the end of intelligible telemetry on 19 September 1958. Approximately 1,500 pages were published.

The geographic positions obtained from SAO were also transformed into a coordinate system centered on the eccentric magnetic dipole of the earth. The details of their transformation were supplied by the Research Projects Laboratory and calculations made by the Computation Laboratory of ABMA. A complete tabulation of satellite positions in this form was supplied to SUI to be used in the analysis of telemetry data. Telemetry recordings were channeled as shown in Figure 1.4.

1.4 RESULTS

1.4.1 Satellite Launchings. Explorer IV was launched from Air Force Missile Test Center, Cape Canaveral, Florida, on 26 July 1958 at 1000 EST. As planned, the launching vehicle was

TABLE 1.2 EXPLORER IV GROUND STATIONS

D = Doppler; I = Interferometer, PM = Phase Modulation; AM = Amplitude Modulation; and O = Optical.

Location	Operator	Tracking Equipment	Telemetering	Location	Operator	Tracking Equipment	Telemetering
Huntsville, Alabama	ABMA	D	PM and AM	Heidelberg, Germany	ABMA	None	AM
CCMTC, Florida	JPL	D	PM	Thule, Greenland	NOTS	D	PM and AM
Blossom Point, Maryland	NRL	I	AM	New Zealand	NOTS	D	PM and AM
Fort Stewart, Georgia	Army	I	AM	Fairbanks, Alaska	NOTS	D	PM and AM
Havana, Cuba	Army	I	AM	Inyokern, California	NOTS	D	PM and AM
Antigua, BWI	RCA	I	AM	Azores	NOTS	D	PM and AM
Quito, Ecuador	Army	I	AM	Johnston Island	AF	D	PM and AM
Lima, Peru	Army	I	AM	Sinop, Turkey	ASA	—	AM
Antofagasta, Chile	Army	I	AM	Berlin, Germany	ASA	—	AM
Santiago, Chile	Army	I	AM	Shemya, Alaska	ASA	—	AM
San Diego, California	NRL	I	AM	Kassel, Germany	ASA	—	AM
Woomera, Australia	NRL	I	AM	Makebetsu, Hokkaido, Japan	ASA	—	AM
Fort Belvoir, Virginia	AMS	D	None	Organ, New Mexico	SAO	O	None
Goldstone, California	JPL	D	PM	Olifantsfontein, South Africa	SAO	O	None
Aberdeen Pvg Gd, Md	BRL	D	None	Woomera, Australia	SAO	O	None
White Sands, New Mexico	BRL	D	None	San Fernando, Spain	SAO	O	None
Van Buren, Maine	ASigC	D	PM and AM	Tokyo, Japan	SAO	O	None
Fort Monmouth, New Jersey	ASigC	D	AM	Naini Tal, India	SAO	O	None
Temple City, California	Amateur	D	PM	Characato, Peru	SAO	O	None
Ibadan, Nigeria	JPL	None	PM	Shiraz, Iran	SAO	O	None
Singapore, Malaya	JPL	None	PM	Curacao, NWI	SAO	O	None
Guam Island	AMS	I	None	Jupiter, Florida	SAO	O	None
Wake Island	AMS	I	None	Villa Dolores, Argentina	SAO	O	None
Johannesburg, South Africa	NRL	I	AM	Haleakala Maui, Hawaii	SAO	O	None
Bonn, Germany	ABMA	None	AM				

fired at an azimuth angle of 44 degrees from north to attain the desired orbit. This was the first departure from the usual southeasterly trajectory used previously for all satellite launching vehicles. During launch, all stages of the Jupiter-C vehicle performed properly, and Explorer IV was placed in orbit.

The launching vehicle for Explorer V was fired from AFMTC on 24 August 1958 at 0117 EST. All stages of the Jupiter-C vehicle functioned properly, but after cutoff and separation of the Redstone booster, the coasting burned-out booster collided with the coasting cluster of the upper stages, creating an error in orientation. For this reason, the satellite did not orbit. The failure of Explorer V to go into orbit did not place the project in jeopardy, because the established orbit of Explorer IV was favorable enough to assure an adequate accumulation of data.

1.4.2 Orbital Characteristics. A preliminary orbit for Explorer IV, based upon data from ten tracking stations, was established by ABMA 5 hours after launching. A more definite orbit was established several days later, based upon data received from additional tracking stations. The final orbital characteristics are shown in Table 1.3. The first passes of Explorer IV are shown in Figure 1.5.

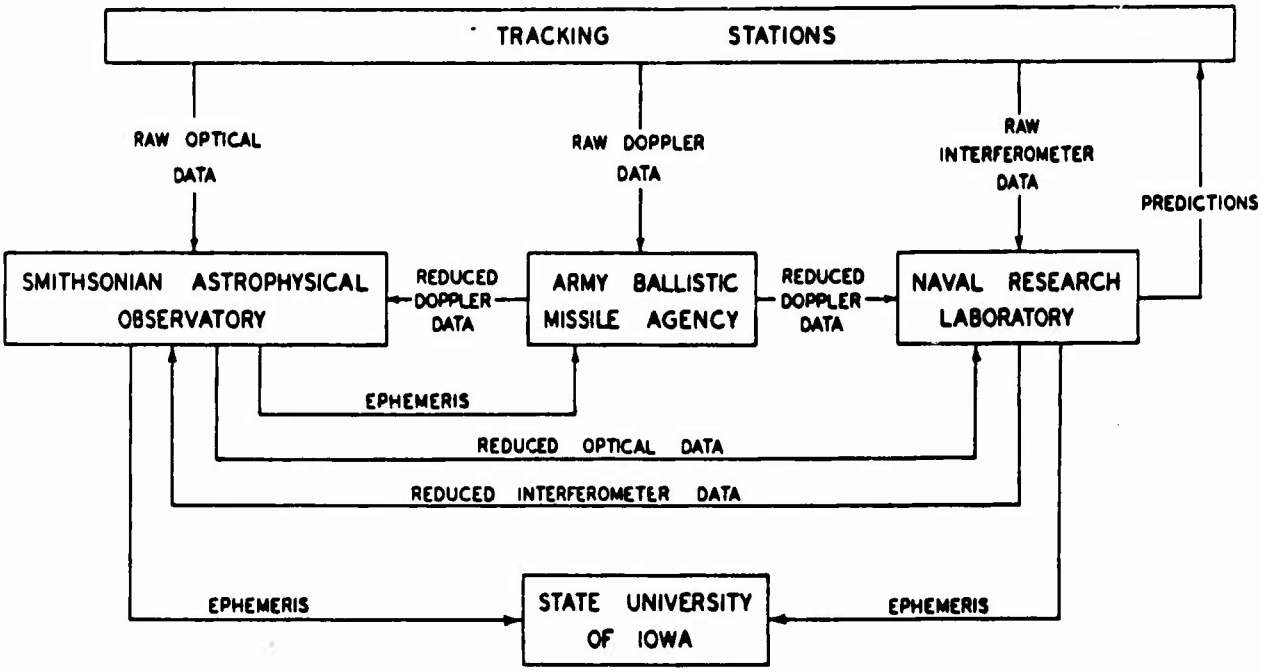

Figure 1.3 Tracking and orbit determination.

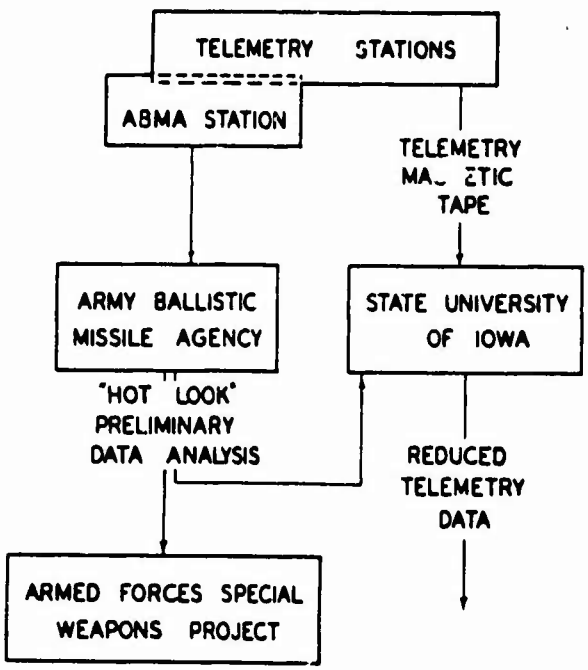

Figure 1.4 Telemetry data processing.

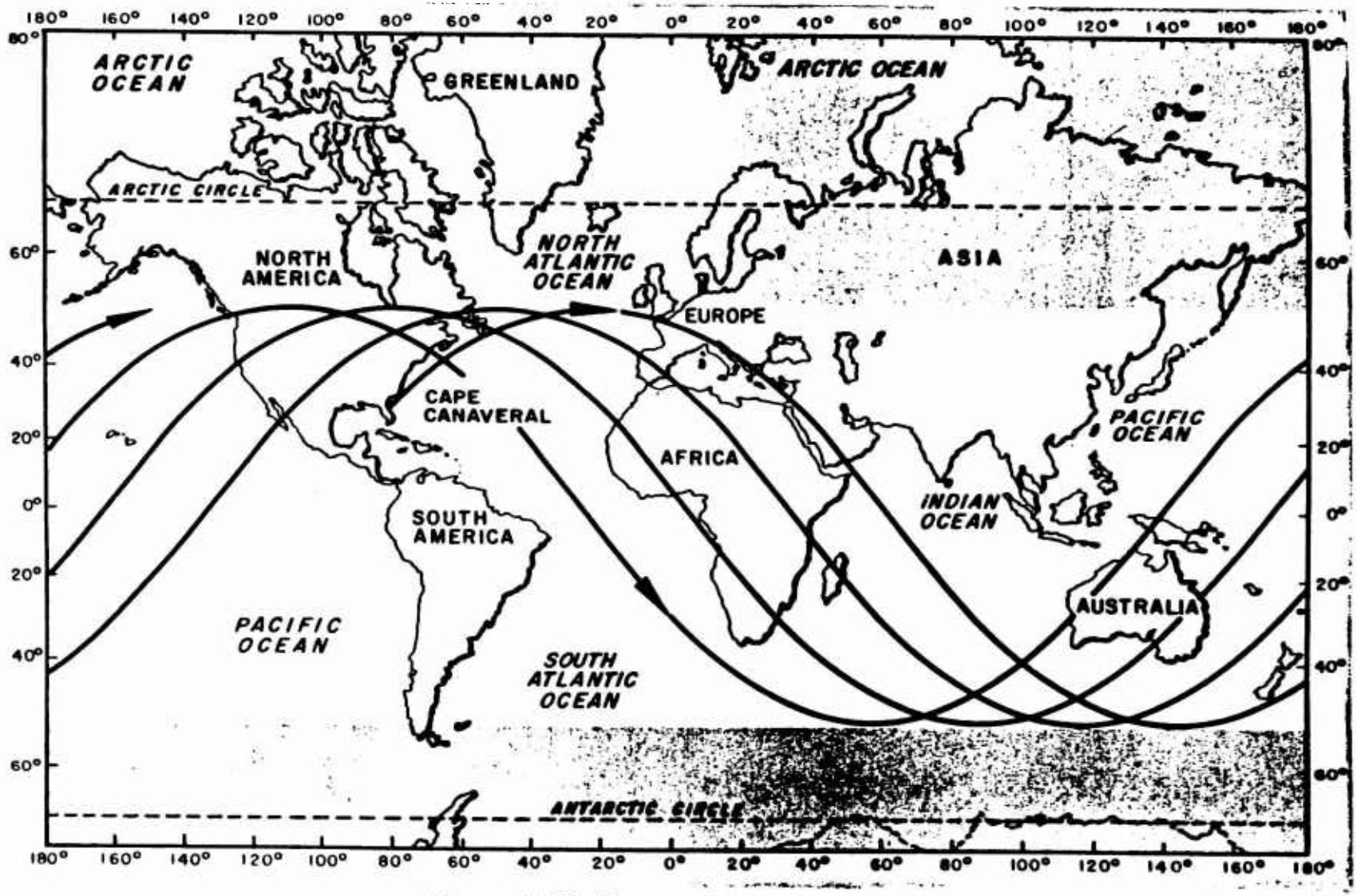

Figure 1.5 First four revolutions of Explorer IV.

1.4.3 Nuclear Shots. The instrumentation of Explorer IV collected data from five nuclear detonations. The first two were Shots Teak and Orange, fired above Johnston Island, T. H., during Operation Hardtack. The data collected from these two shots will be presented in another report.

The last three shots were the Argus tests launched from shipboard in the South Atlantic by the U. S. Navy.

Table 1.4 contains a chronological listing of all satellite and missile launchings.

1.4.4 Natural Background Radiation. Some knowledge of the natural background radiation was necessary for the planning and evaluation of the Argus tests. It would have been difficult, for example, to follow the decay of the Christofilos effect if it had been superimposed on a much stronger background of natural radiation. In addition, it would have been most optimistic to expect militarily useful effects from artificial electron densities that were small compared to those already existing in nature. Further, observation of the distribution of the natural radiation would have been useful in determining the symmetry and orientation of the magnetic field of the earth, a knowledge of which would be necessary if the shell of Argus radiation was to be placed in the most effective position. Finally, knowledge of the spatial and energy distribution of the natural radiation could have been useful in predicting order-of-magnitude lifetimes for radiation shells injected into various parts of space by various injection methods. As a first approximation, it was assumed that a region with a large background of natural radiation would be also a region that would permit a long lifetime for artificially injected radiation.

TABLE 1.3 ORBITAL CHARACTERISTICS

Perigee	159.9 mi
Apogee	1,360 mi
Eccentricity	0.12795
Nodal period	110.11 min
Inclination to orbital plane	50.307 deg

TABLE 1.4 DATA ON ARGUS AND HARDTACK DETONATIONS

PART 1

Event	Date	Location	Altitude
Explorer IV	26 Jul 58	Cape Canaveral	264 to 2,138 km
Teak	31 Jul 58	Johnston Island	76.2 km = 41.1 naut mi
Explorer V	10 Aug 58	Cape Canaveral	—
Orange	11 Aug 58	Johnston Island	38.1 km = 20.6 naut mi

PART 2

Event	Date	Shot Time (Greenwich)	Longitude	Latitude	Altitude
		sec			
Argus 1	27 Aug	0227:52.55 ± 0.01	11° 55′ W ± 30′	38° 48′ S ± 30′	87 ± 16 naut mi 161 ± 30 km
Argus 2	30 Aug	0317:33.79 ± 0.01	8° 43′ W ± 25′	49° 23′ S ± 65′	158 ± 8 naut mi 293 ± 15 km
Argus 3	6 Sep	2212:33.35 ± 0.01	10° 24′ W ± 30′	49° 30′ S ± 20′	405 ± 5 naut mi 750 ± 10 km

The presence of the natural background radiation at high altitudes was established by Explorers I and III (Reference 2). The counting rate was nearly that expected for the cosmic ray background at an altitude below 1,000 km. Above 1,100 km, the counting rate rose rapidly with

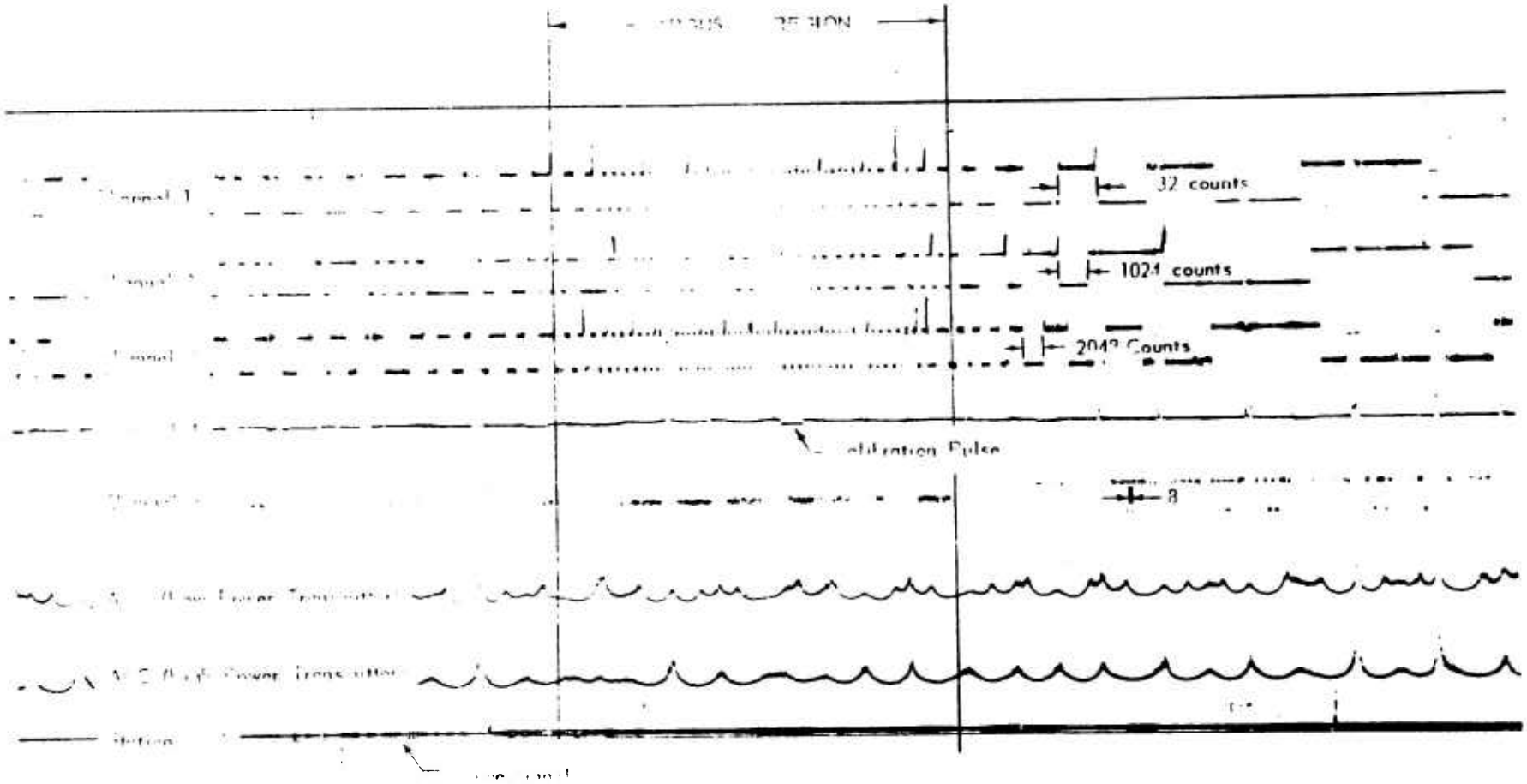

Figure 1.6 Typical telemetry record of Argus effect, Pass No. 454.

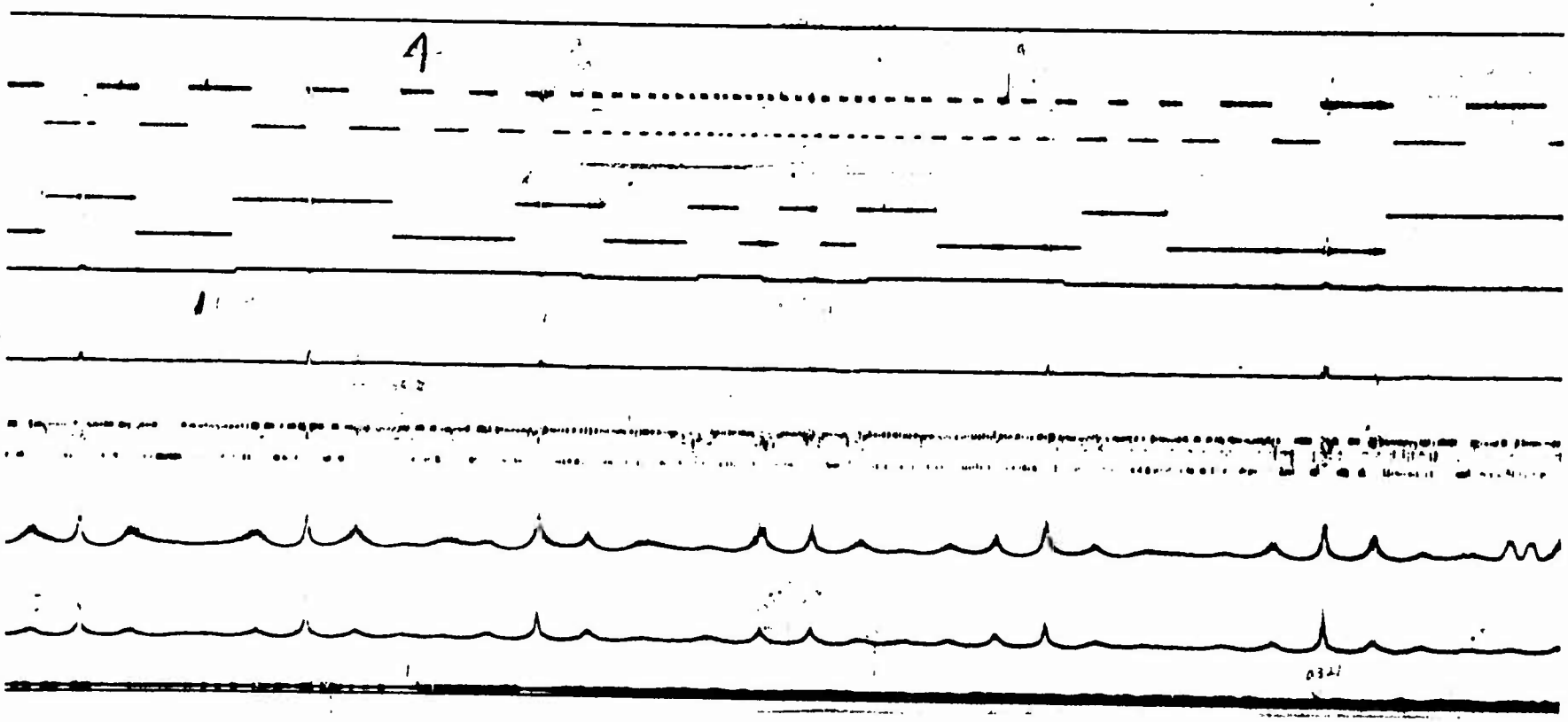

Figure 1.7 Typical telemetry record of Argus effect, Pass No. 453.

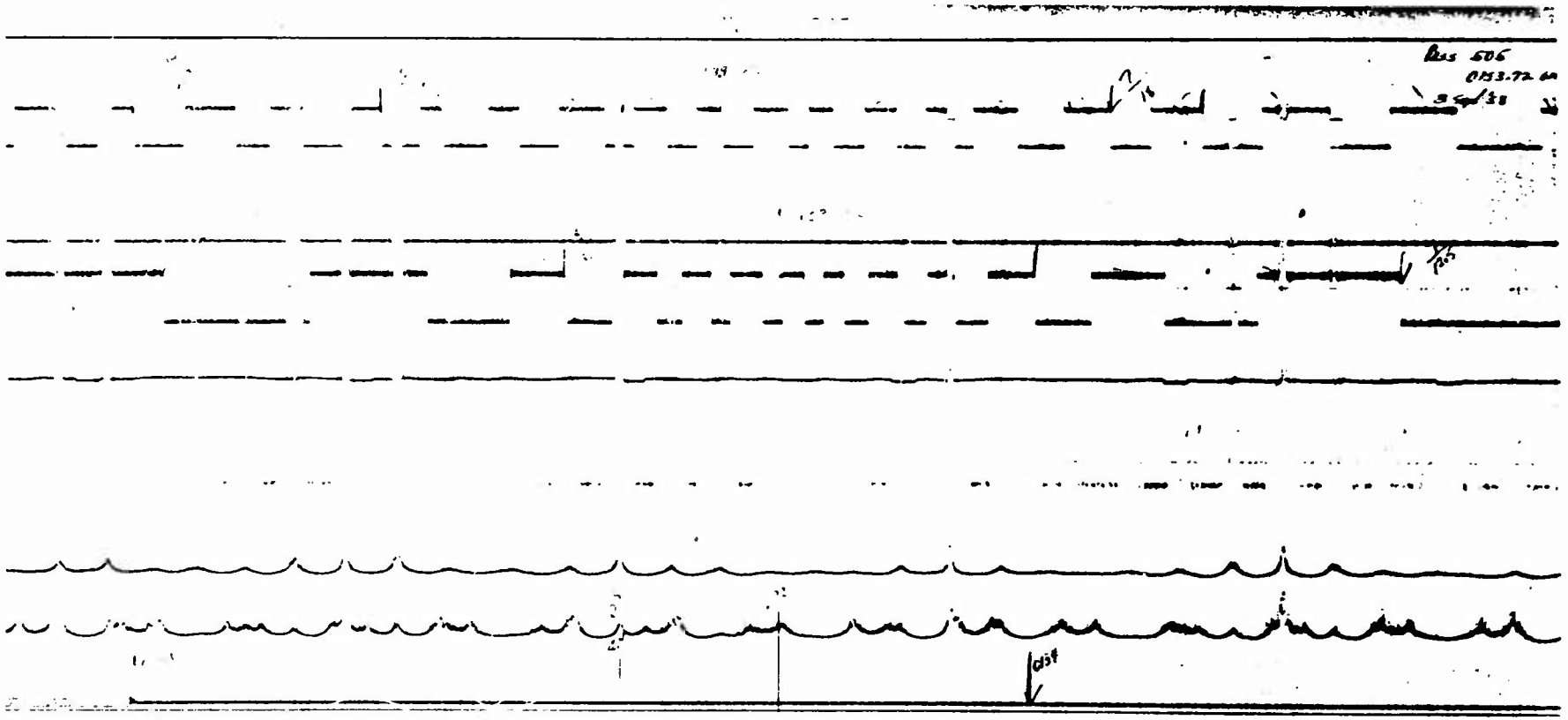

Figure 1.8 Typical telemetry record of Argus effect, Pass No. 505.

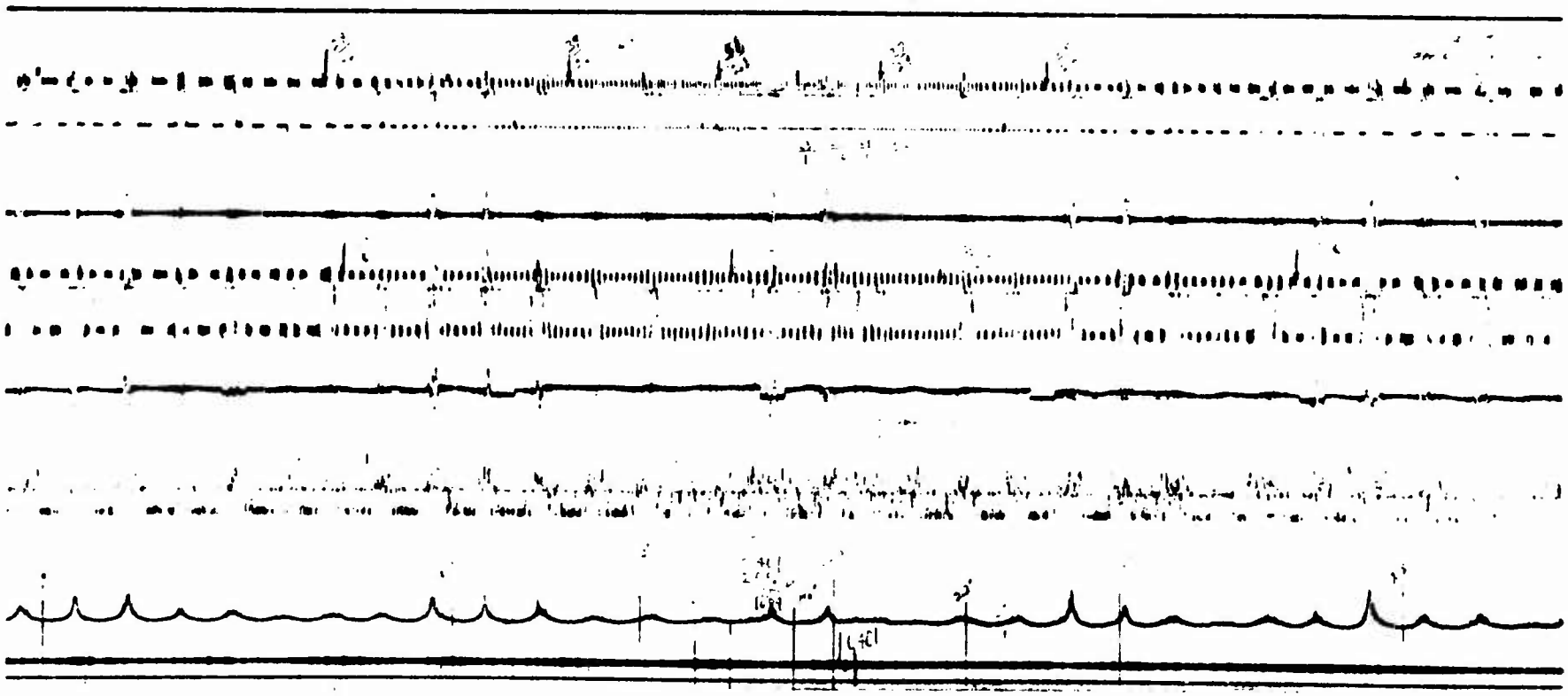

Figure 1.9 Typical telemetry record of Argus effect, Pass No. 559.

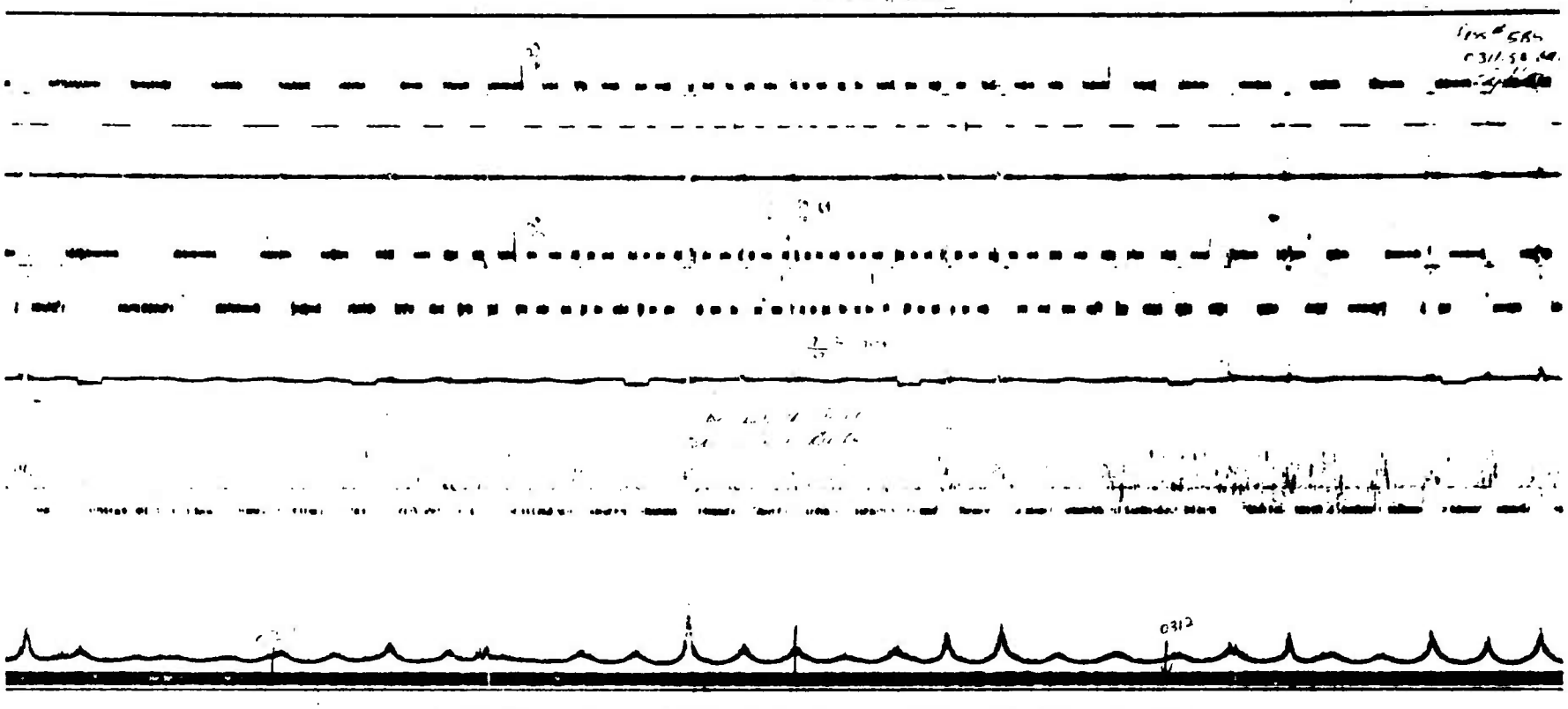

Figure 1.10 Typical telemetry record of Argus effect, Pass No. 585.

altitude and soon exceeded the capacity of the detection system. The wide dynamic range built into the instrumentation of Explorer IV was capable of indicating the intensity of natural radiation at all points on the satellite orbit (Reference 3).

The exact nature of the natural background radiation is not evident from the data of Explorers I, III, and IV. It is reasonable to believe, however, that the region in which the radiation exists is essentially electrically neutral, i.e., that there is a collection of both negatively and positively charged particles. The detection of considerable amounts of bremsstrahlung in the Russian experiments indicates that a large number of electrons with energies in the Mev range are to be found in the radiation (Reference 6). Protons of the same energy would produce practically no bremsstrahlung and are so easily stopped that they would not penetrate the walls of the detection equipment. However, there are those who strongly believe that protons contribute to the counting rate observed in the natural radiation belt (Reference 7).

1.4.5 Radiation Results from Hardtack and Argus Experiments. Shots Teak and Orange, which were fired in the Pacific as part of Operation Hardtack, were essentially different from those of the Argus experiments in that the warheads were larger and the altitudes of detonation were lower (Table 1.4). Increased counting rates associated with Shots Teak and Orange were observed from the satellite. A report on the Teak and Orange measurements will be prepared at a later time.

The Argus experiments were conducted in the South Atlantic. The electrons were injected into a small region of space by a fission warhead of a few kilotons. The atmosphere was rarefied enough to permit electrons, created by beta-decay, to become trapped by the magnetic field of the earth and to undergo a north-and-south motion along the field lines of the magnetic field of the earth. Although the Christofilos effect was observed by the instrumentation of Explorer IV at many points around the earth, it was always within a volume which could be created by the rotation of a small bundle of neighboring magnetic lines of force about the magnetic axis of the earth.

Each of the three Argus shots produced a clearly defined effect on the high-altitude radiation field, which was promptly and successfully detected by the Explorer IV instrumentation. Five typical telemetry records are reproduced in Figures 1.6 through 1.10. The Christofilos effect followed the predicted pattern so well that there was no doubt concerning the origin of the new radiation band, which was narrow enough to be traversed by the satellite in approximately a minute and which, for several days after the shot, was an order of magnitude more intense than the natural background.

Chapter 2
THEORY

A. H. Weber

The theory for the Christofilos electron shield is a single-particle theory; each electron of the lune or shield is acted upon individually by the magnetic field. The extremely low particle density, roughly between 10^{-5} and 1 electrons/cm^3, makes realistic the assumption of a single-particle model. Except for certain phases of the nuclear-bomb burst, as detailed below, there is considered to be no exclusion of the magnetic field, such as in a plasma of high electric conductivity. Hence, throughout this section, the electrons are considered to interact with the various fields but not with each other.

2.1 ENTRAPMENT OF CHARGED PARTICLES BY MAGNETIC FIELDS

As is well known, the basic equation of the force $\bar{F}$ upon a charge $q = e/c$ (e, electron charge 4.803×10^{-10} statcoulombs; c, speed of light in free space 2.998×10^{10} cm/sec) moving with velocity $\bar{v}$ in a magnetic field of flux density $\bar{B}$ at the position of the charge is

$$\bar{F} = e/c\ \bar{v} \times \bar{B} \tag{2.1}$$

In Equation 2.1, $\bar{v}$, in general, has components $v_\perp$ and $v_{/\!/}$, perpendicular and parallel respectively to the magnetic-flux density. The perpendicular component $v_\perp$ results in a cyclotron motion of the electron about $\bar{B}$, radius of gyration a and angular frequency ω_c given by

$$a = \frac{\gamma m_0 v_\perp}{eB},\ \omega_c = Be/\gamma m_0 c, \tag{2.2}$$

where m_0 is the electron rest mass (9.107×10^{-28} g) and

$$\gamma = 1/\sqrt{1 - \beta^2}, \tag{2.3}$$

where

$$\beta = v/c. \tag{2.4}$$

The parallel component of the velocity $v_{/\!/}$ combined with $v_\perp$ produces the primary helical motion of the charge about the B lines.

It follows from the above simple analysis that a charged particle can escape from entrapment upon a B line only by traveling beyond the magnetic field during its helical trajectory into a region free of magnetic fields (assuming that the electron does not collide with other particles during its motion about the magnetic lines of force). If the charged particle traverses a magnetic field of varying B, its instantaneous radius of gyration will vary with the instantaneous value of B.

2.2 EASTWARD DRIFT OF ELECTRONS TRAPPED UPON EARTH'S MAGNETIC FIELD

A charged particle will continue to spiral about the "same" magnetic-flux line, if $\bar{B}$ remains constant in magnitude and direction. However, if $\bar{B}$ varies in either magnitude or direction in space, the entrapped charged particle will drift transverse to the direction of $\bar{B}$.

This drift motion by which the charged particle continuously switches from entrapment upon one "line" of magnetic flux to another is shown by Figure 2.1 for electrons trapped in the earth's magnetic field. In this figure, the drift motion is from west to east and is caused by the decrease in B as the distance from the earth increases. It should be noted that the eastward drift is due to the fact that the instantaneous radius of gyration at P, for example, is larger than that at Q,

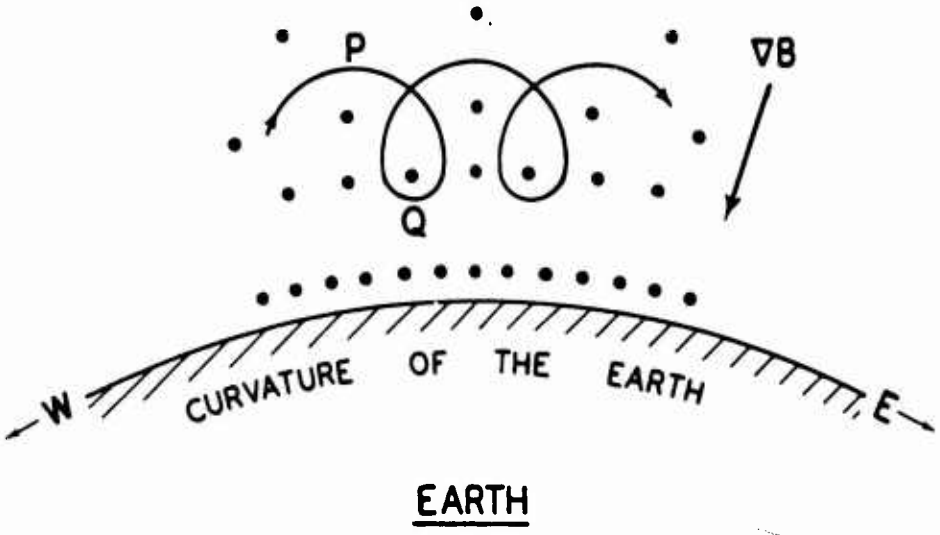

Figure 2.1 A simplified schematic of the easterly drift of electrons arising because of the magnetic field gradient. The view is in the plane of the equator and looking north along the lines of force.

since the magnetic flux density B is smaller at P than at Q because P is farther than Q from the earth's equivalent magnetic dipole.

The charged-particle drift produced by the inhomogeneous magnetic field and depicted by Figure 2.1 has been analyzed in a first-order manner by Alfven (Reference 29) to yield the following expression for the drift speed v_{DG} due to magnetic gradient

$$v_{DG} = \frac{a \nabla_{\perp} B}{2B} v_{\perp} , \qquad (2.5)$$

where $\nabla_{\perp} B$ is the component of the gradient of the magnitude of B in a direction perpendicular to $\bar{B}$, and a and B are as defined previously. For a positive charge, the direction of v_{DG} is given by $\bar{B} \times \bar{\nabla} B$.

If in Equation 2.5 we assume a 1.0-Mev electron, with $a \sim 50$ meters in a field of 1.0 gauss, $v_{\perp} \sim$ the speed of light, and $(\nabla_{\perp} B)/B \sim 3/r$, where r is the radius of the earth, we obtain a drift velocity v_{DG} of about 6 mi/sec. Further, if it is assumed that the drift trajectory of the electron once around the earth averages to a distance of about 12,000 miles, the revolution time will be about 30 minutes.

Although the drift due to the variation of the magnitude of B, specified by v_{DG} in Equation 2.5, appears to be the main drift effect of the Christofilos lune electrons, there are other causes of motion of charged particles transverse to the magnetic field. One of these, the curvature of

the lines of B, causes a centripetal force, which results in a drift speed due to curvature of B lines v_{DC} given by Reference 8.

$$v_{DC} = v_{//}^2/R\omega_c \tag{2.6}$$

where R is the radius of curvature of the B line in question (Figure 2.2).

The direction of v_{DC} is again given by $\bar{B} \times \bar{\nabla} B$ for positive charges and turns out to be eastward also for electrons trapped in the earth's magnetic field.

The total drift speed, v_D, due to both inhomogenieties and curvature of the magnetic flux lines is the sum of Equations 2.5 and 2.6, thus

$$v_D = v_{DG} + v_{DC} \tag{2.7}$$

2.3 REFLECTION OF LUNE ELECTRONS BY MAGNETIC MIRROR EFFECT

Charged particles such as the lune electrons that are trapped upon the earth's magnetic-flux lines may experience reflections in their north-south spiraling motion about the B lines due to

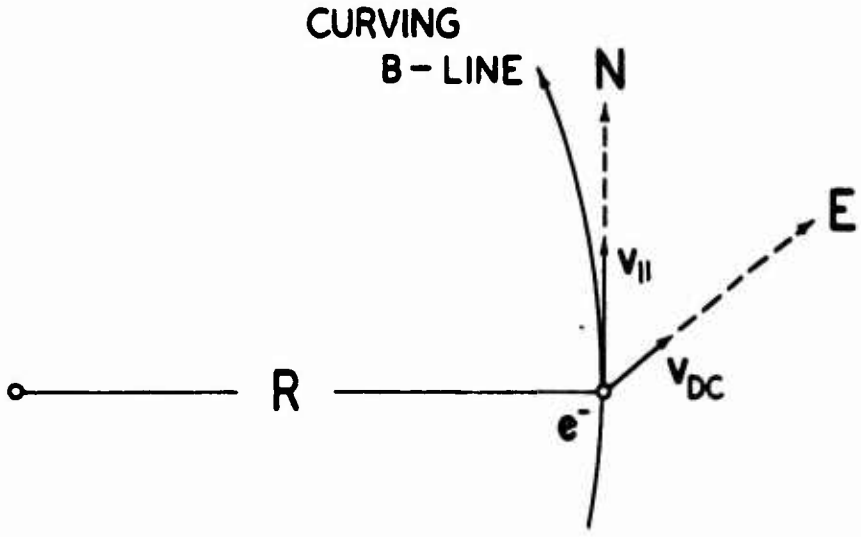

Figure 2.2 The drift associated with curvature of the lines of force. The view is at the equator, with E, N, and R lines mutually orthogonal.

the formation of magnetic mirror points as regions of increasing B are approached, generally near the earth's magnetic poles. Successive reflections of the electrons alternately near the north and south poles of the earth are necessary to preserve the electrons in the lune, as briefly noted above. Figure 2.3 shows the shape of the magnetic field of the earth and a cross section of the electron shield (shaded) formed by magnetically trapped electrons.

The magnetic-mirror effect is discussed in Reference 8 and elsewhere. It is a simple effect and may be described in physical terms by reference to Figure 2.4, which shows what happens to an electron spiraling in from the left-hand side in its magnetically trapped motion from a region of weaker and, essentially constant, magnetic-flux density B_0 (at P on X axis) toward the right-hand side, where the flux density increases steadily. It is to be noted that the electrons spiral clockwise about $\bar{B}$, looking in the direction of the $\bar{B}$ lines. The electron radius of gyration varies inversely as B, so the electron spirals, as shown by Figure 2.4, become tighter as the particle moves from left to right. Another effect also is present: because of the convergence of the B lines, there is always a component of B perpendicular to the X axis. This component, not shown in Figure 2.4, produces a force that is always directed toward the left. The retarding

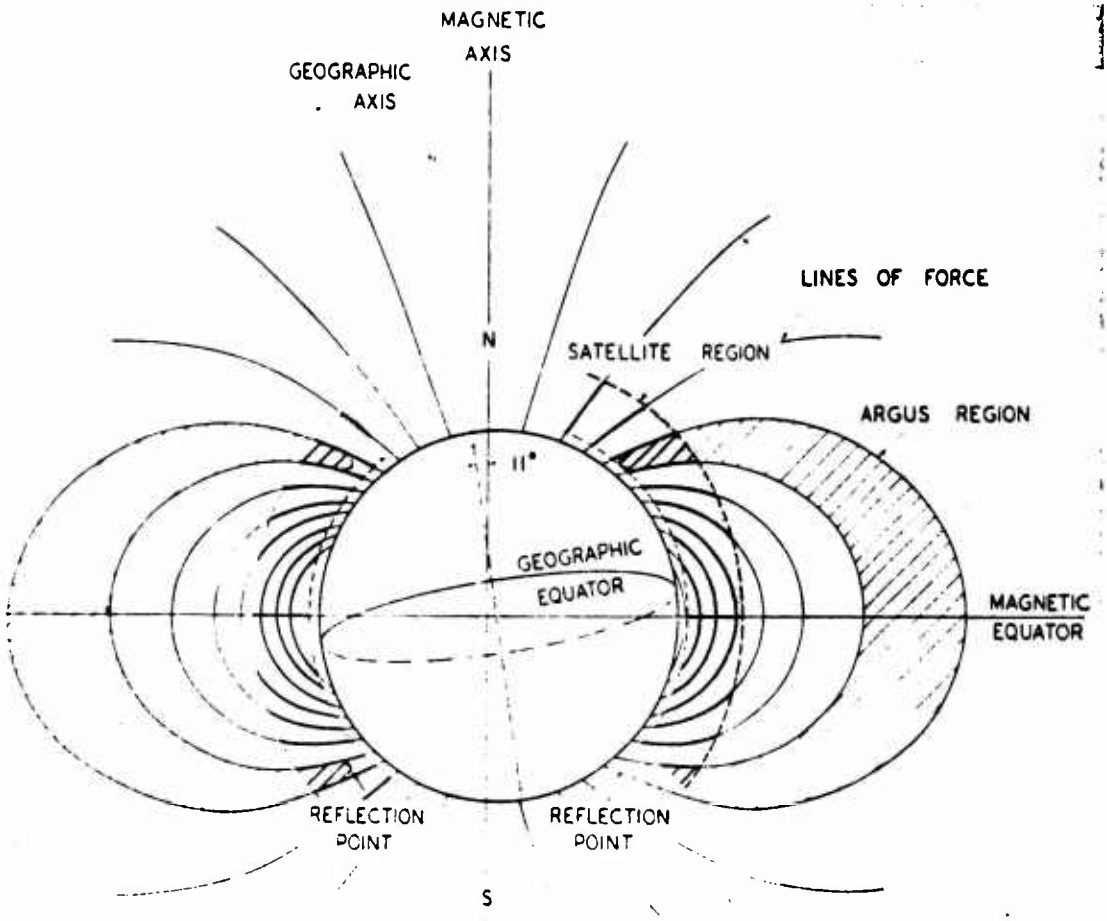

Figure 2.3 A view of the earth showing the magnetic lines of force assumed to be generated by an eccentric magnetic dipole.

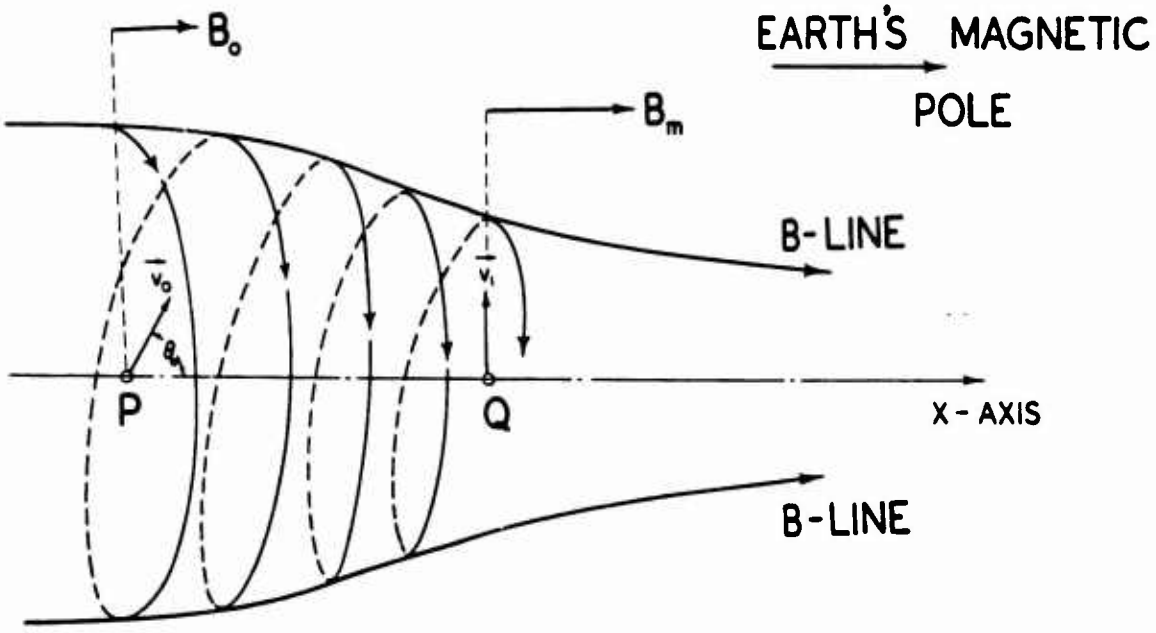

Figure 2.4 The path of an electron as it moves into a more dense magnetic field.

force toward the left eventually reduces the electron speed parallel to the X axis and toward the right to zero; the electron is then reflected and begins to spiral out toward the left.

As shown in Reference 8, the following expression, derived from the constancy of the magnetic moment of the gyrating electron, holds

$$\frac{\sin^2 \theta_0}{B_0} = \frac{\sin^2 \theta}{B} \tag{2.8}$$

where θ and θ_0 are the angles between the total velocity vector $\bar{v}$ and the X axis (Figure 2.4) for the electron at two positions where the magnetic flux density is B_0 and B, respectively. By Equation 2.8, reflection occurs when $\theta = 90$ degrees, which means that the velocity vector has turned until it is perpendicular to the lines of force (X-axis direction in Figure 2.4). Hence, $\sin^2 \theta = 1$ in Equation 2.8 is the magnetic-mirror-reflection condition, and if B is put equal to B_m (magnetic-flux density at mirror point, Q, on X axis) in the equation, the condition may be written

$$B_m = B_0/\sin^2 \theta_0 \tag{2.9}$$

Electrons for which $\theta > \theta_0$ are reflected before they arrive at Q. For example, as shown in Figure 2.5, an electron with a velocity vector making an angle θ_1 with B will be reflected before Q is reached.

The fraction of electrons reflected between P and Q (Figure 2.5) is calculated readily if an isotropic distribution of each charged particle velocity is assumed at P. Considering θ_0 to be the angle at P which results in reflection at Q, it is shown easily that the reflection coefficient of the magnetic mirror R is related to Equation 2.9 as follows:

$$1 - \sin^2 \theta_0 = \frac{B_0}{B_m} = R \tag{2.10}$$

Since R is independent of the particle speed v, each speed has the same reflection coefficient.

2.4 LUNE PRODUCTION, PERIOD, AND LIFETIME

The preceding sections concerned the fundamental physical principles of the Christofilos effect, i.e.: (1) the trapping of electrons upon the magnetic flux lines of the earth; (2) the eastward drift of these electrons resulting from curvature of the magnetic flux lines and the gradient of the magnetic field density; and (3) the reflection of electrons by the "magnetic mirrors" in the earth's magnetic field, formed by the convergence of the magnetic-flux lines as the two magnetic poles are approached. In this section, the production of the electron lune, the lifetime of electrons in the lune, and the revolution period of the lune electrons will be discussed.

2.4.1 Production of Electron Lune. As stated previously, the relativistic electrons of the lune are obtained from the beta-decay of fission fragments and nuclei which are produced in a nuclear explosion. Argus was to use three nuclear bursts: yield, warhead mass, 100 kilograms; height of burst, 700 kilometers; launch latitude, about 45 degrees S magnetic; launch longitude, ~10 degrees W. The treatment in this section assumes these parameters.

The nuclear burst should produce a rapidly expanding ball of radioactive material and bomb debris. In the absence of any containing atmosphere, this ball should expand against a restraining magnetic field. The ball may be pictured as a bubble in the earth's magnetic field with the magnetic flux lines passing around the bubble — the high electrical conductivity of the bubble ex-

cluding the magnetic field initially. The maximum expansion of the ball or bubble within the restraining magnetic field may be calculated roughly by equating all of the burst yield (neglecting radiation losses) to the work done against the restraining magnetic field, thus

$$\text{Yield} = \frac{4\pi R^3}{3} \frac{B^2}{8\pi} \tag{2.11}$$

where R is the maximum radius of the ball or bubble. Equation 2.11 yields R ~ 150 km. A correction for the radiation losses of the highly ionized material within the bubble yields R ~ 100 km.

Since the magnetic field is excluded initially, the 100-km-radius bubble is a plasmoid, which rises upward in the direction of weaker magnetic fields and expands further (Reference 9).

As the bubble expands and cools, its electrical conductivity decreases, the earth's magnetic flux density B penetrates the bubble, and the entrapment of charged particles by the magnetic

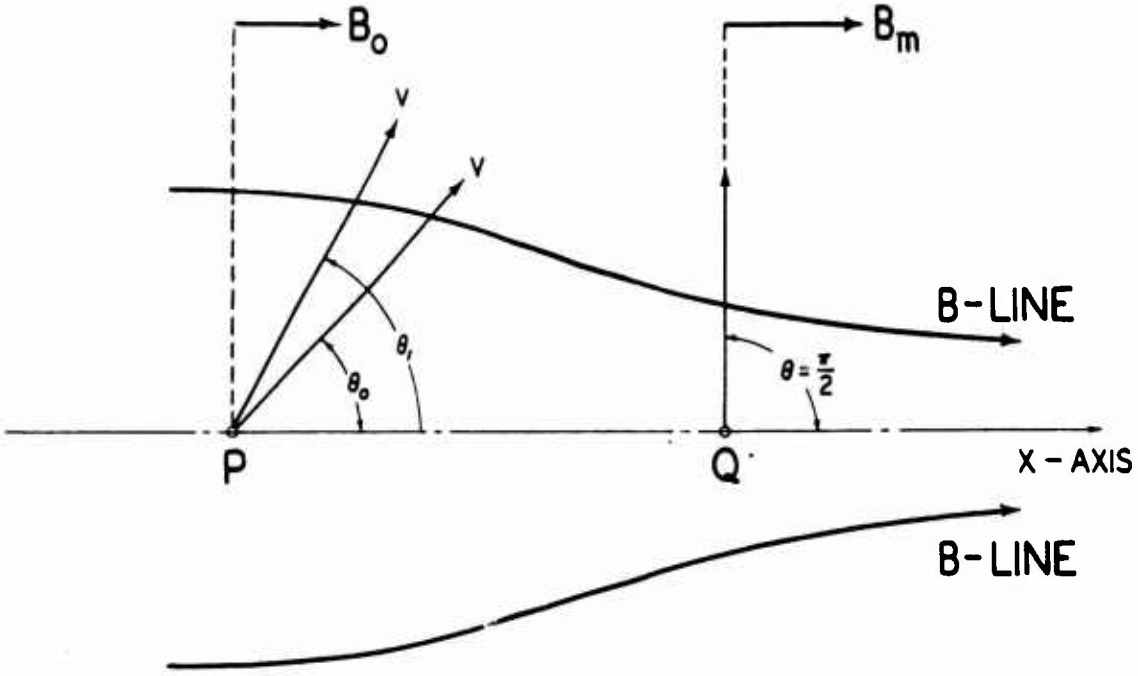

Figure 2.5 An illustration of quantities for derivation of the reflection coefficient of the magnetic mirror of Figure 2.4.

field begins. The exact situation is not known, but the following reasonable assumptions can be made: (1) One half of the beta particles from the neutrons and other fission fragments are lost at once into the lower atmosphere. (2) One half of the neutrons and other fission fragments, which are moving upward, emit beta-decay electrons uniformly along magnetic lines of force through the cooling bubble. (3) The beta-decay electrons are emitted isotropically. These assumptions yield a picture of a tubular volume of electrons. The surface of the tube is formed by the earth's magnetic-flux lines and the ends of the tube are circles of some 100 km in radius located on the earth's surface.

The tube or lune of electrons expands quickly into a shell (Figure 2.3). The shape of this shell can be constructed analytically by the application of the two adiabatic invariants of the electron motion (Reference 10). These fundamental invariants are the magnetic moment of the trapped electron and the integral invariant, $I = \int_B^B v_{//}\, dl$ = constant. This integral of $v_{//}$ along the magnetic flux density line is conserved when the revolution time (see below) is long compared to the

travel time between conjugate mirror points (bounce period). To construct the electron shell at each longitude, the integral I is adjusted to constancy along a surface of constant magnetic-flux density. The resulting shell will not have constant thickness, and the associated electron particle density will vary with the shell thickness, being smaller where the shell is wider, and vice versa.

For the calculations of the revolution time (period for eastward drift of lune-trapped electrons around the earth) and the characteristic lifetime (mean life of a trapped electron) it is necessary to know the energy distribution of the beta-decay electrons emitted in or as a result of the nuclear burst, since both times are energy dependent. Figures 2.6 and 2.7 show the electron energy distributions for both the neutron decay and for typical fission-produced betas.

2.4.2 Revolution Time of Lune Electrons. The time for lune electrons to drift eastward once around the earth in a winding orbit has been calculated roughly for 1 Mev to be about 30 minutes.

The calculation of the average revolution time T_{av} as a function of the electron energy was originally made by Christofilos and appears in Reference 11. The final result obtained by using

TABLE 2.1 AVERAGE REVOLUTION TIMES FOR RELATIVISTIC ELECTRONS OF KINETIC ENERGY E

E	T Average	E	T Average
Mev	min/rev	Mev	min/rev
0.5	57	4.0	9.7
1.0	33	6.0	6.6
2.0	18	8.0	5.2
3.0	12.5		

Equation 2.7, including B as a variable and averaging over all mirror points and trigonometric factors, is

$$T_{av} = \frac{87}{\gamma \beta^2} \text{ minutes} \tag{2.12}$$

where γ and β are defined by Equations 2.3 and 2.4. Equation 2.12 shows that T_{av} varies essentially as the reciprocal of the kinetic energy of the orbiting particle. Table 2.1 lists a few typical values of T_{av}.

Equation 2.12 and the values in Table 2.1 include these assumptions: (1) The earth's magnetic field is approximated by an eccentric dipole (the dipole is shifted 342 km from the earth's center toward the surface point 6.5 degrees N, 161.8 degrees E; the axis of the eccentric dipole intersects the earth's surface at 80.1 degrees N, 82.6 degrees W, and 76.3 degrees S, 121.3 degrees E; the dipole moment is 8.1×10^{25} Gauss cm^3). (2) The trapping B lines of the earth are those intersecting the earth's surface at 45 degrees latitude. (3) Perturbations in the earth's magnetic field at the surface disappear at the high altitudes of the Argus lune. (4) There are no radial drifts.

Reference 11 includes another calculation for T_{av} in which it is assumed that the eastward drift of the electrons occurs at the earth's surface perpendicular to both $\bar{B}$ and $\bar{\nabla} B$, which are known. Hence, the drift line winding around the earth can be plotted accurately. This second calculation that includes the effect of perturbations in the earth's magnetic field gives results close to those of Table 2.1.

2.4.3 Characteristic Lifetime of Lune Electrons. The characteristic lifetime is the mean life of an electron as a function of its initial mirror altitude (minimum altitude). Reference 11 details the calculation of characteristic lifetime for lune electrons and includes the following:

1. The life of an electron in the lune is determined by the small angle scattering cross section for electrons by atmospheric molecules at the mirror point (lowest altitude and, therefore,

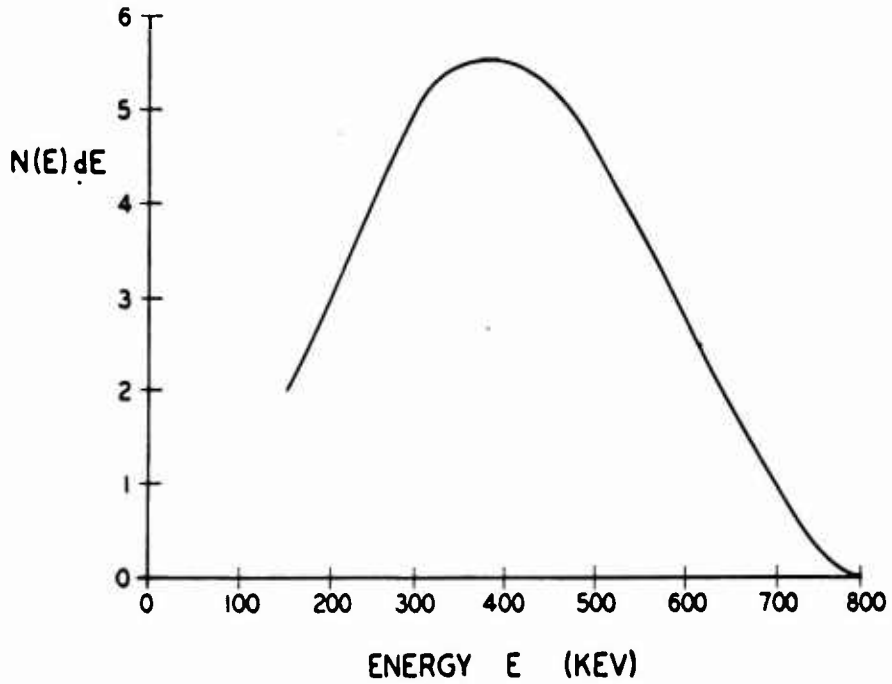

Figure 2.6 Distribution in energy of electrons resulting from the beta-decay of neutrons.

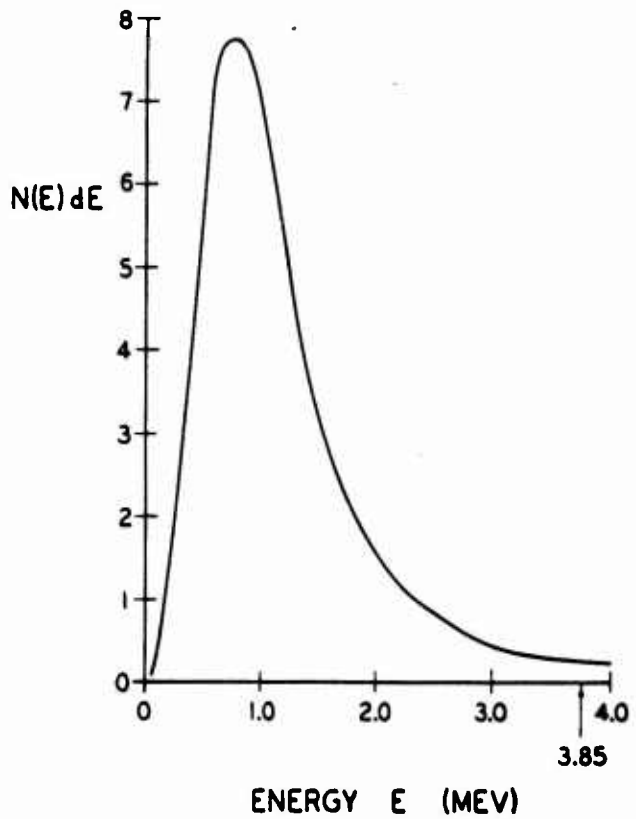

Figure 2.7 Approximate beta spectrum for fission products.

most dense atmosphere). This means that electrons are scattered from a potential mirror point into a mirror point at lower altitude, so that by successive scatterings and reflections the particle's mirror point effectively drifts down to the earth along a B line.

2. The mean life is calculated usually for a B line intersecting the earth at 45 degrees latitude at a dip angle of about 70 degrees.

3. The earth's magnetic-field flux density at 45 degrees latitude is 1.5 times its value at the equator.

4. Because of the earth's eccentric dipole, the atmosphere density will vary with longitude at a given latitude as the lune revolves about the dipole axis; hence, this effect must be averaged in the lifetime calculation.

5. The magnetic moment of gyrating electrons is taken to be constant, which results in constancy for the ratio $B/\sin^2\theta$ where θ is the angle between $\bar{B}$ and the velocity vector.

With these five items included, the resulting expression for the characteristic mean life $\tau(r)$ of a particle of initial mirror point located r from the dipole center is

$$\tau(r) = \frac{f\,10^7\,E^2}{N(r)}\left(\frac{a}{r}\right)^{1/2} \text{ days} \qquad (2.13)$$

where E is the kinetic energy of the electron, N(r) is the atmospheric particle density at the initial mirror point, f is a factor of value 2.0, and a is the scale height defined as the e-folding distance for atmospheric density.

Equation 2.13 shows that the characteristic lifetime varies directly as the square of the kinetic energy of the electrons and inversely as the initial atmospheric particle density. Hence, for long lifetimes, E must be large and the electrons injected at high altitude. Table 2.2 lists values of $\tau(r)$ as a function of initial mirror point, altitude h, for 1-Mev electrons injected at 45 degrees latitude. Other pertinent data are included.

It is important to investigate the decay of the Christofilos effect. This is defined analytically as the change with time of the integral of the mirror point density W(h, t), at mirror altitude h, over the cross-sectional area of the electron shell perpendicular to the B line. The quantity W(h, t) has been investigated (Reference 10) by calculating the change with time of the fission beta spectrum and assuming $\tau(r) \propto E^2$, Equation 2.13, where E is between 0.5 and 6 Mev.

$$W(h, t) = \text{constant}\left[\frac{1}{1 + t/\tau(r)}\right] \qquad (2.14)$$

For short times $t << \tau(r)$, W(h, t) should be constant whereas for long-lived electrons, $t >> \tau(r)$, Equation 2.14 predicts a 1/t law. There are questions as to whether observations at times shorter than the characteristic mean life $\tau(r)$ may be made. Thus, the constant part of the decay may not be observable in the satellite data.

2.5 ELECTRON DENSITIES

Following the development of his theory, Christofilos proposed a test with artificial electron injection for which electron density and flux could be calculated. It was suggested that the source of the electrons be the various beta-decay processes involved in a nuclear explosion at a suitably high altitude and that radiation detectors be carried by a satellite.

Calculations of particle densities and fluxes of magnetically trapped relativistic electrons resulting from nuclear bursts have been made (References 11 and 12). Electrons, both from beta-radioactive fission products and neutron decay, have been considered. Because of the relatively long half life (about 12 minutes) of the neutron and its long mean free path at high altitudes, the electrons from neutron decays are widely dispersed. Further, as shown in Figures 2.6 and 2.7,

the higher energies of the fission-product betas mean a longer lifetime in the electron shield. By Equation 2.13, the characteristic lifetime is proportional to the square of the particle energy.

Hence, it turns out that the neutron decay processes result in an electron particle density of roughly one thousandth of that of the corresponding electron particle density resulting from beta radioactivity of the fission products. It must be emphasized that the greater electron density resulting from fission product beta-decay is useful only if these betas escape from the bomb bubble (fireball) of high electrical conductivity to become trapped upon the earth's magnetic-flux lines. It is not known what fraction of the betas escape from the fireball, but it is expected that

TABLE 2.2 CHARACTERISTIC LIFETIMES OF 1-MEV ELECTRONS AS A FUNCTION OF INITIAL MIRROR POINT, 45 DEGREES LATITUDE INJECTION

Altitude (of initial mirror point)	Air Density	Scale	Characteristic Lifetimes	
			Centered Dipole	Eccentric Dipole
h, km	N, atoms/cm^3	Height, km	days	days
0	5.4×10^{19}	10	1.4×10^{-14} *	1.8×10^{-13} *
100	1×10^{14}	20	1.1×10^{-8} *	1.0×10^{-7} *
200	2.5×10^{10}	50	7.0×10^{-5}	4.0×10^{-4}
300	3.5×10^{9}	100	7.1×10^{-4}	2.6×10^{-3}
400	1.2×10^{9}	100	2.0×10^{-3}	7.3×10^{-3}
500	4.5×10^{8}	100	5.5×10^{-3}	2.0×10^{-2}
600	1.8×10^{8}	100	1.4×10^{-2}	5.1×10^{-2}
700	6.5×10^{7}	100	3.7×10^{-2}	0.14
800	3×10^{7}	100	8.2×10^{-2}	0.30
900	1×10^{7}	100	0.24	0.88
1,000	4.4×10^{6}	100	0.50	1.8
1,100	1.7×10^{6}	100	1.3	4.7
1,200	8×10^{5}	100	2.8	10.2

* Less than time for one revolution. Hence, particles with these mirror point altitudes die on their first encounter with the atmosphere.

additional information on this point will be obtained from a more intensive study of the Argus experiments.

The calculation of the trapped-electron particle density and flux, making several simplifying and reasonable assumptions, is sketched as follows:

1. The total number of fission-produced electrons N_e for a [ ] high-altitude fission burst is, assuming production of six betas per fission event,

$$N_e = [\quad] \times 1.3 \times 10^{23} \frac{\text{fissions}}{\text{kiloton}} \times 6 \frac{\text{electrons}}{\text{fission}} \times \frac{1}{2}$$
$$= [\quad] \text{ electrons} \qquad (2.15)$$

where the factor ½ is used because of the assumption that half the beta decay occurs under conditions favorable to reasonable lifetimes, with the other half being lost rather quickly by collisions with the atmosphere and bomb material. It is probably optimistic to consider that each fission event results in three electrons available for entrapment; if one electron per fission is used instead, [ ] electrons is obtained for N_e.

2. The total number of fission-produced electrons N_e fill the shell-like space generated by the revolving lune. The volume of this shell may be calculated by integrating $\int A\,ds$ where $A = 2\pi rd$, r is the radius of the shell measured from the dipole center; d is the thickness of the shell, which is assumed roughly constant and taken equal to the initial fireball diameter of 200 km; and ds is the element of distance along a line of force. Also, for simplicity, the mirror-

point density is considered to be constant. A detailed discussion of these assumptions may be found in Reference 11. Finally, the number of entrapped electrons/cm^3 n_e is calculated to be

$$n_e \sim 10^{-3} \text{ electrons/cm}^3 \tag{2.16}$$

3. The electron flux, defined as $n_e v$, is approximated ($v \sim c$) and averaged over all directions by

$$n_e v \sim \frac{n_e c}{4} = \frac{10^{-3} \times 3 \times 10^{10}}{4} \sim 8 \times 10^6 \text{ electrons/cm}^2 \text{ sec}, \tag{2.17}$$

TABLE 2.3 ARTIFICIAL AND NATURAL TRAPPED ELECTRON PARTICLE DENSITIES, FLUXES AND ENERGIES

Source of Relativistic Electrons	Electron Particle Density, N_e	Electron Flux	Kinetic Energy
	number/cm^3	(number/cm^2)/sec	
Argus nuclear burst (Christofilos electrons); fission produced beta particles	(0.3 to 1.0) $\times 10^{-3}$	(2.5 to 8) $\times 10^6$	Maximum > 3.5 Mev, peak of spectrum ~ 0.5 Mev; (Figure 2.8)
Natural, Van Allen radiation at ~ 2,000 km altitude	0.5	10^9	Maximum > 5 Mev, peak of spectrum ~ 0.05 Mev

If one electron per fission is used instead of three, the values of Equations 2.15, 2.16, and 2.17 are reduced by a third, to yield

$$N_e \sim \quad \text{electrons},$$
$$n_e \sim 0.3 \times 10^{-3} \text{ electrons/cm}^3,$$
$$n_e v \sim 2.5 \times 10^6 \text{ electrons/cm}^2 \text{ sec} \tag{2.18}$$

The theoretically expected electron-particle densities and fluxes due to artificial injection may be compared with naturally present values of these same quantities. This comparison is presented in Table 2.3, which includes also similar calculations for a Hardtack-type burst.

A crude estimate of actual count rates to be expected for the Argus nuclear burst (Table 2.3) employing a G-M counter such as used in Channels 1 and 3 of Explorer IV (Table 2.4) may be made as follows:

Assuming direct counting of beta particles (relativistic electrons enter the counting volume of the G-M tube) and 0.5 cm^2 as the effective incident surface A for the Anton G-M counter (Table 2.4), the counting rate N_T is

$$N_T = n v A \sim 2 \times 10^6 \times 0.5 = 10^6 \text{ counts/sec} \tag{2.19}$$

TABLE 2.4 SUMMARY OF RADIATION-DETECTION INSTRUMENTATION OF EXPLORER IV SATELLITE

Channel	Detector	Shielding	Radiation Measured	Solid Angle	Counting-Flux Factor To obtain counts per cm^2 per sec per steradian	Scale	Center Frequency
1	D—Geiger-Mueller counter (Anton 302; cylinder 7 × 7 mm approximately). The Shielded G-M Detector	1.2 g/cm^2 of Fe plus 1.6 g/cm^2 of Pb	Electrons of energy greater than 5 Mev; protons of energy greater than 40 Mev; X rays of energies greater than 80 kev with low efficiency.	Approaches 4 π for more energetic particles	Output counts × $\frac{1}{3}$	64X	400 cycles/sec ± 7.5 pct
2*	A—Scintillation detector: RCA photomultiplier 6199 viewing National Radiac Scintilon (plastic scintillator) diam. 0.30 in., length 0.070 in. A Pulse-Height Detector	0.14 g/cm^2 of Al, through window	Electrons of energy 0.58 Mev to greater than 3 Mev; protons of energy greater than 9.5 Mev; X rays of energies greater than 0.4 Mev with low efficiency. (Shielding plus electronic cutoff: 0.7 Mev for electrons.)	Designed to view $\frac{1}{40}$ of sphere. Detector aligned perpendicular to axis of satellite	(1) 0.6 to 3 Mev: Output counts × 10 (2) Greater than 3 Mev; Output counts × $\frac{1}{3}$	2,048X	560 cycles/sec ± 7.5 pct
3	C—Geiger-Mueller counter; same as Channel 1. The Unshielded G-M Detector	1.2 g/cm^2	Electrons of energy greater than 3 Mev; protons of energy greater than 30 Mev.	Approaches 4 π for more energetic particles	Same as Channel 1	2,048X	730 cycles/sec ± 7.5 pct
4	B—Scintillation Detector: RCA photomultiplier 6199 viewing cesium-iodide (thallium loaded) crystal diam. 0.30 in., length 0.080 in. A total energy integrator, not a pulse-height detector, employing an electrometer tube circuit. The Analog Detector	0.2 mg/cm^2 of Al plus 0.8 mg/cm^2 of Ni; increases to about 1 g/cm^2 as detector approaches a 4 π detector.	Electrons of energy greater than 20 kev for window, electrons of energy greater than 3.5 Mev when performing as approximately a 4 π counter; protons of energies greater than 0.4 Mev; X rays are detected efficiently.	Designed to view $\frac{1}{100}$ of sphere; actually becomes a 4 π counter at higher energies. Detector aligned perpendicular to axis of satellite and 180 degrees opposite to Channel 2 detector.	For total energy calibration see Figure 1	None, d.c.	960 cycles/sec ± 7.5 pct
5*	A—Same as Channel 2. (The output of Channel 2 detector feeds two scaling circuits of 2,048X and 16X)	Same as Channel 2	Same as Channel 2	Same as Channel 2	Same as Channel 2	16X	1,300 cycles/sec ± 7.5 pct

* Channels 2 and 5 have a built-in scaler deadtime resulting in the following formula for obtaining the true count rate N in terms of the observed count rate n. $N = n/(1-n)/11{,}000$. The temperature coefficient of the amplifier of Channels 2 and 5 is large. Above 40 C the amplifier gain is decreased by about one half, which effectively increases the lower energy cutoff of the detector. In the temperature range −10 to 40 C the performance is satisfactory. Channels 2 and 5 contain a built-in radioactive source Tl^{204}, to yield about 0.5 detector counts per sec.

Assuming conversion of electrons into bremsstrahlung which, in turn, are counted by the G-M detector, N_T is

$$N_T = nvA \times \eta \times A_\gamma \times \epsilon \tag{2.20}$$

where η is the bremsstrahlung production efficiency for electrons and is taken to be 0.003, A_γ is the absorption coefficient for bremsstrahlung photons and is taken to be 0.5 for photons of 100-kev mean energy, and ϵ is the G-M counter efficiency for bremsstrahlung photons of the stated mean energy and is taken to be 0.01. Thus, using these values in Equation 2.20 yields

$$N_T = 2 \times 10^6 \times 0.003 \times 0.5 \times 0.01 \sim 18 \text{ counts/sec} \tag{2.21}$$

The natural background counting rate N_B at altitudes below those which the Van Allen high count rate begins is expected to be about 1 count/sec. Hence, considering Equations 2.19 and 2.21 to yield the maximum and minimum counting rates, respectively, the signal minus background counting rate $N_T - N_B$, for the Argus experiments should be

$$18/\text{sec} \leq N_T - N_B \leq 10^6/\text{sec} \tag{2.22}$$

Chapter 3
RADIATION INSTRUMENTATION for EXPLORER IV

The apparatus installed in Explorer IV is shown in block diagram form in Figure 3.1. An outline sketch of the physical arrangement of components in the satellite payload is shown in Figure 3.2. Salient characteristics of the four radiation detectors were as follows:

3.1 DETECTOR A

Circular disk of plastic scintillator (National Radiac Scintilon), thickness 0.178 cm, diameter 0.762 cm, cemented on the face of an RCA 6199 photomultiplier (PM) tube. The PM tube was mounted with its axis orthogonal to the longitudinal axis of the payload and with the scintillator near an open hole in the wall of the payload shell. The scintillator's unidirectional geometrical factor (defined by $G = R/\epsilon j$, where j is the unidirectional intensity in particles $cm^{-2}sec^{-1}$ steradian^{-1} through an aperture covered by 0.14 g/cm^2 of aluminum. The geometrical factor as a function of stopping power rose rapidly for stopping power greater than 1.6 g/cm^2 to an asymptotic value of $G = 4.2$ cm^2 steradian (or $G_0 = 0.334$ cm^2) for stopping powers greater than 5 g/cm^2. The collimating apertures were such that the area of the scintillator "visible" through the foil had its full value for a cone of a half angle of 6 degrees and fell linearly to zero at a half angle of 19 degrees. The electronic bias was selected so that about 5 percent of the beta rays from a Tl^{204} source on the outside of the stopping foil were recorded. The upper limit of the beta spectrum of Tl^{204} is 780 kev. A weak Tl^{204} source was permanently deposited on the foil of the flight instrument to provide an overall check on performance of the system; it gave an average background of the amplifier. Overall response of the system was well represented by the following equation:

$$R = \frac{r}{1 - r\tau} \tag{3.1}$$

in which r = apparent counting rate, $\tau = 91$ μsec, R = true counting rate. Two scaling factors were provided in order to extend the dynamic range of the system: Channel 2 with a scaling factor of 2,048 and Channel 5 with a scaling factor of 16.

Detector A (the plastic scintillator) counts electrons having energies exceeding 700 kev; protons having energies exceeding 9.5 Mev; with considerably lower efficiency, X rays having energies exceeding about 400 kev; and with rapid diminishing efficiency, particles or X rays of progressively lower energies than those specified (electronic pile-up of pulses). In a sample preflight test with an X-ray machine irradiating Detector A at 1,400 r/hr, it was necessary to raise the accelerating voltage to 200 kv before an observable counting rate occurred. Detectors C and D were simultaneously driven far beyond their dynamic range, a situation never encountered in flight.

3.2 DETECTOR B

Circular disk of CsI(Tl) scintillating crystal, thickness 0.203 cm, diameter 0.762 cm, cemented to the face of an RCA 6199 photomultiplier tube. Mounting of the assembly was similar to that of Detector A, except that its aperture faced in the opposite direction. A thin layer of aluminum (about 0.2 mg/cm^2) was first evaporated onto the crystal. Then it was further shielded by a nickel foil of 0.8 mg/cm^2 thickness. This arrangement permitted exposure of the detector

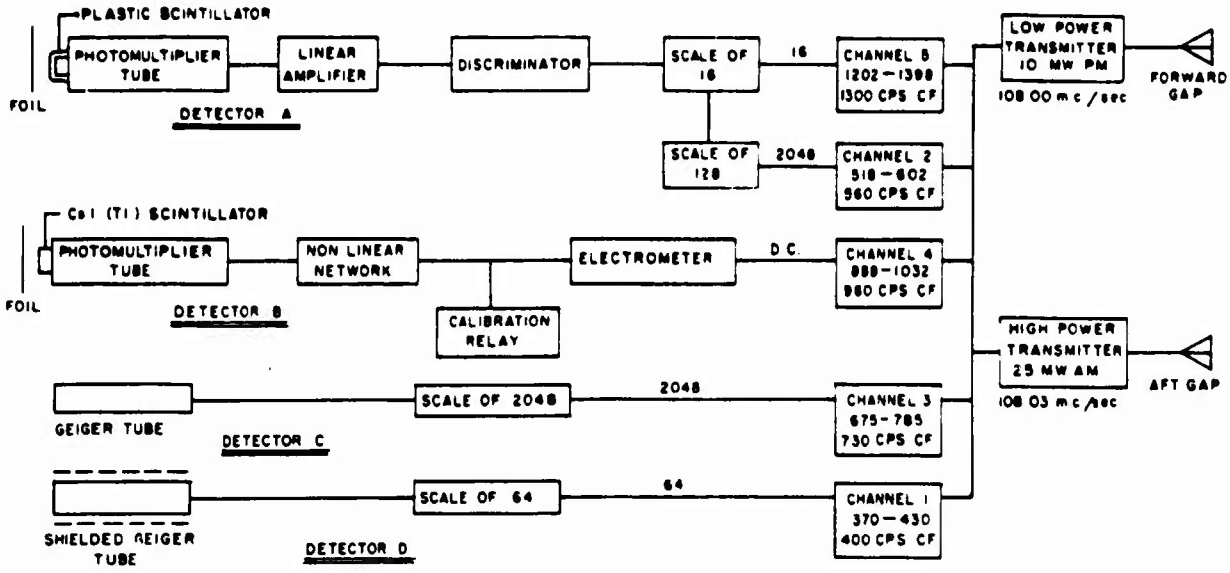

Figure 3.1 Schematic of satellite instrumentation.

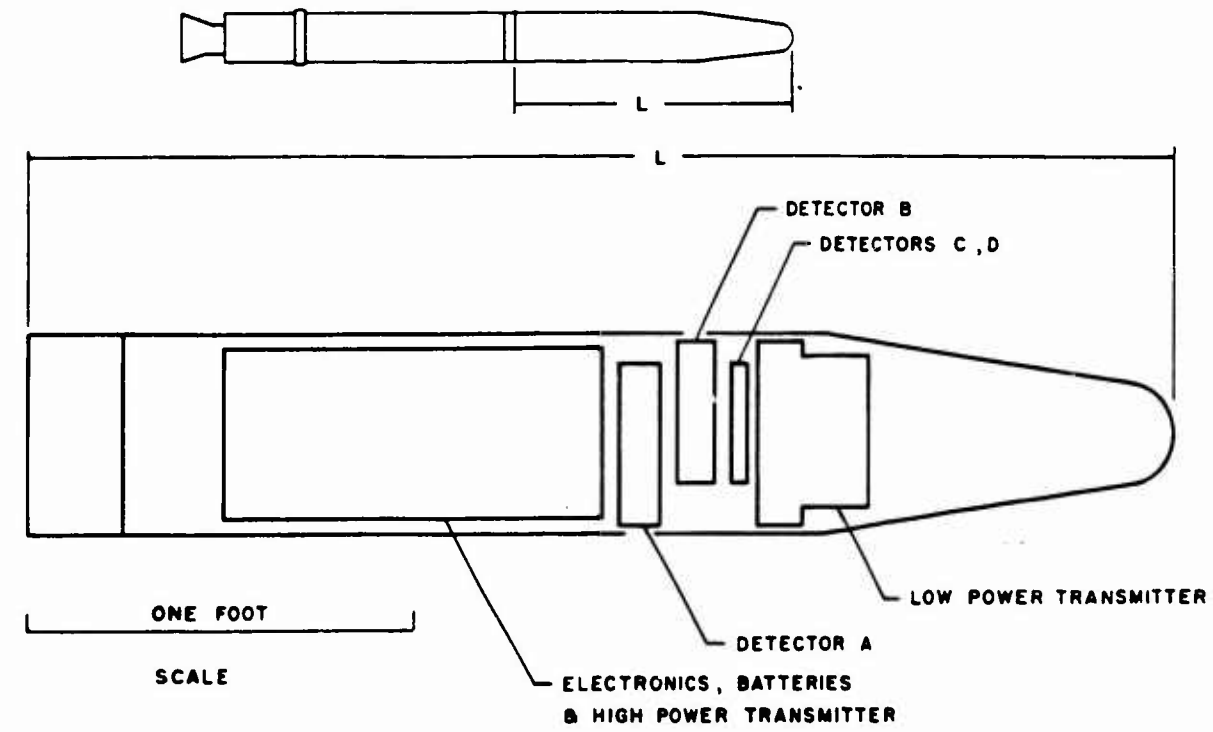

Figure 3.2 Payload configuration of satellite.

to direct sunlight without any detectable response. The nickel foil was cemented to and supported by a plastic disk having seven closely spaced No. 46 drill-size holes. The geometrical factor G was 0.0235 cm^2 steradian for a stopping power of 1 mg/cm^2 and rose rapidly to an asymptotic value of 4.4 cm steradian (or G_0 = 0.350 cm^2) for a stopping power greater than 5 gm/cm^2. The angular opening angles were very nearly the same as for Detector A. The anode current of the

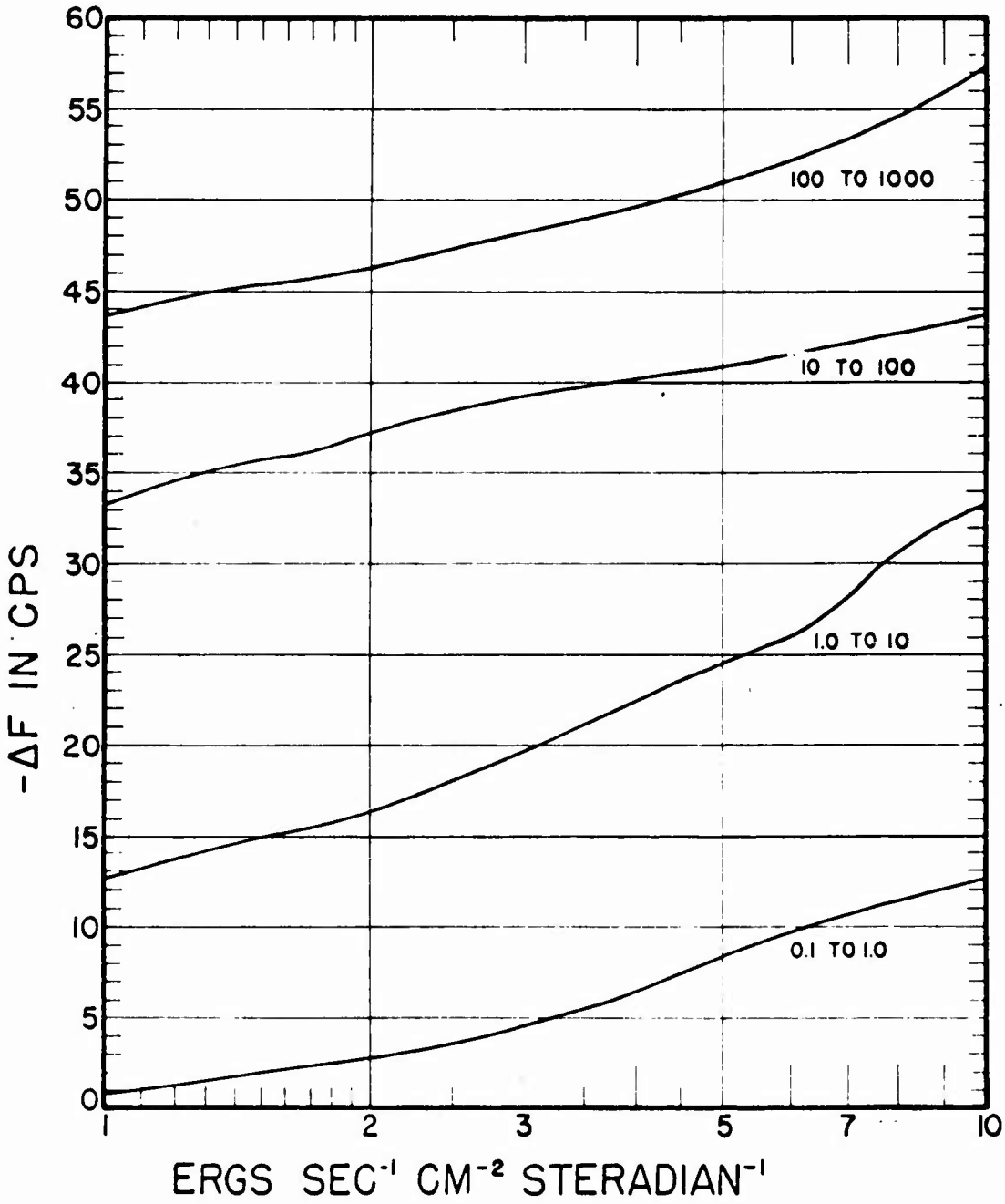

Figure 3.3 Calibration curves for Channel 4.

photomultiplier tube was passed through a nonlinear Zener diode network, whose output voltage was applied to the grid of a hard vacuum electrometer tube and thence to the subcarrier oscillator. The frequency deviation of the subcarrier was approximately proportional to the logarithm of the anode current of the photomultiplier tube over a range of six decades. The absolute calibration of the system was determined with the help of a polonium alpha-particle source of known strength (Figure 3.3). The constant of the system was 1 amp = 0.47×10^8 ergs/sec of ionization

energy dissipated in the crystal by a fast, singly charged particle. The workable dynamic range extended from about 10^{-1} erg/sec to 10^{5} erg/sec. The zero of the electrometer was checked periodically throughout flight at 20-second intervals by connecting the grid of the electrometer tube to a fixed reference potential for 1.7 seconds.

Detector B has distinctively different properties from Detector A. Its foil will stop electrons having energies of about 20 kev, or protons having energies of 400 kev. And it is an efficient detector of X rays.

3.3 DETECTOR C

The basic detector was an Anton-type 302 Geiger tube. It was not deliberately shielded but was more or less surrounded by a miscellany of electronic components and mechanical structure such that the omnidirectional geometric factor G_0 was 0.13 cm^2 for a stopping power of 1.2 g/cm^2 and approached its full value of 0.705 cm^2 for stopping power of greater than 5 g/cm^2 (Figure 3.4).

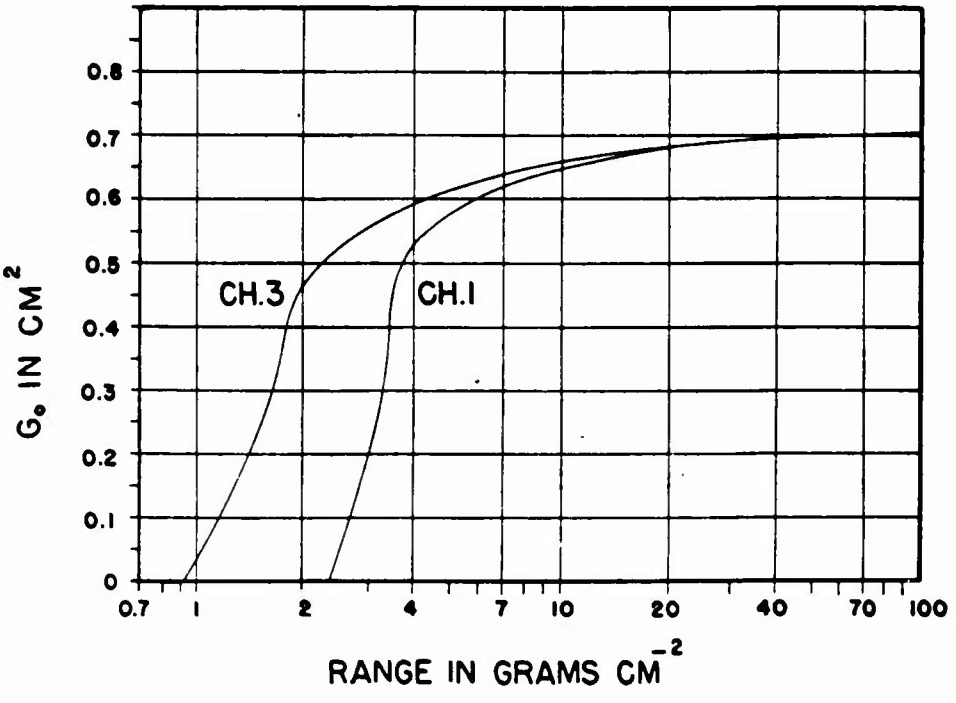

Figure 3.4 Calibration curves for Channels 1 and 3.

The material in the low stopping power case was mainly stainless steel. The performance of the overall circuit was found in detailed calibrations to be well represented by the following equation:

$$r = Re^{-R\tau} \tag{3.2}$$

where r is the apparent rate, R the true rate and $\tau = 62.5 \pm 1.3$ μsec. The useful dynamic range for filtered 50-kv X rays, for example, extended up to about 20 r/hr. The maximum value of r was 5,900 counts/sec and the value of r was very nearly proportional to radiation intensity at rates below 1,000 counts/sec. No difficulty was experienced in practice in resolving the ambiguity presented by the fact that r was a double-valued function of radiation intensity. The maximum value of r was easily read on the telemetered record due to the large scaling factor, namely, 2,048.

Detector C responds to electrons of energy exceeding 3 Mev, to protons of energy exceeding 30 Mev, and with much lower efficiency, X rays of energy exceeding some tens of kev.

3.4 DETECTOR D

The basic detector was again an Anton-302 Geiger tube. This detector responded to electrons of energies exceeding 5 Mev, protons of energy exceeding 40 Mev, and with much lower efficiency, X rays of energy exceeding about 80 kev. The tube was surrounded by a lead cylinder of 1.6 g/cm^2 thickness and was further shielded on the ends by lead plugs of somewhat greater thickness; G_0 = 0.13 cm^2 for a total stopping power (lead plus stainless steel) of 2.8 g/cm^2, and G_0 approached its full value of 0.705 cm for stopping powers greater than 6 g/cm^2 (Figure 3.4). The maximum observable counting rate of Detector D was determined by the information bandwidth of the telemetering system. It was about 1,500 counts/sec under favorable conditions. The low scaling factor of 64 was selected in order to get a determination of satisfactory telemetering reception by a given station on a given pass. This information is summarized in Table 2.4.

Periods as brief as 1 or 2 minutes were anticipated and did indeed occur not uncommonly, though many stations were successful in receiving workable signals for up to 15 minutes and, in rare cases, longer.

Every reasonable effort was made to assure reliable operation of all elements of the apparatus over a large range of temperature. The entire detector assembly operated reliably from −30 C to +120 C, though the characteristics of Detectors A and B had small, known temperature coefficients. The practical low limit for the complete payload package was about 0 C (determined by mercury batteries) and the practical high limit was about +60 C (determined by the germanium transistors used in the transmitters). Temperature of the interior of the payload of the satellite was determined roughly from the frequency of the subcarrier oscillators. It lay always in the range +10 C to +50 C during its orbital flight.

All components and completely assembled payloads were subjected to a full program of acceleration, vibration, shock, vacuum, and temperature cycling tests. No attempt was made to pressure-seal the payload shell. The operation of all high-voltage (up to 700 volts) circuits was assured by foam-potting and thorough vacuum testing.

Mallory mercury batteries were used throughout for powering the electronic apparatus.

Many potential improvements in the apparatus will doubtless occur to the reader, as they did to the experimenters during the development. But there were severe restrictions on power drain, physical arrangements, weight and information-bandwidth, and on available time, which precluded extensive refinements.

Chapter 4
DISCUSSION and CONCLUSIONS

The artificial satellite, Explorer IV, carrying radiation instruments (Table 2.4) to detect Argus electrons, was successfully placed in orbit on 26 July 1958 by the U.S. Army Jupiter-C vehicle. The first Argus nuclear shot occurred on 27 August 1958. During the month between the launching of Explorer IV and Argus Shot 1, data were transmitted continuously by the satellite, permitting both a detailed, world-wide study of the natural radiation background present in the huge space traversed by Explorer IV and also observations of effects produced upon the natural background by Shots Teak and Orange, Operation Hardtack, 31 July 1958 and 11 August 1958, respectively. This month-long series of observations carried out by many of the ground stations (Table 1.2), such as the one at Huntsville, Alabama, provided the accurate patterns of the radiation background essential for the separation of the Argus electrons from the natural background.

Hence, within a few hours after Argus 1, the Army Ballistic Missile Agency (ABMA) was able to report the positive experimental observation of the Christofilos effect, and then to confirm these initial observations by even more definite and positive observations of Explorer IV piercings of the Argus shell within a few hours of Argus 2 (30 August 1959). The observations of the Huntsville group were quickly confirmed and supplemented by the data received at many ground stations and were reduced and interpreted by the State University of Iowa (SUI) group under direction of James Van Allen.

The initial observations strikingly confirmed the main features of the theory, summarized in Chapter 2 and given in References 1, 10, 11, 12, and 13. It was specifically demonstrated that:

1. The electrons artificially injected into the earth's magnetic field were definitely and precisely contained within a shell, fixed relative to the earth so as to be considered attached to the rotating earth, with the inner and outer surfaces of the shell conforming in shape to the magnetic flux lines of the earth (Figure 2.3). Excursions of Explorer IV through the shell, repeated over periods of days and weeks, established that the shell shape and position relative to the earth were quite stable. No radial drifting of the shell was observed.

2. The shell thickness varied with the magnetic latitude and longitude, as expected from an eccentric dipole approximation of the earth's magnetic field. The shell thickness was some 100 to 200 kilometers, as measured by increased count rates of the satellite detectors during complete traversals of the shell.

3. There was definite decay of the Christofilos effect associated with characteristic lifetimes of the electrons contained in the shell. This was established in a rough quantitative way by observing the satellite detector counting rates for consecutive piercings of the shell in approximately the same regions of space (relative to the earth). These observations resulted in rough decay plots (counting rate versus time) which were useful in distinguishing the Argus shots. Also, these original decay plots were consistent with the calculated characteristic lifetimes.

4. The eastward drift of the lune electrons was demonstrated in the quick development of the injected particles into a shell enveloping the entire earth at the middle latitudes.

The "revolution time" was observed rather strikingly during Argus 2 in that a satellite pass to the west of the injection longitude penetrated the developing electron shell 2 minutes 10 seconds after the burst time for Argus 2. This unusual and fortuitous experimental observation is shown by Figure 1.7, illustrating a telemetered recording of the data during Satellite Pass 453. The observed increased count rate was associated with the shot made 2 minutes 10 seconds before because the observation fitted well into the pattern of later observations for the same Argus

shot. Since the satellite was west of the shot longitude and since electrons drift eastwardly, the increased count rate was attributed to electrons that had traveled almost completely around the earth and, according to Table 2.1, had energies greater than 8.0 Mev.

Following the results observed and analyzed in a rapid, semiquantitative way, it became clear that a more complete and thorough study of the Argus experiments should be made. Hence, during the first two weeks of February, ARPA invited some fifty scientists to an Argus conference at the Lawrence Radiation Laboratory under the chairmanship of Paul Adams of ARPA. This working session presented the first opportunity after the experiment for the scientists involved in the various Argus missions (Table 1.1) to meet and compare results in detail.

After brief introductory presentations from each part of the project, a number of working groups were established, as follows: (1) nuclear planning, (2) space experiments, (3) laboratory experiments, (4) theory, (5) military implications, and (6) data analysis. A report of this conference has been published (Reference 14).

The results of the data analysis working group in analyzing the data obtained from Explorer IV is of particular significance. Dr. George Bing, the local chairman of the conference, was also chairman of the data analysis working group. The other members were: Donald Chandler, Rolf Dyce, William Karzas, John Killeen, Charles Lundquist, Hans Mark, Carl McIlwain, Paul Nakada, Theodore Northrup, Ralph Pennington, Russell Shelton, James Van Allen, and Ernest Vestine.

The group started with some 130 data sheets reduced from the satellite observations by the SUI group. An explanation of these and typical examples are given in Appendix B. The entire collection is contained in a supplement to this report.

A need recognized from the outset by those who had previously worked with the satellite data was for some way to characterize equivalent points in the magnetic field of the earth, where similar counting rates would be expected at a given instant of time. For a dipole, this would have been a simple problem, due to the cylindrical symmetry about the axis and the symmetry with respect to the magnetic equatorial plane. However, the magnetic field of the earth is not adequately represented by a magnetic dipole. The first step toward the solution of this problem was effected by Ernest Vestine, who supplied detailed harmonic expansions for the magnetic field of the earth, some containing as many as 48 terms. He also supplied a computer program which could be used to locate points on the surface of the earth intersected by a flux line through any given point in space. This program, employing 48 terms, was used to project positions where the satellite pierced the electron shell to the surface of the earth in both hemispheres. The result of this program is shown in Figure 4.1. For each nuclear shot, the consistency of the points projected into both hemispheres is of note. This result engendered confidence in the Vestine representation of the magnetic field and formed the basis for representing the total data during the Livermore meetings.

Using the Vestine model also, with an interpolational program from Rand, William Karzas supplied field strength values for each observed traversal of the shell. Ralph Pennington developed a program for computing the shell thickness from the time the satellite spent in the shell and the angle between the satellite orbit and the normal to the shell, the normal being calculated from an eccentric dipole model of the field. These and other important data are presented in Tables 4.1, 4.2, and 4.3.

The magnitude of the field at an observation point proved to be useful as a single parameter characterizing position, replacing the three variables of latitude, longitude, and altitude. Figures 4.2, 4.3, 4.4, 4.5, and 4.6, which resulted from the Livermore conference, are decay curves corresponding to small ranges of magnetic field intensity B. These curves compare favorably with the $1/t$ dependency expected.

Figure 4.7, also produced at the Livermore conference, shows the product of count rate, shell thickness, and elapsed time after the event plotted versus field strength, B. For the case of electrons injected into a small region of space, from geometrical considerations, this product should increase with increasing field strength. Figure 4.7 shows the opposite behavior. This was interpreted to mean that injection was spread out along the lines of force, rather than

TABLE 4.1 ARGUS SHOT 1

Date	Time	t_E	Lat N+, S−	Long E+, W−	Alt	B	Ch 1	Ch 3	Ch 2 Max	Ch 2 Min	Ch 4 Max	Ch 4 Min	Δt ½	Δt 1/10	D ½ = Thickness
		hrs	deg min	deg min sec	km	Gauss	$R-\left(\frac{R_1+R_2}{2}\right)$	difference					sec	sec	km
27 Aug	0227:53	0.0	−38 30	−11 30	160	—	—	—	—	—	—	—	—	—	—
27 Aug	0416:30.8	1.80	+18 13	−73 05	1,497.5	0.228	1,218	100,000	100,000	8,700	12.2	1.5	<20	27	—
27 Aug	0607:50	3.67	+22 51	−96 41 30	1,398	0.251	349	7,800	42,000	7,300	4.39	0.70	32	43	120
27 Aug	0759:22	5.52	+27 55	−119 11	1,285	0.252	95.4	4,000	9,200	1,100	0.70	0.20	16	37	65
27 Aug	0841:58	6.23	−18 47	+40 09	715	0.250	8.3	155	1,044	37.4	—	—	18	53	82
27 Aug	0845:10	6.28	−26 43	+47 38	872	0.249	250	7,150	30,500	<1,679	—	—	30	61	158
27 Aug	1114:55	8.78	−21 04	+146 36	2,114	0.206	232	8,000	28,000	1,000	5.04	1.06	—	—	—
28 Aug	0027:25	21.98	+37 54	4 41	1,057	0.271	5.22	145	245	20	—	—	39	78	72
28 Aug	0356:46	25.48	+17 54	−72 54	1,538	0.228	33.8	2,850	7,600	1,600	0.75	0.17	34	63	108
28 Aug	0548:00	27.33	+22 29	−96 33	1,442	0.245	44.5	1,240	3,146	546	>−0.032	−0.045	30	52	110
28 Aug	0739:34	29.20	+27 39	−119 08	1,328	0.260	16.4	590	1,012	68.7	—	—	—	—	—
28 Aug	0825:45	29.97	−27 15	+48 39	841	0.254	6.5	Noise	38*	92	—	—	—	—	—
29 Aug	0007:27	45.65	+37 51	+5 02	1,106	0.266	1.72	150	181	12	—	—	33	64	60
29 Aug	0336:25	49.13	+17 22	−72 52	1,596	0.216	51.7	1,600	2,355	330	0.41	0.02	32	58	101
29 Aug	0527:39	51.0	+22 01	−96 32	1,500	0.238	32.4	800	694	332	−0.073	0.020	29	54	108
29 Aug	0719:15	52.85	+27 23	−118 58	1,383	0.253	7.9	330	—	—	—	—	26	53	104
29 Aug	2346:58	69.32	+37 41	+5 16	1,158	0.260	3.4	125	126	11.5	—	—	41	90	79
30 Aug	0315:37	72.82	+17 04	−72 32	1,647	0.211	123	800	913	179	0.20	−0.03	37	77	116
30 Aug	2325:57	92.97	+37 20	+5 24	1,215	0.253	21	90	290	6	0.005	−0.025	38	67	73
31 Aug	0913:54	102.79	−28 15	+23 47	736	0.240	56	225	1,090	18	—	—	30	117	149
31 Aug	2304:34	116.63	+37 05	+5 56	1,264	0.248	32	140	24	6	0.026	0.074	47	80	87
1 Sep	2242:46	140.27	+36 50	+6 24	1,320	0.242	24	145	246	2	0.135	0	40	76	76
2 Sep	2220:35	163.90	+36 37	+7 03	1,373	0.236	≥4	180	—	—	0.078	0.004	36	94	67
3 Sep	2157:59	187.52	+36 22	+7 43	1,428	0.230	12	90	—	—	0.014	0.025	52	109	102
4 Sep	2134:57	211.01	+36 08	+8 45	1,470	0.226	<28.5	40	—	—	—	—	45	82	87
5 Sep	0448:20	218.23	+26 37	−113 06	1,701	—	—	~15	—	—	—	—	—	—	—
6 Sep	2047:30	258.22	+32 45	+6 54	1,642	—	—	~100	—	—	—	—	—	—	—

*Serious error.

TABLE 4.2 ARGUS SHOT 2

Date	Time	t_E	Lat N+	Lat S−	Long E+	Long W−	Alt	B	Ch 1 $R-\left(\frac{R_1+R_2}{2}\right)$	Ch 3	Ch 2 Max	Ch 2 Min	Ch 4 Max	Ch 4 Min	Δt $\frac{1}{2}$	Δt $\frac{1}{10}$	$D\frac{1}{2}$ = Thickness
		hrs	deg	min	deg	min	km	Gauss	Difference						sec	sec	km
30 Aug	0317:34	0.0	−40	30	−8	10	290	—	—	—	—	—	—	—	—	—	—
30 Aug	0320:22	0.03	+27	22	−63	04	1,423	0.257	113	180	104	49	−0.002	0	15	43	50
30 Aug	0510:20	1.87	+29	05	−88	54	1,387	0.275	227	8,500	22,000	557	3.0	0.33	18	40	69
30 Aug	0701:43	3.73	+33	41	−111	05	1,277	0.292	71	3,400	4,100	690	0.42	0.08	14	31	58
30 Aug	0819:12	5.02	−30	57	+166	07	2,114	0.221	156	>5,000	10,210	380	—	—	—	—	—
30 Aug	0853:17	5.58	+38	30	−131	36	1,153	0.303	22	~1,290	—	—	—	—	—	—	—
30 Aug	1009:47	6.87	−28	24	+141	15	2,124	0.226	44	4,500	8,000	700	—	—	25	44	106
31 Aug	0116:30	21.98	+39	55	−17	44	1,144	0.273	Noise	>150	—	17	—	—	—	—	—
31 Aug	0259:19	23.68	+27	16	−62	31	1,473	0.251	22	1,300	1,500	300	0.124	0.007	26	53	85
31 Aug	0449:13	25.52	+28	51	−88	29	1,414	0.269	—	265	490	>19	—	—	37	53	140
31 Aug	0606:18	26.80	−35	16	−170	56	2,067	0.218	34	1,250	1,874	~171	—	—	27	62	113
31 Aug	0832:06	29.23	+38	10	−131	25	1,210	0.295	4	250	163	58	0.063	0.017	21	—	88
31 Aug	0948:32	30.52	−28	22	+142	04	2,116	0.226	24	1,326	—	—	—	—	—	—	—
31 Aug	1023:46	31.10	+42	45	−150	25	1,079	0.303	4.8	140	>34	>18	—	—	19	40	79
1 Sep	0055:32	45.63	+40	33	−15	51	1,172	0.271	5.6	230	−62	14	—	—	39	85	70
1 Sep	0237:51	47.33	+27	00	−61	49	1,520	0.245	12	560	371	72	−0.037	0.002	28	58	94
1 Sep	0427:38	49.17	+28	25	−87	57	1,491	0.262	4.3	370	210	77	0.07	0.02	21	56	78
1 Sep	0544:43	50.45	−35	22	−170	02	2,034	0.221	18	~400	1,454	<477	—	—	25	64	103
1 Sep	0618:58	51.02	+33	15	−110	10	1,383	0.279	4.3	180	77	38	—	—	—	—	—
1 Sep	0736:10	52.30	−31	24	+167	27	2,074	0.225	15	870	760	244	—	—	24	52	102
1 Sep	0926:53	54.15	−28	30	+142	54	2,994	0.228	15.1	950	—	—	—	—	—	—	98
2 Sep	0033:59	69.27	+40	46	−14	36	1,273	0.267	—	220	151	>25	—	—	43	102	81
2 Sep	0405:39	72.80	+27	55	−87	25	1,544	0.255	5.9	440	457	63	—	—	16	42	60
2 Sep	0556:59	74.65	+32	43	−109	44	1,440	0.272	5.8	330	316	261	—	—	20	41	82
2 Sep	0904:43	77.78	−28	42	+143	45	2,077	0.230	13	670	287	89	—	—	21	44	89
3 Sep	0011:49	92.90	+40	36	−13	56	1,265	0.261	—	~280	—	—	—	—	38	89	69
3 Sep	0153:45	94.60	+26	45	−60	12	1,616	0.231	12.7	690	—	—	—	—	21	58	69
3 Sep	0343:16	96.42	+27	40	−86	51	1,599	0.249	9.0	530	—	—	0.009	−0.003	18	46	67
3 Sep	0534:35	98.28	+32	19	−109	13	1,497	0.265	1.3	290 (peak)	—	—	—	—	not known	not known	—
3 Sep	2349:15	116.52	+40	26	−13	10	1,318	0.255	3.0	180	—	—	—	—	76	143	130
4 Sep	0131:07	118.22	+26	38	−59	13	1,663	0.229	6.6	360	—	—	0.042	0	53	99	170
4 Sep	0511:45	121.90	+31	51	−108	40	1,554	0.258	1.14	140	—	—	0.080	0	34	65	136
4 Sep	0628:45	123.18	−31	51	+170	01	2,005	0.230	5.8	317	—	—	—	—	—	—	—
4 Sep	0703:18	123.75	+36	46	−129	41	1,435	0.267	−2.6	90	—	—	0.14	0.06	37	89	154
5 Sep	0108:09	141.83	+26	49	−57	41	1,690	0.225	0.6	50	—	—	0.035	0.044	65	111	207
5 Sep	0257:08	143.65	+26	48	−85	18	1,693	0.237	~0.4	~32	—	—	−0.112	0.060	42	76	154
6 Sep	0044:35	165.45	+26	39	−56	31	1,734	0.220	1.0	~130	—	—	—	—	—	—	—
6 Sep	0233:36	167.27	+26	47	−83	58	1,735	0.233	1.9	55	—	—	0.024	0.012	65	131	236
6 Sep	0428:11	169.17	+37	35	−98	05	1,493	0.286	8.5	~30	—	—	—	—	—	—	—

TABLE 4.3 ARGUS SHOT 3

Date	Time	t_E	Lat N+	Lat S−	Long E+	Long W−	Alt	B	Ch 1 $R-\left(\frac{R_1+R_2}{2}\right)$	Ch 3 Difference	Ch 2 Max	Ch 2 Min	Ch 4 Max	Ch 4 Min	Δt $\frac{1}{2}$	Δt $\frac{1}{10}$	$D\frac{1}{2}$ = Thickness
		hrs	deg	min	deg	min	km	Gauss							sec	sec	km
6 Sep	2212:33	0.0	−48	30	−9	40	740	—	—	—	—	—	—	—	—	—	—
6 Sep	2240:16	0.45	+42	11	−5	34	1,398	0.249	963	~70,000	—	—	3.80	1.56	~7.9	~93	105
7 Sep	0021:30	2.13	+28	13	−53	28	1,749	0.220	903	64,000	—	—	—	—	52	75	164
7 Sep	0209:54	3.97	+27	12	−82	12	1,729	—	494	~35,000	—	—	3.39	0.120	21	59	77
7 Sep	0400:58	5.80	+31	23	−104	57	1,685	0.245	394	31,400	—	—	—	—	23	44	92
7 Sep	0516:54	7.07	−33	38	+171	47	1,874	0.245	271	7,400	—	—	—	—	52	80	223
7 Sep	0552:25	7.65	+36	08	−126	24	1,579	0.254	284	7,200	—	—	1.5	0.33	39	79	161
7 Sep	0707:40	8.92	−80	18	+148	16	1,927	0.246	236	6,000	—	—	1.3	0.32	48	92	205
7 Sep	0743:59	9.52	+40	45	−146	18	1,459	0.260	155	6,200	—	—	—	—	34	68	139
7 Sep	2030:45	22.30	+47	00	+36	43	1,262	0.284	10.3	850	—	—	0.31	0.12	54	100	21
7 Sep	2216:20	24.05	+42	31	−3	18	1,433	0.247	106	5,000	—	—	0.25	0.07	74	189	94
7 Sep	2357:18	25.73	+28	22	−51	47	1,781	0.216	231	5,500	—	—	0.86	0.27	70	120	217
8 Sep	0145:25	27.53	+26	54	−80	54	1,811	0.227	151	7,200	—	—	≥0.48	0.18	28	83	101
8 Sep	0336:26	29.38	+30	59	−103	59	1,735	0.240	128	6,500	—	—	0.57	0.05	28	69	111
8 Sep	0452:19	30.65	−34	01	+172	52	1,832	0.249	92	5,624	—	—	—	—	—	—	—
8 Sep	0527:54	31.25	+35	47	−125	22	1,632	0.249	93	4,900	—	—	—	—	29	70	118
8 Sep	0643:03	32.50	−30	40	+149	26	1,888	0.250	58	3,200	—	—	—	—	27	76	116
8 Sep	2151:54	47.65	+42	49	−1	12	1,464	0.244	80	2,300	—	—	0.264	0	63	134	88
8 Sep	2332:33	49.33	+28	15	−50	16	1,808	0.212	54.8	—	—	—	—	—	—	—	—
9 Sep	0120:37	51.13	+26	43	−79	25	1,843	0.223	63	2,300	—	—	0.05	0.03	38	90	138
9 Sep	0427:24	54.23	−34	30	+174	03	1,775	0.255	25	1,400	—	—	—	—	28	79	119
9 Sep	0503:01	54.83	+35	28	−124	09	1,671	0.245	66	2,750	—	—	0	0.013	28	69	113
9 Sep	1941:15	69.47	+46	53	+39	13	1,357	0.274	8.0	520	—	—	—	—	56	91	20
9 Sep	2122:08	71.23	+42	58	+0	47	1,505	0.241	38	1,450	—	—	—	—	76	146	87
10 Sep	0055:29	74.70	+26	29	−77	59	1,875	0.220	52	1,600	—	—	—	—	54	109	194
8 Sep	2006:09	45.88	+47	00	+37	58	1,306	—	8.8	450	—	—	—	—	57	100	17
10 Sep	0210:46	75.97	−39	18	−163	59	1,629	0.262	13.4	650	—	—	—	—	40	91	164
10 Sep	0246:16	76.55	+30	17	−101	34	1,815	0.232	31	1,930	—	—	—	—	29	85	111
10 Sep	0402:09	77.82	−34	53	+175	14	1,729	0.259	16.4	790	—	—	0.11	0.012	36	7	154

TABLE 4.3 CONTINUED

Date	Time	t_E	Lat		Long		Alt	B	Ch 1	Ch 3	Ch 2 Max	Ch 2 Min	Ch 4 Max	Ch 4 Min	$\Delta t_{1/2}$	$\Delta t_{1/10}$	$D_{1/2}$ = Thickness
			N+	S−	E+	W−											
		hrs	deg	min	deg	min	km	Gauss	$R-\left(\frac{R_1+R_2}{2}\right)$	Difference					sec	sec	km
10 Sep	0437:43	78.42	+35	05	−123	08	1,722	0.240	23.8	1,615	—	—	—	—	39	96	160
10 Sep	0552:57	79.67	−31	16	+152	14	1,799	0.259	12.2	625	—	—	—	—	46	86	197
10 Sep	0742:40	81.50	−29	35	+126	35	1,825	0.259	>12	--	—	—	—	—	—	—	—
10 Sep	1915:54	93.05	+46	42	+40	17	1,413	0.268	3.2	275	—	—	—	—	62	102	37
10 Sep	2101:56	94.82	+43	02	+2	41	1,548	0.237	17.8	920	—	—	—	—	71.2	143	X
11 Sep	0029:58	98.28	+26	14	−76	26	1,909	0.216	18.2	1,500	—	—	0	−0.04	38	113	137
11 Sep	0220:41	100.13	+29	58	−100	07	1,855	0.228	16.8	1,130	—	—	—	—	45	123	177
11 Sep	0412:03	101.98	+34	42	−121	49	1,769	0.236	17.2	750	—	—	—	—	42	105	169
11 Sep	1850:10	116.62	+46	30	+41	28	1,467	0.263	≥3.06	—	—	—	—	—	—	—	—
11 Sep	2036:26	118.38	+43	12	+4	58	1,587	0.234	10.9	550	—	—	—	—	75	164	86
11 Sep	2217:45	120.08	+30	31	−42	20	1,871	0.205	16.6	960	—	—	—	—	56	111	166
12 Sep	0003:45	121.85	+25	23	−75	23	1,951	0.210	10.4	900	—	—	—	—	?	?	—
12 Sep	0154:40	123.70	+29	31	−98	39	1,895	0.224	17.6	720	—	—	—	—	35	79	137
12 Sep	1824:04	140.18	+46	22	+42	46	1,514	0.259	5.4	—	—	—	—	—	—	—	—
12 Sep	2010:32	141.97	+43	18	+7	12	1,620	0.231	8.0	550	—	—	—	—	73	147	84
12 Sep	2152:02	143.65	+31	15	−39	34	1,887	0.203	20.3	1,000	—	—	—	—	71	147	198
13 Sep	0624:52	152.20	−30	14	+131	38	1,696	0.274	2.42	105	—	—	—	—	32	77	132
14 Sep	0101:36	170.82	+28	42	−95	18	1,955	0.218	13.3	800	—	—	—	—	37	110	144
14 Sep	0252:53	172.67	+33	09	−117	47	1,895	0.224	8.6	600	—	—	—	—	37	90	152
15 Sep	0034:36	194.37	+28	23	−93	40	1,986	0.215	16.4	510	—	—	—	—	45	96	175
15 Sep	0225:46	191.22	+32	45	−116	09	1,931	0.221	11.8	620	—	—	—	—	39	115	159
16 Sep	0158:21	219.75	+32	17	−144	28	1,782	—	7.8	500	—	—	—	—	46	93	183
16 Sep	2339:20	241.43	+27	10	−90	06	2,025	0.209	11.1	660	—	—	—	—	42	109	160
17 Sep	0130:25	243.28	+31	38	−112	43	1,985	0.216	5.5	450	—	—	—	—	42	100	170
17 Sep	1939:10	261.43	+36	04	−22	01	1,947	0.197	10.9	500	—	—	—	—	95	151	220
17 Sep	2311:12	264.97	+26	56	−87	55	2,043	0.208	2.8	610	—	—	—	—	40	94	153
18 Sep	0102:17	266.82	+31	25	−110	33	2,008	0.214	0	390	—	—	—	—	56	112	227
19 Sep	2026:01	310.22	+27	31	−54	44	2,061	0.195	—	~300	—	—	—	—	—	—	—

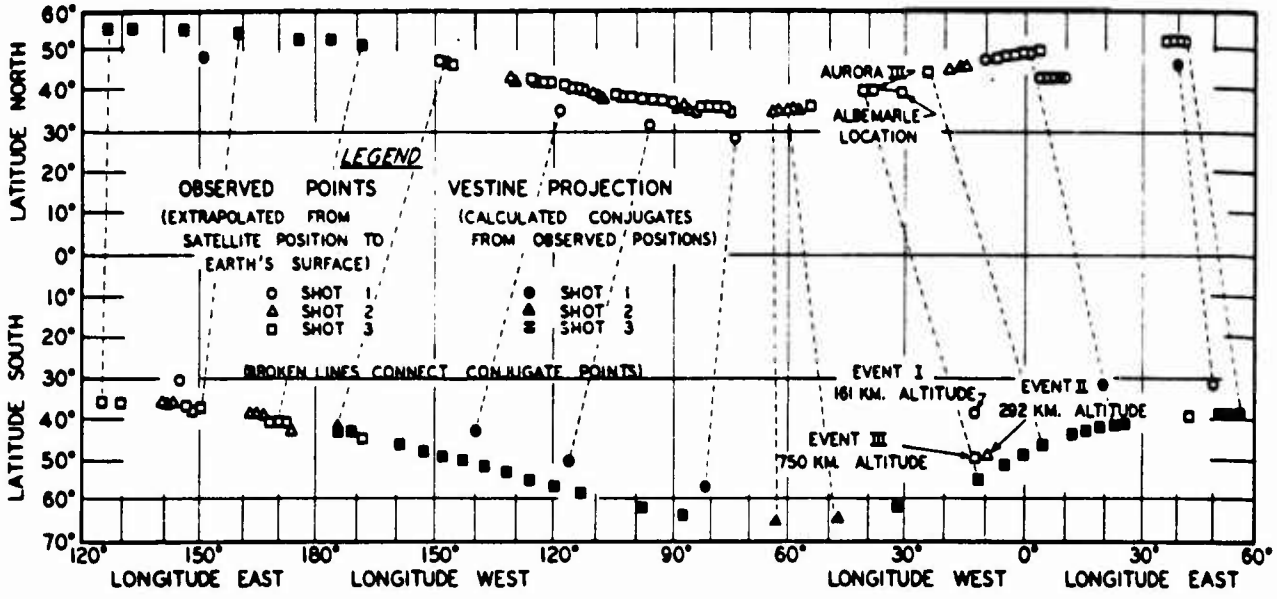

Figure 4.1 Extrapolations of Argus observations along lines of force to the surface of the earth.

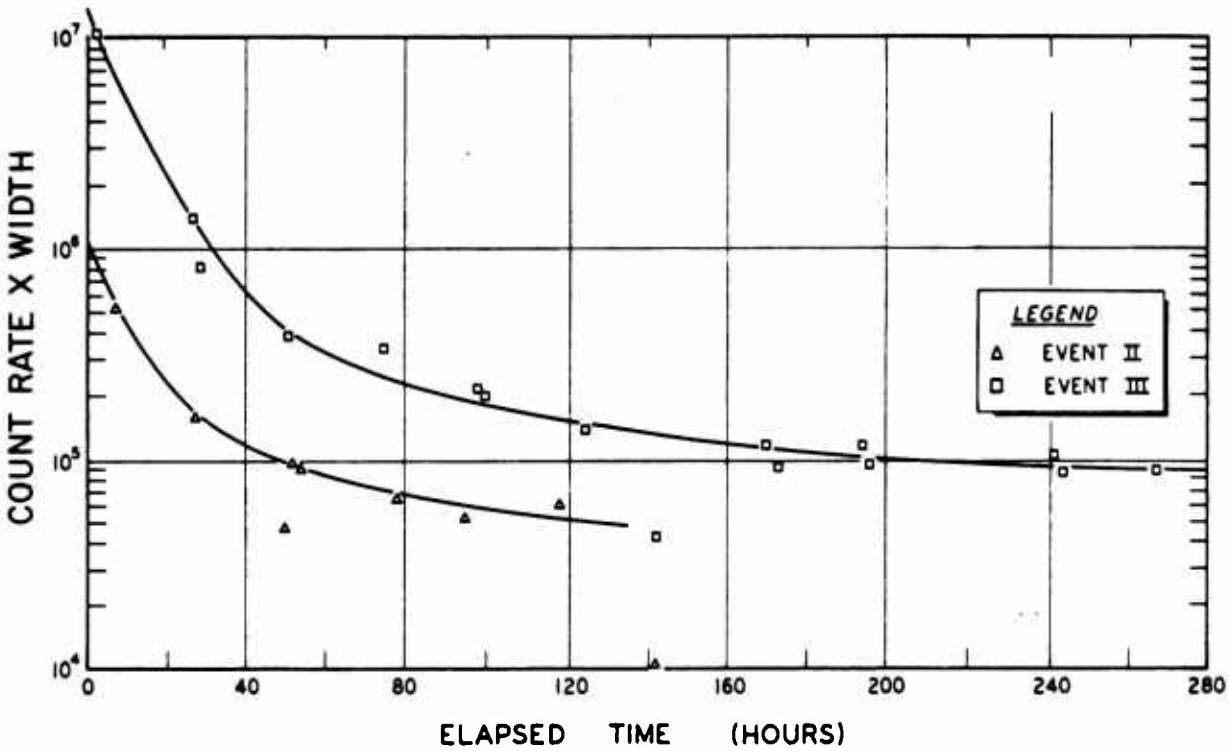

Figure 4.2 Product of count rate (Ch. 3) and width versus elapsed time, Shots 2 and 3. B = 210 to 230 milligauss.

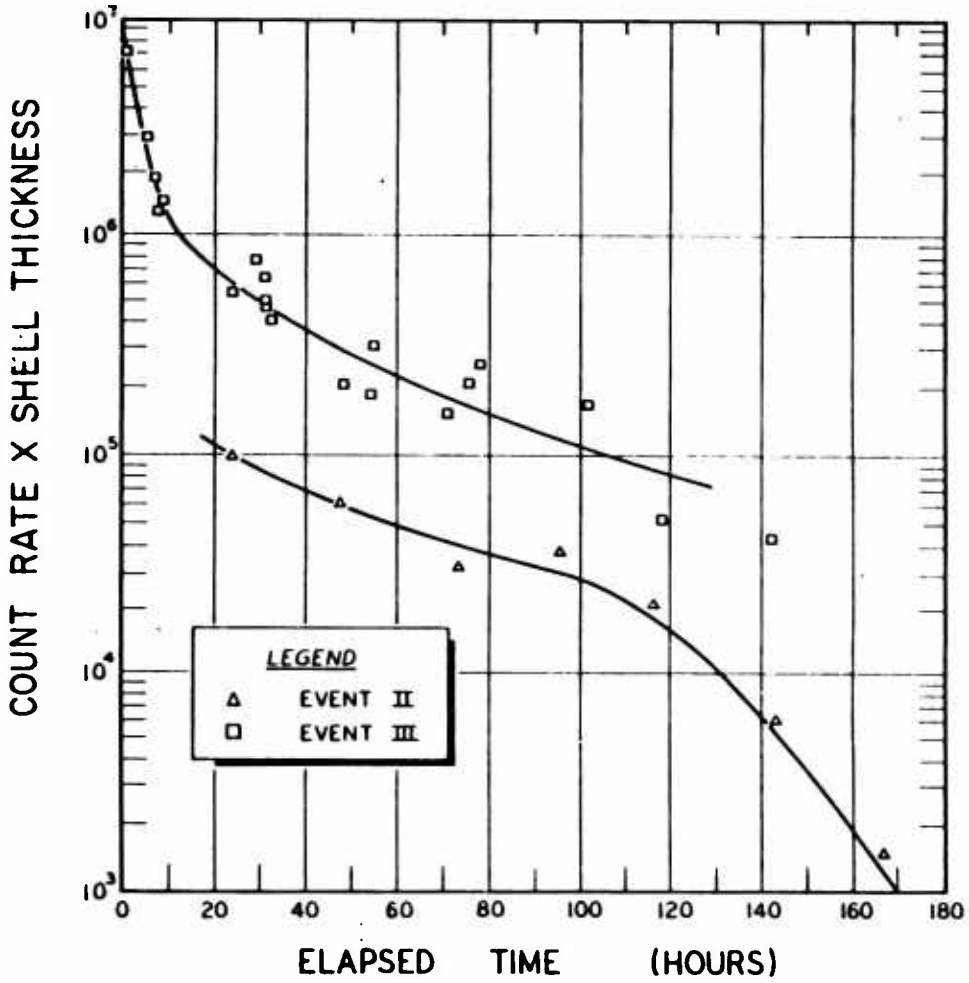

Figure 4.3 Product of count rate and shell thickness versus elapsed time, Shots 2 and 3. B = 230 to 255 milligauss.

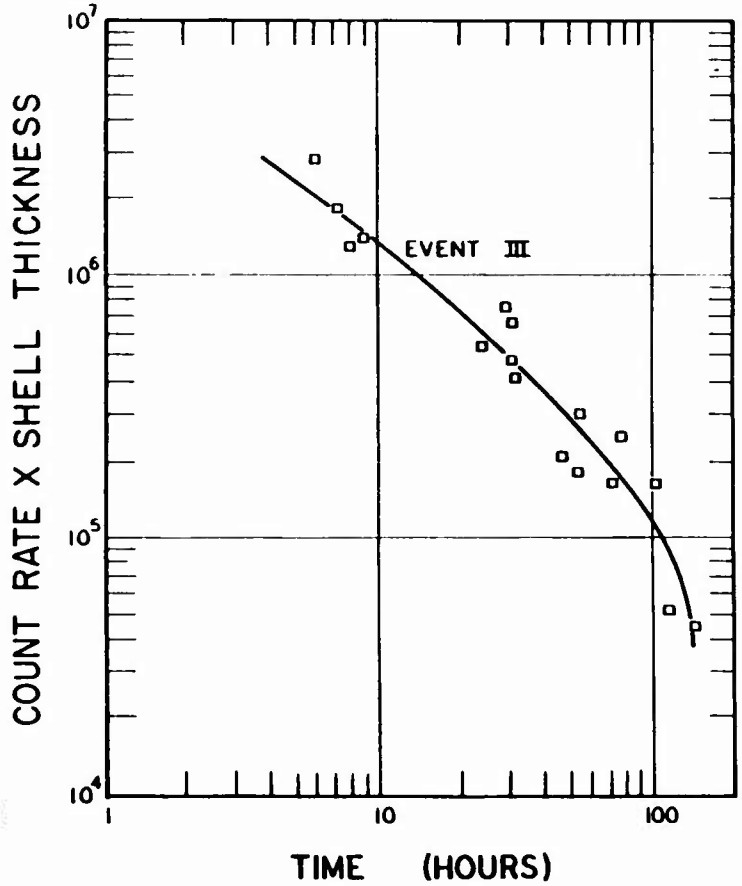

Figure 4.4 Product of count rate and shell thickness versus elapsed time, Shot 3. B = 230 to 255 milligauss.

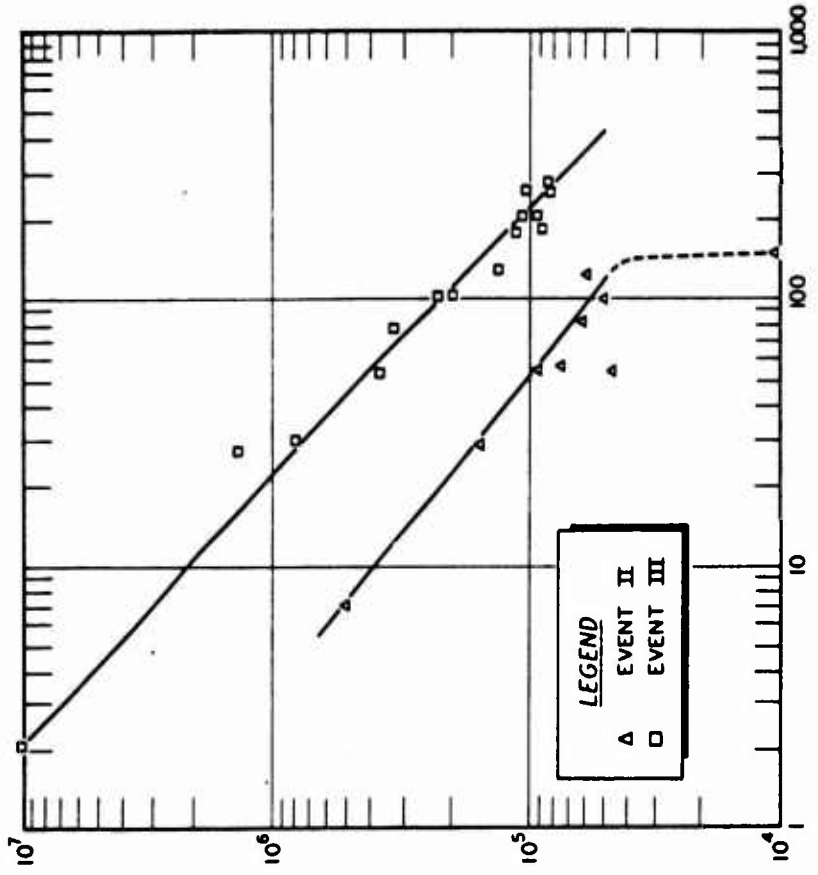

Figure 4.6 Product of count rate and shell thickness versus elapsed time, Shots 2 and 3. B = 210 to 230 milligauss.

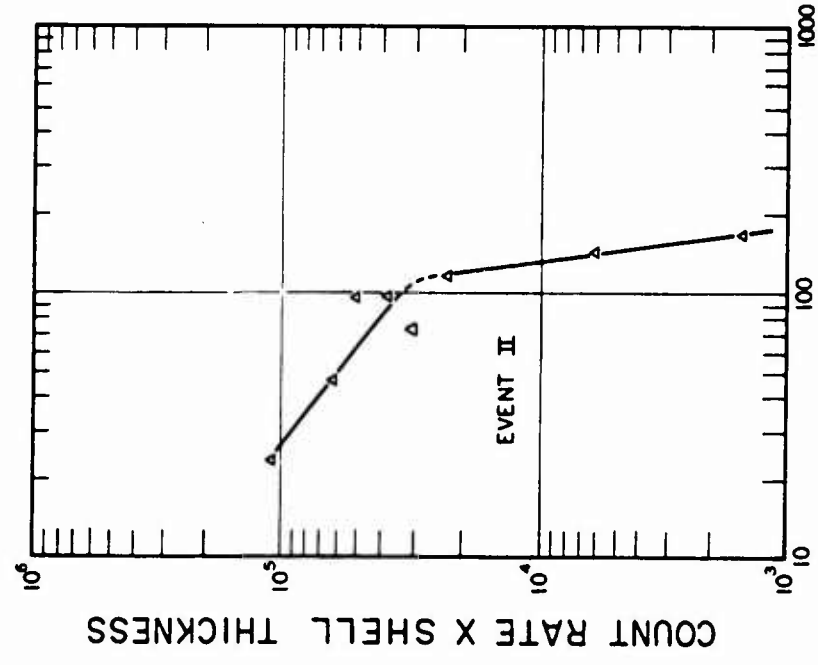

Figure 4.5 Product of count rate and shell thickness versus elapsed time, Shot 2. B = 230 to 255 milligauss.

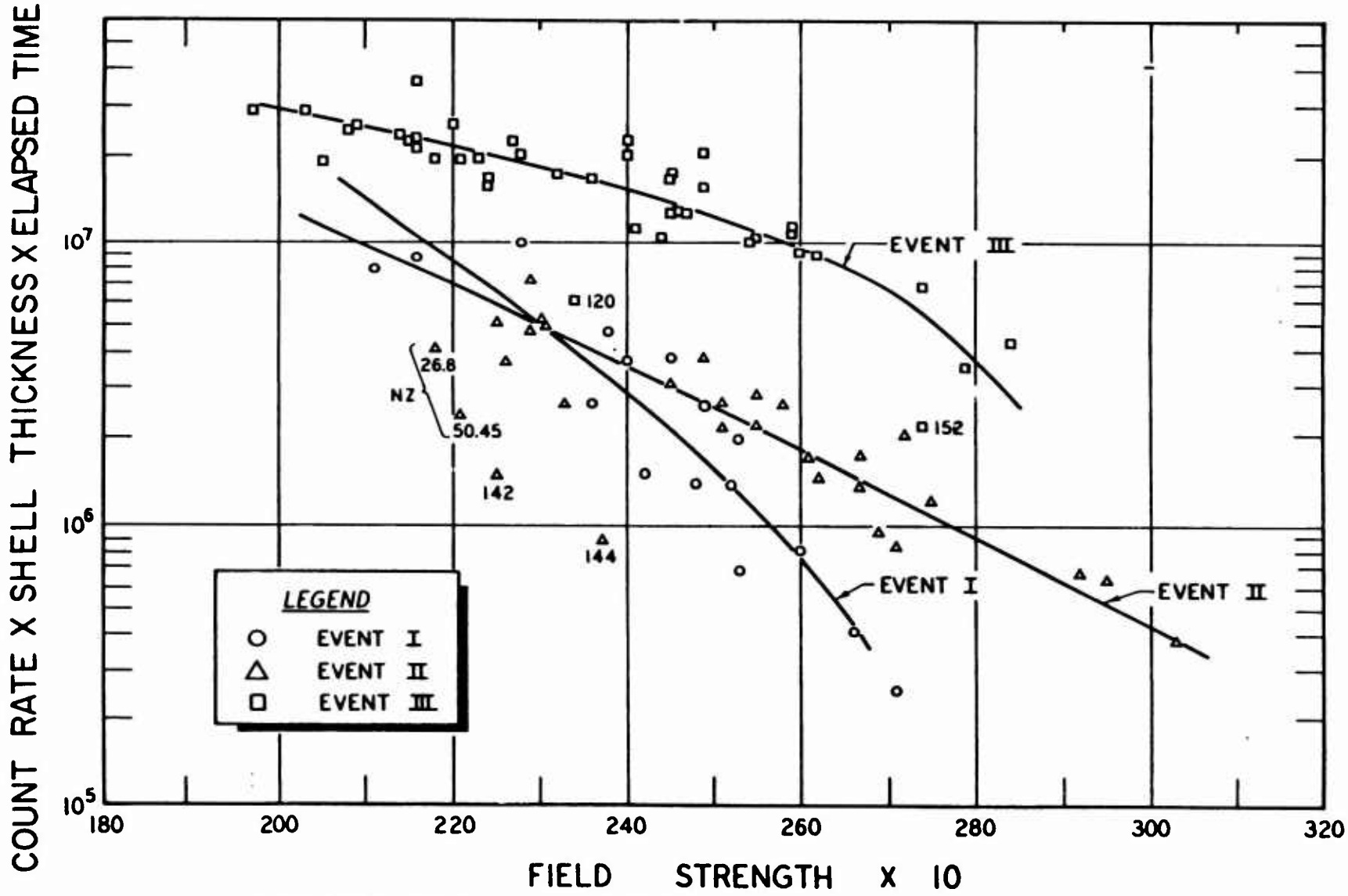

Figure 4.7 Product of count rate, shell thickness and elapsed time versus field strength, Shots 1, 2 and 3.

being confined to a volume near the burst point. Particles were still being reflected at the greatest altitudes reached by the satellite. The recognition of this qualitative observation of mirror point distribution was one of the results of the conference. It made impossible the exact calculation of the total number of electrons trapped.

Other important topics considered by the data analysis working group were the use of the "integral invariant" (Reference 15) to further characterize an Argus shell in the irregular magnetic field of the earth and the problem of the angular distribution of the radiation. The final analysis of these and many other topics remained after the conference as further "homework" for the members.

Subsequent to the Argus working session at Livermore (February 1959), further analyses of the data were made by the various participating groups. These studies include magnetic-field plotting, by a computer program under the direction of E. H. Vestine; satellite roll and tumble motion study, by R. J. Naumann; and further investigation of the nature of the geomagnetically-trapped particles (natural effect) indicating an energetic proton component, by J. A. Van Allen.

A final and up-to-date summary of the Argus experiments was presented in an unclassified meeting at the National Academy of Sciences in Washington, D. C., 29 April 1959. Papers presented at this meeting include References 10, 13, 16, and 17.

The conference at Livermore (4 through 17 February 1959), the Argus meeting at the National Academy of Sciences (29 April 1959), the AGARD meeting at NATO Headquarters in Paris (26 through 28 May 1959) indicate a continuing activity and interest in the Argus experiments. Although several important and interesting conclusions have been drawn, considerable detailed evaluation of the data needs to be done. Among the several aspects of the satellite experiment that merit further attention are a more detailed study of the energy and directional distribution of the Christofilos radiation, the derivation of an injection model, and the comparison of recent theoretical studies with the experimental data.

Appendix A
RADIATION MEASUREMENTS

The existence of a high intensity of corpuscular radiation in the vicinity of the earth was discovered by apparatus carried by Satellite 1958 Alpha, launched at 0348 U.T. on 1 February 1958. The discovery was confirmed and knowledge of the distribution of radiation was greatly extended with more elaborate equipment in Satellite 1958 Gamma, launched at 1738 U.T. on 26 March 1958. A preliminary account of this work has been given (Reference 2).

A full report will be made as soon as comprehensive reduction of the observation has been completed.

The data from 1958 Alpha and 1958 Gamma showed that:

1. The intensity of radiation up to some 700 km altitude was in good accord with that to be expected for cosmic rays only, when proper account was taken of the increasing opening angles of geomagnetically allowed cones with increasing altitude and of the concurrent shrinking of the solid angle subtended at the observing point by the solid earth.

2. Above some 1,000 km (this transition altitude being longitude and latitude dependent) the intensity of radiation increased very rapidly with increasing altitude, in a way totally inconsistent with cosmic ray expectations.

3. At the higher altitudes (~2,000 km) the true counting rate of a Geiger tube with a geometric factor[2] $G_0 = 17.4\ cm^2$ and with total shielding of about 1.5 g/cm^2 of stainless steel (extrapolated range for electrons of energy 3 Mev, or range for protons of 30 Mev) exceeded 25,000 counts/sec. Hence, the omnidirectional intensity exceeded 1,700 $cm^{-2}\ sec^{-1}$ if the radiation consisted wholly of penetrating charged particles ($\epsilon = 0.85$); or it exceeded some $10^6\ cm^{-2}\ sec^{-1}$ if the radiation consisted wholly of electrons whose range was less than 1.5 g/cm^2 ($E < 3$ Mev) but whose bremsstrahlung was sufficiently energetic to penetrate the absorber with little attenuation ($E \gtrsim 50$ kev).

4. Since the atmospheric path length between altitudes of, for example, 1,000 km and 700 km was negligible compared to the effective wall thickness of the counter, it was evident that the primary radiation was restrained from reaching lower altitudes by the earth's magnetic field and must, therefore, consist of charged particles.

It was proposed in Reference 19 that the radiation was corpuscular in nature, was presumably trapped in Stoermer-Treim (Reference 20) lunes about the earth, and was intimately related to that responsible for aurora. On the basis of these tentative beliefs, it was thought likely that the observed trapped radiation had originally come from the sun in the form of ionized gas, which may or may not have been subjected to acceleration in the outer reaches of the earth's magnetic field, in some such manner as discussed by Chapman and Ferraro.

The existence of such radiation had been presaged by earlier rocket observations in the northern and southern auroral zones (References 21 and 22). Indeed, further specific experiments on the arriving auroral radiations have been planned (Reference 23) for satellites in high inclination orbits; but it had not been anticipated that the auroral soft radiation would be encountered at such low altitudes and low latitudes as was found with 1958 Alpha and 1958 Gamma to be the case.

A.1 ORBIT OF EXPLORER IV

In order to obtain wide geographical coverage, we requested an orbit as steeply inclined to the geographical equator as feasible. The Army Ballistic Missile Agency (ABMA) and the Patrick Air Force Base agreed to shoot on a northeasterly bearing from Cape Canaveral, Florida, so as to produce an orbital inclination of about 51 degrees. This was accomplished. An inclination of 90 degrees would, of course, have been desirable, but this was judged unwise from a range safety point of view. The inclination of 51 degrees permitted a great extension of knowledge over what would have been possible with the inclinations of 34 degrees of previous U.S. satellites.

The satellite was tracked by radio interferometric methods by ten Minitrack stations, with optical methods by stations of the Smithsonian Institution Astrophysical

---

[1] This appendix consists of excerpts from State University of Iowa Report 58-10, "Radiation Observations with Satellite 1958 Epsilon."

[2] The omnidirectional geometric factor G_0 is defined so that the omnidirectional intensity of isotropic radiation is given by $J_0 = R/\epsilon G_0$, where J_0 is the flux of particles from all directions through a sphere of unit cross section (J_0 measured in $cm^{-2}\ sec^{-1}$); R is the true counting rate of the detector and ϵ is its efficiency for the radiation in question. For a cylindrical counter of effective length l and effective diameter a, $G_0 = 0.25\ \pi\ a\ l\ (1 + a/2\ l)$. See Reference 18.

Observatory's (SAO) network and by other stations and various methods. A smoothed orbit was computed by the Vanguard Computing Center and jointly by the SAO and ABMA groups. Altitudes above the international geoid and geographic latitude and longitude were tabulated at each minute of real time. Precision of the presently available ephemeris is typically such as to locate the satellite with high probability within a sphere of radius 10 km. Table A.1 lists two typical sequences of entries. An overall view of the history of the orbit is provided by Table A.2 and Figure A.1.

TABLE A.1 SAMPLE OF EPHEMERIS OF 1958 EPSILON

(Courtesy Army Ballistic Missile Agency and Smithsonian Institution Astrophysical Observatory.)

Day	U.T.	Longitude East	Latitude	Height
		deg		km
2 August 1958	0015	292.25	−28.10	2,054.8
	0016	294.19	−29.91	2,080.9
	0017	296.19	−31.67	2,104.7
	0018	298.28	−33.39	2,126.1
	0118	110.52	+38.15	267.9
	0119	114.78	+40.56	278.2
	0120	119.38	+42.78	272.5
	0121	124.31	+44.79	270.9
	0122	129.61	+46.55	273.3
	0123	135.23	+48.02	279.7
		etc.		

In addition, ABMA has computed recently an ephemeris in terms of eccentric geomagnetic coordinates.

TABLE A.2 PRINCIPAL ORBITAL PARAMETERS OF 1958 EPSILON

(Courtesy Vanguard Computing Center.)

Mean Date	Altitude of Apogee	Altitude of Perigee	Period
	km	km	min
28 Jul 58	2,210	262	110.2
1 Aug 58	2,203	257	110.1
5 Aug 58	2,194	257	110.0
9 Aug 58	2,184	256	109.9
13 Aug 58	2,172	256	109.7
17 Aug 58	2,161	258	109.6
21 Aug 58	2,150	257	109.5
25 Aug 58	2,140	258	109.4
29 Aug 58	2,127	258	109.3
2 Sep 58	2,115	258	109.1
6 Sep 58	2,100	262	109.0
10 Sep 58	2,084	267	108.9
14 Sep 58	2,079	262	108.8
18 Sep 58	2,070	261	108.7

A.2 OBSERVATIONS

A.2.1 Remarks Concerning Data. For the entire operating lifetime of 1958 Epsilon, we have now received at the SUI data center some 3,600 recorded passes. The original records are made on magnetic tape with coded absolute time signals. The mixed-audio signal from the five subcarriers is played back through a set of five bandpass filters and frequency discriminators to a multichannel, pen-and-ink Offner oscillograph. Several hundred of the records have been surveyed thus far and detailed reading and tabulation of the data from a substantial number of selected records have been accomplished. A typical pass yields workable data over a several minute period. The rf radiation pattern of the satellite is that of a linear antenna fed asymmetrically. Hence, nulls in the signal strength occur periodically as the satellite tumbles. The angular motion was originally a pure rotation about the longitudinal axis of the cylindrical satellite. But by early August the motion had become a propellor-like

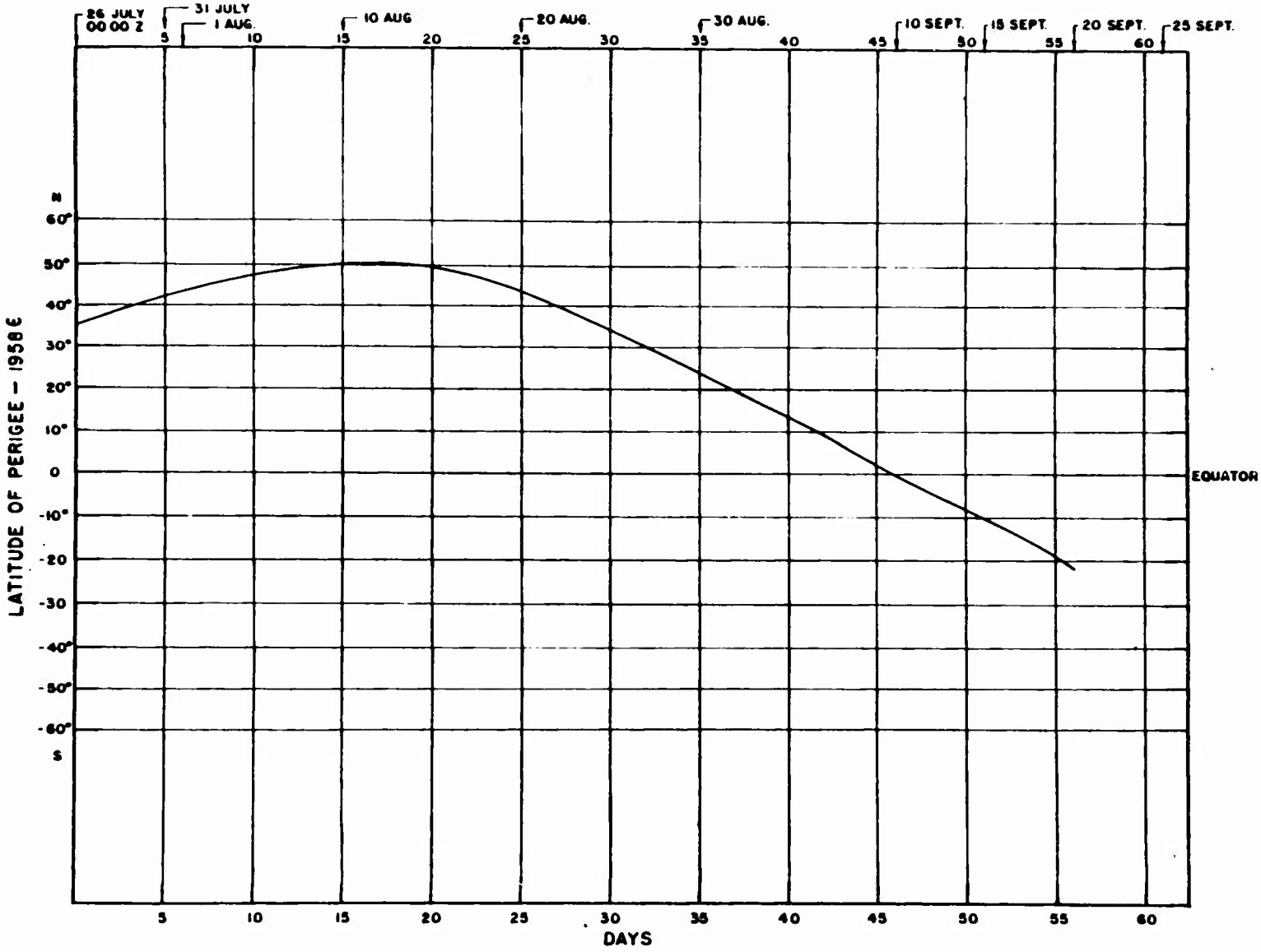

Figure A.1 Latitude of perigee versus time.

tumbling motion with a period of about 7 seconds, and a slow rotation about the longitudinal axis (period over 1 minute).

A.2.2 Sample Sets of Data. In Table A.3 are tabulated a number of sets of data for illustrative purposes.

A.2.3 Altitude, Latitude and Longitude Dependence of Intensity. In geographical longitude 80 degrees ± 20 degrees west and low latitudes, the intensity as measured by all detectors increases slowly up to some 800 to 1,000 km, then increases very rapidly to the highest altitude reached (2,200 km). The increase in the region 1,000 to 2,200 km is by approximately a factor of 0.02/km.

more full and detailed knowledge of the distribution and nature of the radiation.

TABLE A.3 SOME SAMPLE OBSERVATIONS WITH 1958 EPSILON

Telemetry Station	U.T.	Detector D Channel 1 (True Rate)	Detector A * Channel 2 or 5 (True Rate)	Detector C Channel 3 (True Rate)	Detector B † Channel 4		Longitude East	Latitude	Altitude
		counts/sec	counts/sec	counts/sec	ergs/sec-cm²-steradian		deg	deg	km
Woomera	1047, 5 Aug	10.4	310	470	0.2 Aver		130.2	−36.4	2,080
	0839, 6 Aug	39.4	390 Aver 60 Min	74	0.45 Min 0.9 Max		143.0	−24.9	1,841
	1321, 12 Aug	6.2	580	62	—		143.0	−46.0	2,142
Antofagasta	0550, 14 Aug	—	14,500	10,500	5 Min 20 Max		290.9	−18.4	1,685
	2353, 3 Aug	—	30,000 Min 110,000 Max	11,400	21 Min 76 Max		287.0	−26.4	1,959
Patrick Air Force Base	1131, 6 Aug	1.9	2.2	—	—		281.4	+26.6	474
	1517, 15 Aug	1.1	1.5	—	—		259.5	+60.0	277
	2220, 30 Jul	1.2	40	—	—		280.8	+25.9	1,035
Singapore	2316, 1 Aug	0.8	1.3	—	—		104.0	+3.5	676
Blossom Point	0940, 15 Aug	2.8	40 Aver 130 Max 20 Min	38	—		295.6	+43.5	458
Santiago	0346, 14 Aug	670	2,900 Min 30,000 Max	1,430	1.7 Min 13 Max		286.9	−43.4	2,133
	0213, 2 Aug	910	8,000 Aver	1,660	4 Min 20 Max		282.1	−41.3	2,210
Antigua	2208, 1 Aug	1,280	4,800	1,420	2.2 Min 6.5 Max		291.2	+8.9	1,328
					Min	Max			
Huntsville	0631, 19 Aug	—	12,100	4,100	0.9	5	275.0	+1.6	1,492
	0632	1,220	11,700	2,020	0.7	3.5	276.6	+3.9	1,442
	0633	950	2,700	980	0.55	2.4	278.4	+6.3	1,390
	0634	470	1,230	466	0.37	0.8	280.2	+8.7	1,337
	0635	180	630	180	0.23	0.35	282.0	+11.1	1,284
	0636	51	220	48	0.14	—	283.9	+13.6	1,230
	0637	17	74	—	0.1	—	285.9	+16.0	1,176
	0638	3.3	76	—		—	288.0	+18.5	1,122
	0639	2.2	115	—		—	290.1	+21.0	1,067
	0640	3.8	68	—		—	292.4	+23.5	1,013
	0641	2.5	44	—		—	294.8	+26.0	959
Quito	0046, 28 Jul	—	14,500	5,600	20 Aver		278.9	+2.5	1,694
	0048, 28 Jul	—	45,000	9,900	60 Aver		282.0	−1.9	1,783

* Where not otherwise indicated, the rates of Detector A are apparent average values over a tumbling cycle. Due to saturating characteristics of the detector, these apparent averages are much too low when the maximum true rate exceeds 5,000/sec. True rates are available from more detailed data reduction.

† The directional energy fluxes of Detector B are as attributed to a geometrical factor of 0.0235 cm² steradian.

It is seen that, in a broad way, the earlier results of 1958 Alpha and 1958 Gamma have been amply confirmed with a diversity of detectors of quite different properties. The detectors of 1958 Epsilon, designed with the knowledge of the earlier results, have provided a vastly

In order to gain a more-comprehensive idea of the geographical distribution of intensity, the counting rate of each detector has been written on a large chart representing a meridian section through the earth and its atmosphere. A different chart is used for each of several longitudinal sectors of the earth. The numbers on each chart progressively produce a two-dimensional array, as the position of perigee moves in latitude and as the corresponding data are reduced and plotted. We then sketch in contours of approximately constant counting rate. Four such charts are shown in Figures A.2, A.3, A.4, and A.5. It is seen that all contours at 80 degrees ± 20 degrees west have approximate symmetry about a plane through latitude 14 degrees south. It is of special interest that a given contour lies at some 800 to 1,000 km higher altitude in the southern hemisphere at 140 degrees ± 20 degrees east than it does in the northern hemisphere at 80 degrees ± 20 degrees west. Indeed, the corresponding contours on the two charts become acceptably complementary if such an altitude displacement is made. This fact provides additional support for the belief in magnetic trapping since the altitude displacement is quite suggestive of the eccentricity of the magnetic axis of the earth. Also, 14 degrees south is near the location of the magnetic dip equator at 80 degrees west.

It is particularly noteworthy that the contours of constant intensity bend outward from the earth at high latitude, both north and south. The outer latitude limits of the greater radiation belt have a striking similarity to the latitudes of the auroral zones. The possible significance of this feature is discussed later.

In Figure A.6 is given a speculative extension of the observed contours under the surmise that contours of constant intensity have a shape at great altitudes resembling that of magnetic lines of force. A partial and tentative confirmation of this pattern has been obtained recently by our radiation measurements in the Pioneer I flight of 11 October 1958.

A.2.4 Anisotropy of Radiation. The axes of Detectors A and B (Section 3) are at right angles to the longitudinal axis of the satellite. Hence, as the satellite rolls and tumbles, these two detectors sweep out a complex motion on a unit sphere centered on the satellite. A strong modulation of the counting rate of Detectors A and B is observed at all points in space, where their rates are sufficiently high to permit such an analysis. The situation has been particularly clear after the angular motion of the satellite approached pure tumbling. The observed ratio of maximum to minimum intensities on Detectors A and B ranges from 2 to 50 in a preliminary survey. And, of course, it must be noted that some particles may be sufficiently penetrating to enter the detectors from directions outside of their nominal acceptance cones. The maxima from A and from B are in phase, as are their minima. Since A and B look in diametrically opposite directions, it appears that the angular distribution of the radiation is disk-like in nature. There were no on-board devices for measuring absolute orientation. But we have hope that study of the pattern of nulls in the rf signal may provide some knowledge of the absolute orientation of the disk. For example, a pass nearly directly over the excellent receiving station at Huntsville, Alabama, showed that maxima of intensity were nearly coincident with the rf nulls. Hence, the disk was horizontal to within ± 30 degrees. This is consistent with its perpendicularity to the local magnetic field vector.

Figure A.7 gives an illuminating example of the nature of the anisotropy. The interpretation of Figure A.7 on the assumption that the disk-like character of the angular distribution of the radiation is as follows. When the longitudinal axis of the satellite was perpendicular to the plane of the disk, the axis of Detector B lay in the plane of the disk; hence, there was little or no modulation due to roll of the satellite about its longitudinal axis. When the longitudinal axis of the satellite lay in or nearly in the plane of the disk, there was the greatest amplitude modulation of the intensity due to roll — with the maximum values being equal to the constant, unmodulated value of the preceding situation. In the latter situation the axis of Detector B cuts through the disk of radiation twice per roll cycle.

When coupled with the further fact that the maxima of response of Detectors A and B are in phase in time, examples such as that shown in Figure A.7 appear to establish conclusively the disk-like character of the angular distribution. We have been unable to visualize any other time-stationary situation which will account for the observations. The flatness of the disk is a function of the latitude and altitude. A fuller study of this matter is in progress.

It already appears safe to conclude that the angular distribution of the radiation provides an important substantiation of our belief in magnetic trapping. See Figure A.8 (not to scale) for a schematic view of the way in which magnetic trapping in the earth's field gives rise to a disk-like angular distribution at altitudes near the mirror altitude.

A.2.5 Temporal Fluctuations. A number of important geophysical fluctuations occurred during the observing periods of 1958 Alpha, 1958 Gamma and 1958 Epsilon. Of special interest is the great auroral event of 10 - 11 February 1958. The 1958 Alpha data during February are now being studied in detail. Inasmuch as the intensity is a rapidly changing function of altitude and is also a function of latitude and longitude, any apparent temporal fluctuations must be critically examined to assure that proper account has been taken of spatial dependences.

Aono and Kawakami (Reference 24) have examined some 1958 Alpha observations made in Japan in early February and have suggested that temporal variations in the intensity at the lower fringe of the radiation belt were associated with the value of planetary magnetic index K_p, and with the ionospheric state as measured by the $f_0 F_2$ value. If these conclusions are substantiated by more comprehensive studies, it may be poss-

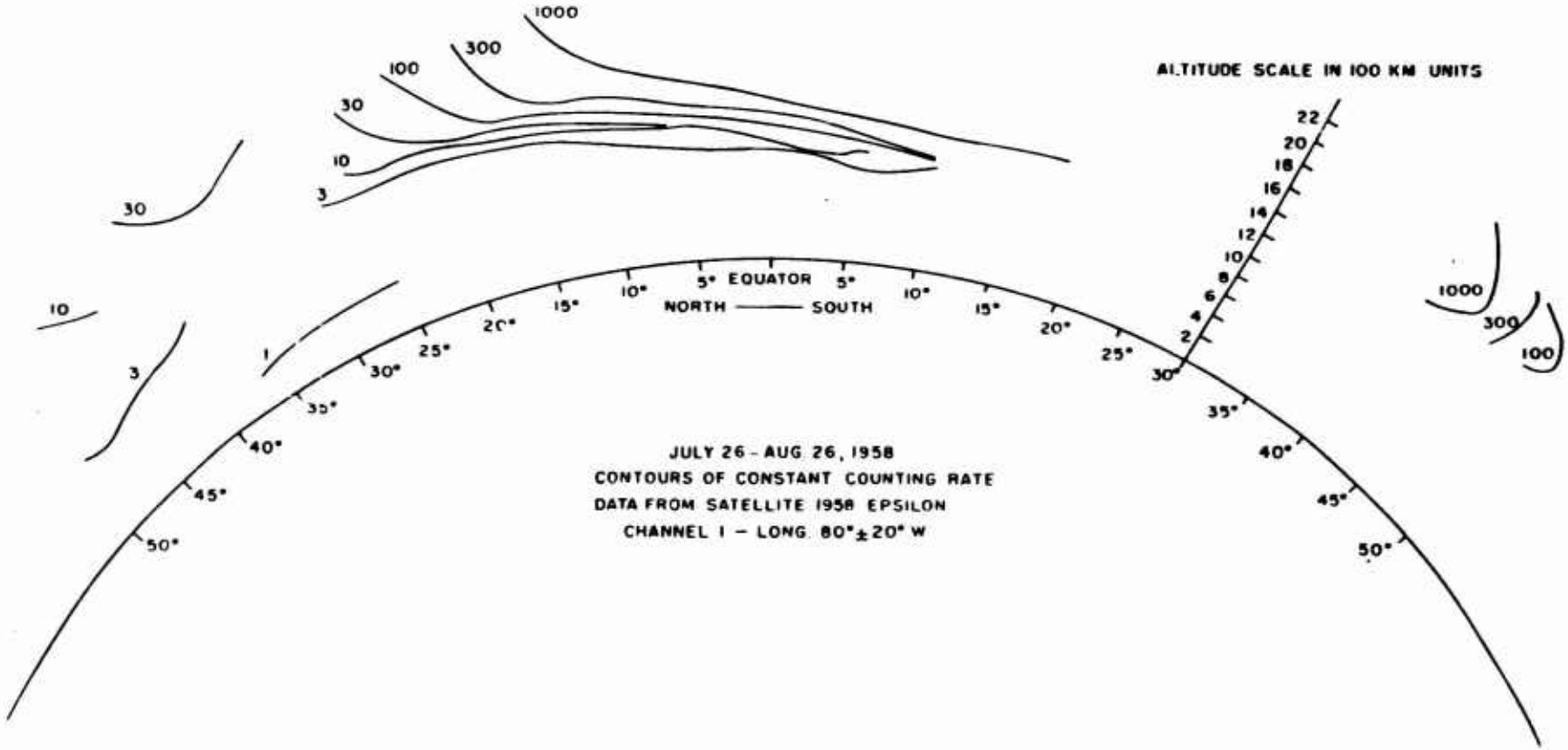

Figure A.2 Contours of constant counting rate data from satellite 1958 Epsilon, July 26 to August 26, 1958. Channel 1, long. 80° ± 20° W.

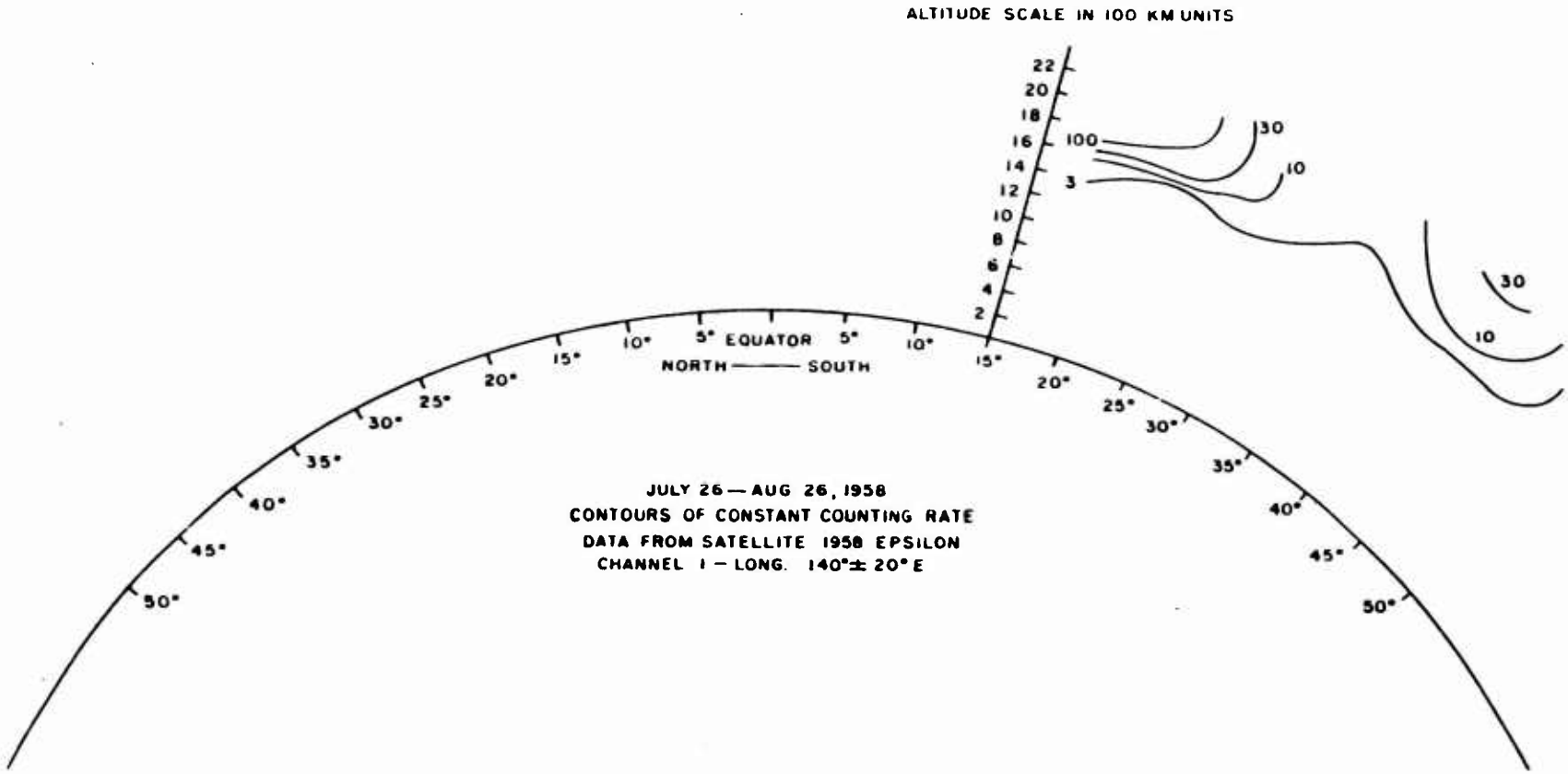

Figure A.3 Contours of constant counting rate data from satellite 1958 Epsilon, July 26 to August 26, 1958. Channel 1, long. 140° ± 20° E.

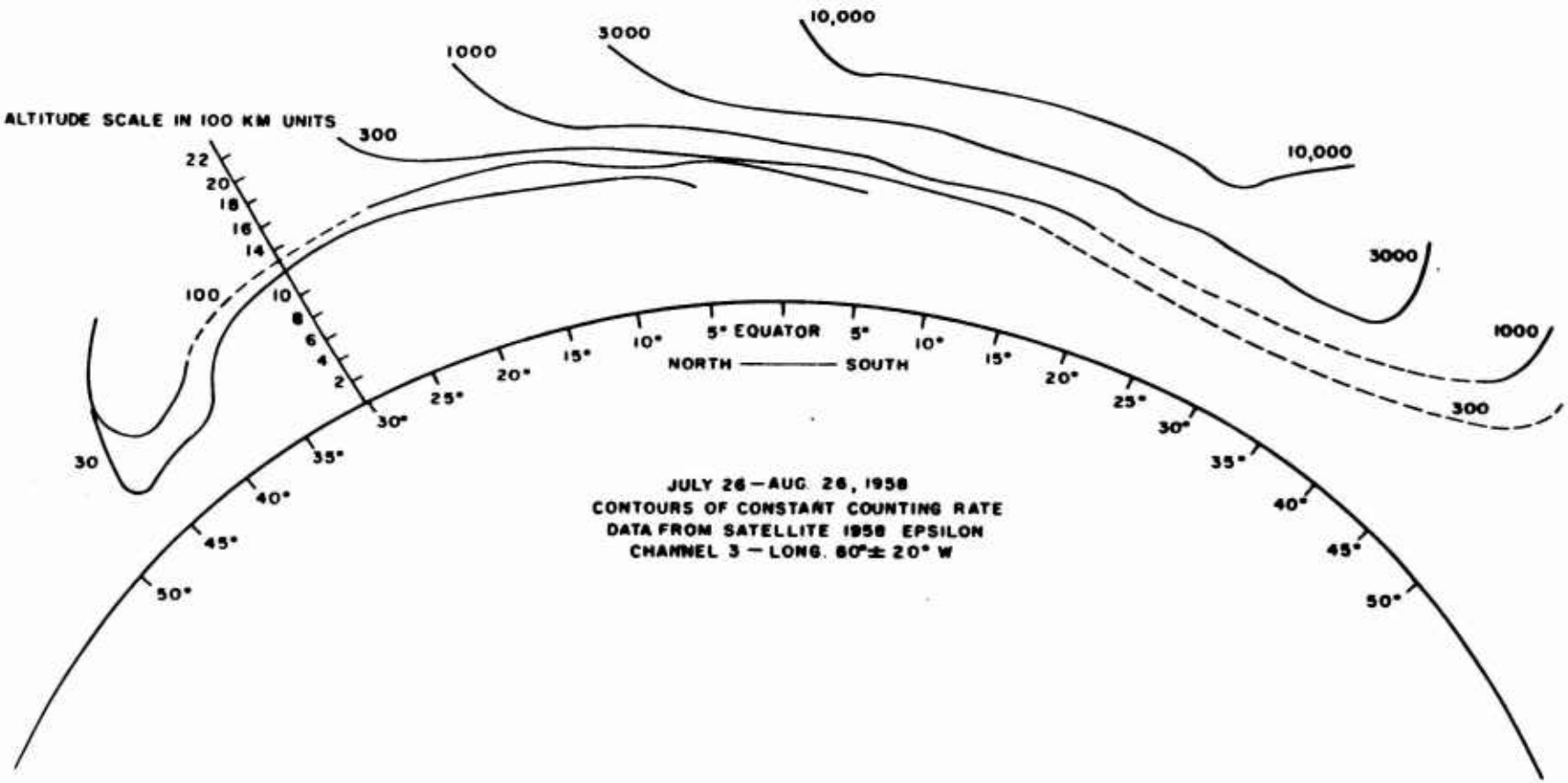

Figure A.4 Contours of constant counting rate data from satellite 1958 Epsilon, July 26 to August 26, 1958. Channel 3, long. 80° ± 20° W.

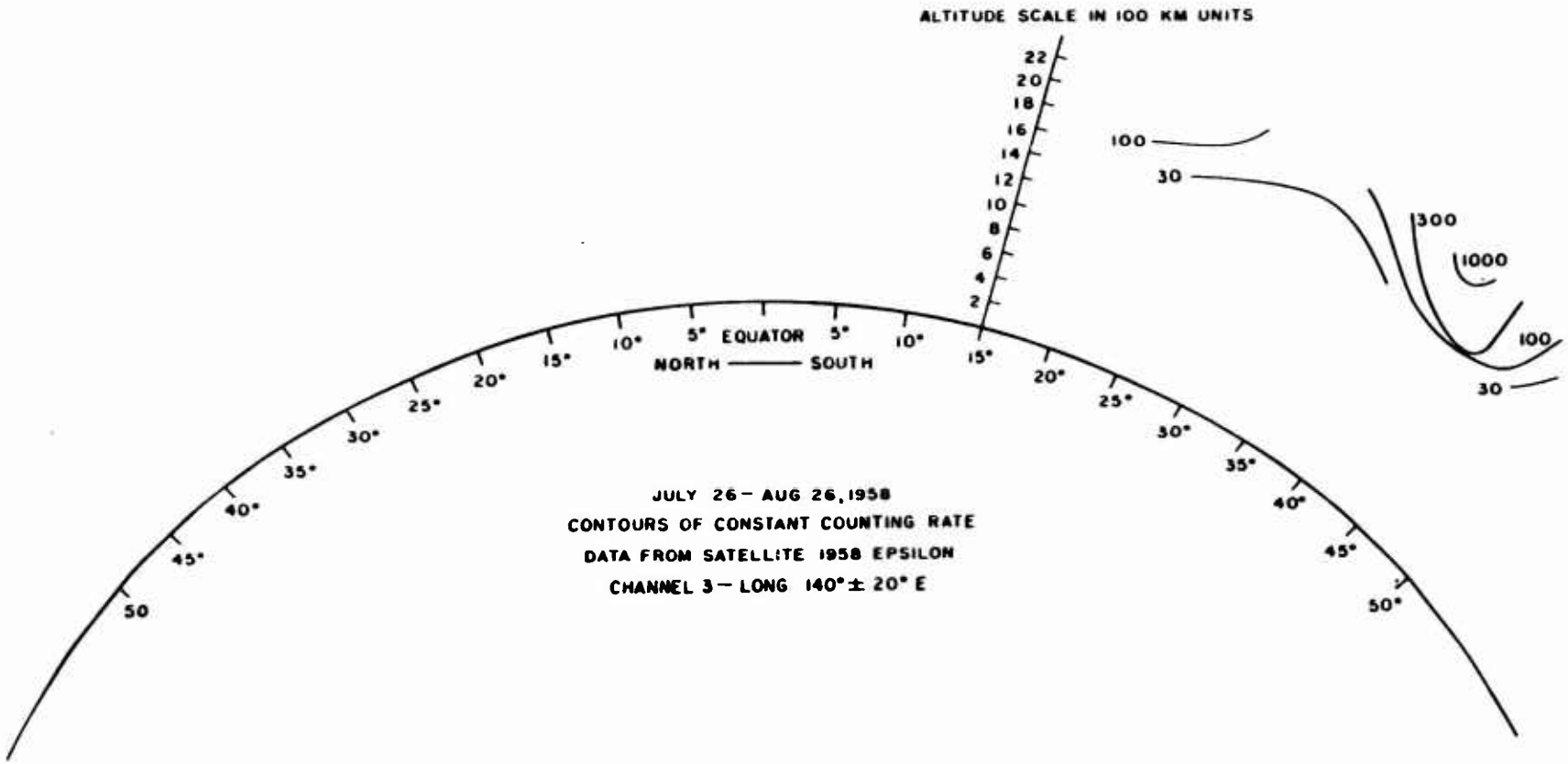

Figure A.5 Contours of constant counting rate data from satellite 1958 Epsilon, July 26 to August 26, 1958. Channel 3, long. 140° ± 20° E.

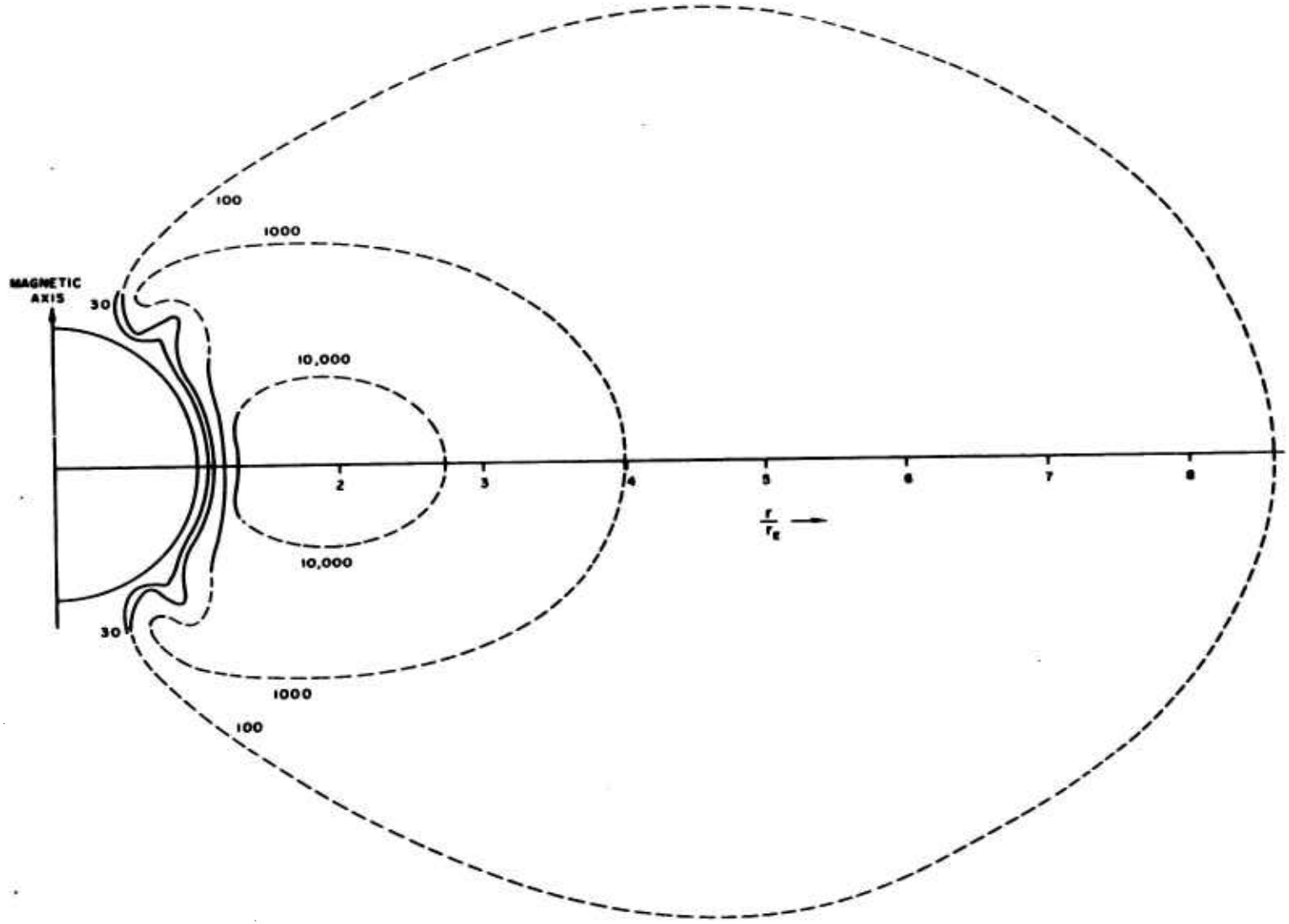

Figure A.6 Speculative extension of Explorer IV counting rate contours. (This picture has been revised on basis of data from Pioneers III and IV.)

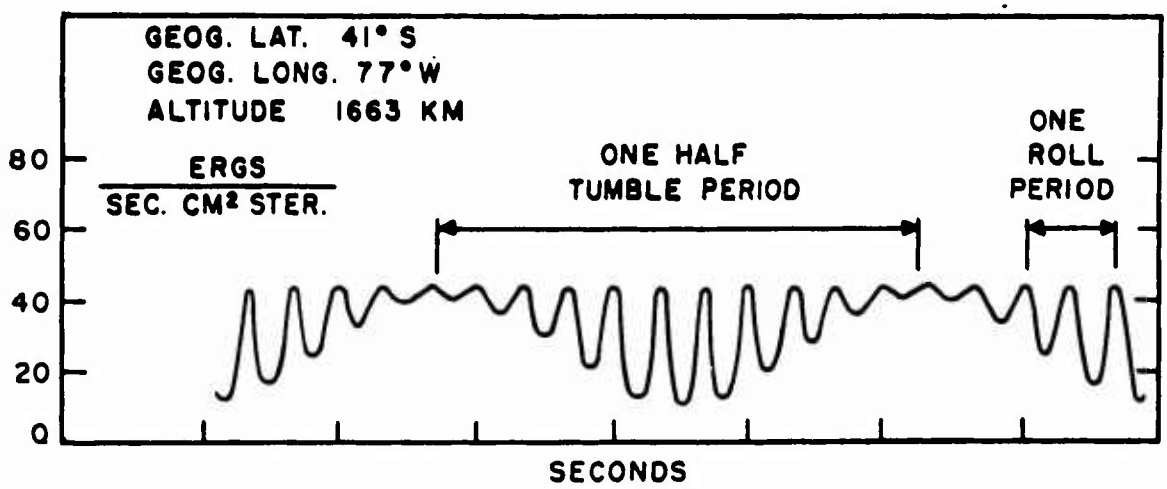

APPEARANCE OF CHANNEL 4 — 1 AUG. 1958, 0817 U.T.

Figure A.7 Appearance of Channel 4, 1 August 1958, 0817 U. T.

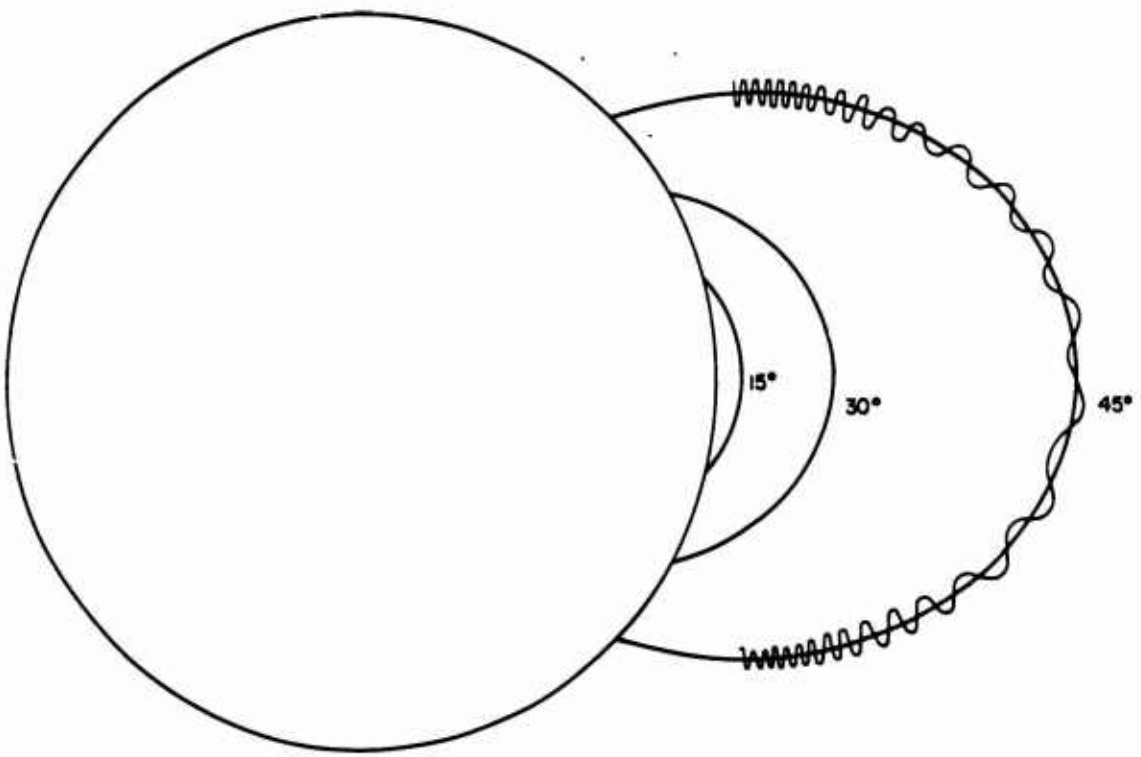

Figure A.8 Motion of charged particle along line of force.

ible to reach conclusions of importance on the origin of the trapped radiation. If its intensity does indeed fluctuate with solar activity, then it would appear that the reservoir of trapped radiation is replenished from time-to-time by fresh batches of solar gas. It is conceivable that the total quantity of trapped radiation may fluctuate little from day-to-day, the most readily observable effect of the arrival of new gas being perturbations of the reservoir. Such perturbations would likely be evidenced by an enhanced leakage rate at the lower and lateral boundaries.

No detailed study of temporal fluctuations in 1958 data has yet been made. As an overall impression, the pattern of selected intensity contours has been stable during the month 26 July to 26 August. But this statement has precision to only a factor of two at present. The intensities have a latitude and longitude dependence in addition to the sharp altitude dependence. Hence, we must reserve judgment on the matter of temporal fluctuations during this period pending a closer study of the observed data.

At one time we were tempted to believe that there was a marked diurnal variation. But more thoughtful inspection showed that this effect was largely, if not wholly, a composite of altitude, latitude and longitude dependence. The possibility for such confusion results from the fact that the satellite's orbit is only slowly varying in an inertial frame of reference and, therefore, has a more-or-less fixed relationship to the solar vector for a period of a few days. Hence, there is, in general, an apparent local time variation of the intensity observed at any chosen station.

A.2.6 Nature of the Radiation. In the design of the detectors for 1958 Alpha our working point of view was strongly conditioned by our earlier observations at rocket altitudes in the auroral zones (References 21 and 22). The most definitive were those of McIlwain in early 1958 at Fort Churchill and those of Meredith et al. of the U.S. Naval Research Laboratory (NRL), also at Fort Churchill. These sets of observations showed that the energetic radiation within and beneath visible auroras had a variable activity. It appeared that electrons having an energy spectrum rising very steeply toward low energies were usually the dominant component. An addition, protons (or at least nucleonic type particles) were present with a somewhat similar spectrum but with a particle intensity at a given kinetic energy several orders of magnitude less than that of electrons.

A dominant feature of the 1958 Alpha observations is the apparent spatial variability of the composition of the radiation. Such variability is most simply illustrated by noting the variability of the ratios of counting rates (or outputs) of the several detectors. (See Table A.3 for examples.) We regard it as unwise at this time to attempt to make a definitive statement concerning the composition of the radiation and the spectra of the several components. On any reasonable view of the origin of the trapped radiation, it would be supposed that electrons and protons are the principal components. If this be assumed, then the problem is to determine their respective absolute energy spectra and angular distributions as a function of position in space and as a function of time.

The 1958 Epsilon observations with the diversity of detectors are consistent with auroral type soft radiation being present in the radiation belt. But, in addition, there appears to be a component which is considerably more penetrating than usually observed there (Reference 25).

Detector A (the plastic scintillator) counts electrons having energies exceeding 700 kev; protons, having energies exceeding 9.5 Mev; with considerably lower efficiency, X rays having energies exceeding about 400 kev; and with rapidly diminishing efficiency, particles or X rays of progressively lower energies than those specified (electronic pile-up of pulses).

Detector B has distinctively different properties. Its foil will stop electrons having energies of about 20 kev, or protons having energies of 400 kev. And it is an efficient detector of X rays.

Detector C responds to electrons of energy exceeding 3 Mev, to protons of energy exceeding 30 Mev, and with much lower efficiency, X rays of energy exceeding some tens of kev.

Detector D responds to electrons of energies exceeding 5 Mev, protons of energy exceeding 40 Mev, and with much less efficiency, X rays of energy exceeding about 80 kev.

The marked aspect modulation of the output of Detectors A and B shows that the radiation which is mainly responsible for their response has a range between 140 mg/cm^2 and 5 g/cm^2 for A and between 1.0 mg/cm^2 and 5 g/cm^2 for B. Unfortunately, these ranges are quite large. Detectors C and D also exhibit a mild aspect sensitivity but their surroundings are more nearly isotropic.

Each set of simultaneous observations with Detectors A, B, C, and D provides, in effect, a set of four independent, and complicated, equations in terms of the various unknown properties of the radiation.

We are not yet prepared to report a range spectrum of radiation nor are we able to offer a definite appraisal of the important matter of whether the more penetrating component consists of protons, of electrons or of X rays resulting from the stopping of electrons in the various portions of the apparatus. It appears probable that a tentative appraisal will result from more thorough study of the observations and from the further experimental tests on one of the spare payloads which are presently being undertaken.

One of the central questions has to do with the importance of the bremsstrahlung from electron impact on the material of the immediate environment of the detectors. The bremsstrahlung is much more penetrating than its parent electrons and, for an electron spectrum which falls off very steeply toward higher

energies, one can readily estimate that, despite the lower detection efficiency, it is possible for the bremsstrahlung to falsely extend the apparent particle spectrum.

A complete knowledge of the physical nature of the radiation is, of course, of the utmost importance in clarifying its origin. Further flights of more elaborate detection systems (e.g., magnetic spectrometers) will be necessary to accomplish this.

A.3 REMARKS ON INTERPRETATION

On the basis of the evidence presented above, we regard it as established that the great radiation belt around the earth consists of charged particles, temporarily trapped in the earth's magnetic field. The rapid diminution of intensity at the lower altitudes is almost certainly due to atmospheric scattering and absorption. The dominant loss mechanism for electrons is scattering. Thus, if an electron is trapped along a specified magnetic line-of-force (See Figure A.8), the guiding center of its corkscrew path spends most of its time near the points at which the velocity of the particle is nearly orthogonal to the magnetic line (the mirror points). The cumulative effect of multiple coulomb scattering is to drive the mirror point to lower altitudes where the lifetime is rapidly reduced. If one adopts as a crude criterion for loss from the trapping region an r.m.s. scattering of one radian, then the lifetime in the reservoir can be estimated as a function of mirror altitude.

Due to the eccentricity of the earth's magnetic field, a given magnetic shell (locus of lines of force having $\cos^2 \lambda/p$ = const.) has its lowest altitude above the earth, for any given λ, at the longitude of the mid-Atlantic Ocean. Because of the radial component of grad $\underline{H}$ there is a systematic drift in longitude of trapped particles (electrons toward the east and protons toward the west) as they corkscrew their way back and forth from northern to southern hemisphere. The period of drift around the earth of 1-Mev electrons, for example, on the line of force meeting the earth at λ = 45 degrees is about 30 minutes.

Hence, the loss of particles from the reservoir is mainly caused by collisions at the longitude of minimum altitude.

Based on these simple ideas and on an extrapolation of the Sterne-Jastrow satellite atmosphere, the mean trapped lifetime of 1-Mev electrons is estimated to be of the order of 10^4 seconds for a mirror altitude of 400 km over the mid-Atlantic and 10^6 seconds (or about 10 days) for a mirror altitude of 1,000 km. The lifetime T is proportional to the square of the electron's energy. The sample values given above possess considerable uncertainty but do serve to give some feeling for the physical situation.

The effective loss of protons from the reservoir is dominated by collisional energy loss, not by scattering. For example, a 1-Mev proton has an estimated lifetime of 3×10^5 seconds for a mirror altitude over the mid-Atlantic of 1,000 km, and a 10-Mev proton, 6×10^6 seconds. From the above considerations, it is reasonable to expect that, irrespective of the origin of the radiation, its composition and the spectra of its various components will be functions of position.

A quasi-stationary state in the radiation belt will result when the time-average injection rate I of new particles is equal to the leakage or output O. Neglecting many important details and assuming that O is proportional to Q, the quantity of radiation present in the reservoir and to the reciprocal of T, the mean storage time in the reservoir, we have the simple equation for the well-known leaky bucket problem, namely

$$I = O = \frac{Q}{T} = \frac{nV}{T} \qquad (A.1)$$

Where n is the average number density and V is the volume of the reservoir.

If, for example, we assume a trapping region having a volume equal to that of a sphere of radius 4 earth radii (10^{29} cm^3) and adopt an average number density of energetic particles of 1/cm^3, then

$$Q = 10^{29} \text{ particles}$$

or some 10^5 moles. A sample pair of values for T and I might be 10^7 seconds and 10^{22} particles/second, respectively.

The equilibrium spectrum of stored particles will presumably be a much less steep function of energy than the spectrum of injected particles since T diminishes rapidly toward lower energies for loss by either scattering or absorption.

It is difficult to avoid the belief that auroras are related to the trapped radiation. Specific reasons for this belief are the following: (1) the contours of constant intensity (Figures A.2, A.3, A.4, and A.5) are more-or-less bounded as they turn away from the earth at high latitudes by a cone which lies at the lower latitude edge of the auroral zone; (2) the nature and intensity of the radiation in the reservoir appears to resemble that encountered at low altitudes (100 to 150 km) in the auroral zone; (3) there is preliminary evidence that fluctuations in the intensity of radiation on lower fringes of the radiation belt are correlated with magnetic and ionospheric activity — as are the auroras; (4) there is sufficient stored energy in the radiation belt to supply the time-averaged auroral intensity if the mean storage life is of the order of 10^7 seconds; and (5) there is observed to be a more-or-less steady leakage of soft radiation into the auroral zone, even in the absence of visible auroras.

For the various reasons listed above, we propose that the radiation belt is the reservoir whose leakage of particles is the direct cause of visible auroras. It is further suggested that solar plasma replenishes the reservoir from time-to-time, working its way into the outer reaches of the earth's magnetic field when its

density is sufficiently great, then being trapped in the field. On the occasion of the arrival of new batches of gas, the pattern of magnetic field lines at great altitudes and, hence, at high latitudes, is distorted, thus permitting the leakage of particles from the reservoir into lower altitudes at a rate exceeding that which is usual for the quiescent situation. The total quantity Q of plasma in the reservoir may fluctuate only slightly on such occasions, though it may be presumed that Q will vary with the general level of solar activity, averaged over a period of time of the order of T. Insofar as gradient $\bar{H}$ has a longitudinal component, there will be a radial drifting tendency, of the same nature as the longitudinal drifting tendency previously mentioned. The importance of this effect has not been assessed, but it may well provide the dominant mechanism for feeding plasma to low altitudes in the equatorial region.

It has been suggested by Christofilos (private communication), Vernov (Reference 26), Kellog (Reference 27) and Singer (Reference 7) that the radioactive decay of outward moving neutrons resulting from cosmic ray interactions in the atmosphere (neutron albedo) may provide an injection mechanism of significant intensity. The charged particle, cosmic ray albedo has been the subject of considerable study during the past 10 years, particularly in this laboratory and by Winckler and associates at the University of Minnesota. The confinement to Stoermer-Treiman lunes has been intrinsic to discussions of the phenomenon. But since injection occurs at altitudes such as 30 km, it has usually been supposed that charged albedo makes only a one-way transit to the conjugate latitude in the opposite hemisphere. The essential attractiveness of albedo neutrons is their ability to escape from the denser regions of the atmosphere, then to inject their decay products at an altitude where the storage life is long. The mean decay lifetime of the neutron at best is about 12 minutes. Almost all upward moving thermal neutrons, therefore decay within the trapping region of the earth's magnetic field (tentatively assumed to extend to about seven earth radii). Their charged decay products are electrons with energies up to 782 kev and quite low energy recoil protons. Of the order of a few tenths of one percent of fast neutrons (having a typical energy of, say, 40 Mev) decay during their traversal of the trapping region. Their charged decay products are protons of energies comparable to their own energy and electrons having a spectrum similar to that of thermal-neutron-decay electrons.

We find a number density of the order of, or greater than, $10^{-6}/cm^3$ of particles sufficiently penetrating to correspond to 40-Mev protons, if indeed these are the particles which actuate Detector D. Hence, by Equation (A.1),

$$I \cdot T = 10^{23} \qquad (A.2)$$

or

$$\frac{I}{A} \cdot T = 2 \times 10^{4}\ cm^{-2} \qquad (A.3)$$

Where A is the area of the surface of the dense atmosphere $= 4.2 \times 10^{18}\ cm^2$. If 0.1 fast neutrons per square centimeter per second emerge from the atmosphere and if 0.3×10^{-2} of their decay products are captured in the earth's field, then T must be of the order of 10^8 seconds, a high but perhaps not inconceivable value.

Thermal neutrons inject their decay electrons at lower altitudes and with an efficiency several hundred times as great as that for fast neutrons. Hence, they appear to be a more promising source of trapped electrons, having energies of the order of several hundred thousand electron volts.

Although it seems plausible from the above that outward moving cosmic ray neutrons may make a significant contribution to the intensity of the more penetrating component of the trapped radiation, we do not believe it is likely that their overall contribution is the dominant one. This view arises from several lines of thought. First, as noted above, we feel that the trapped radiation is probably the direct source of auroras. If this be so, then it is appropriate to note that the rate of supply of energy from cosmic ray neutron injection is inadequate by perhaps a factor of 10^4 to produce the time-averaged auroral intensity. Second, the energy spectra of electrons and protons from neutron decay are quite different from those observed in auroral displays and those apparently also present in the radiation belt, though the latter point is not yet well established. Moreover, by either scattering or absorption, there is a strong tendency to deplete the low energy end of the spectrum relative to that of the injected particles. Hence, the equilibrium spectrum of neutron-decay products in the reservoir will be even poorer at low energies than at injection, which is already much too depleted to agree with the observations. Third, the entire body of knowledge concerning solar terrestrial relationships (specifically the time association between solar flare and auroras and magnetic storms) seems to demand the arrival of solar plasma in the outer reaches of the earth's atmosphere. Of course, some of the solar plasma may enter the auroral zones directly and not via the belt of trapped radiation.

The outward projecting horns at high latitudes on the contours of constant radiation intensity (Figures A.2, A.3, A.4, and A.5) are of considerable interest. They suggest that the atmosphere is sufficiently heated there that levels of given atmospheric pressure are several hundreds of kilometers above the corresponding levels at low latitudes (Reference 28). This can presumably happen if radiation leakage from the reservoir is favored there, as indeed it appears to be. The portion of the atmosphere which is ionized is constrained laterally by the magnetic field and it is possible that there are plumes of ionized terrestrial gas extending out from the earth's atmosphere (T. Gold) like those observed in the sun's corona. Even in neutral gas, some elevation of the levels of constant pressure can be maintained in dynamic equilibrium.

The radiation belt may well be the seat of a distributed ring current encircling the earth; and the pertur-

bations of the belt due to arrival of solar plasma may be directly responsible for magnetic storms. No detailed study of this possibility has yet been made.

Also, it may well be that steady leakage of energetic particles contributes significantly to the general heating of the atmosphere at all latitudes.

It is a matter of considerable interest to investigate above the F region of the atmosphere the low frequency electromagnetic (synchrotron) radiation which is expected to result from trapped electrons. Indeed such observations may contribute importantly to knowledge of the energy spectra and nature of the trapped particles.

Appendix B
SATELLITE DATA

Raw data was received from the tracking stations in the form of magnetic tapes. These were played back to obtain strip charts, excerpts from which are given in Figures 1.7 through 1.11. The significance of the different lines is explained in Figure 1.7. These figures also illustrate the evident superposition of the Argus effect on the natural background. During the period of increased counting rate, the satellite may be visualized as passing through the shell of electrons injected by the Argus shots.

In processing the data, Van Allen's group at the State University of Iowa (SUI) made two corrections, one for background and another for nonlinearity of the detecting instruments. While the satellite was passing through the electron shell, the natural radiation background was varying and the counting rate associated with the Christofilos effect was changing at times by more than an order of magnitude in less than a minute. In addition, the satellite was tumbling and the counting rate was varying according to the degree of anisotropy of the radiation and the detection system.

Faced with these problems, SUI proceeded as follows: Channels 1 and 3 were observed to be reasonably well-behaved; i.e., had less ripple, caused by anisotropy of the counters, superimposed on the count rate envelope. The count rate was established 1 minute before and 1 minute after the satellite passed through the most intense part of the shell. The average of these two count rates, $(R_1 + R_2)/2$ in the data sheets, was called average background and was subtracted from the true count rate.

By observing the count rate of the detector as a function of dose in an X-ray machine, SUI plotted a curve of count rate versus dose. This curve was used to correct for the nonlinearity of the detector in obtaining the true count rate. The true count rate is that which would be observed with the counter if it were perfectly linear in response and had zero dead time.

By establishing the time at which the maximum count rate occurred, the satellite ephemeris could be consulted to obtain the satellite location.

Channel 3 was chosen for further analysis. The thickness of the shell is determined by the time required for the satellite to traverse the shell and the angle which the satellite path makes with the normal to the shell. Accordingly, SUI tabulated the time required for the satellite to move from a point at which the count rate had increased to half of the maximum, to a point at which the count rate had decreased to half of the maximum. In addition, the time of one-tenth maximum, defined in a similar way, was determined for Channel 3.

Channels 2 and 4 were orientation sensitive, which indicated somewhat the degree of anisotropy of the velocity distribution of the radiation. A large ripple was superimposed on roughly the same type of envelope observed for the Christofilos effect in Channels 1 and 3. The general procedure was to establish the count rates for each region considered; for example, the ripple was examined 1 minute before the peak of the envelope, and a maximum (peak of the ripple) and a minimum (valley of the ripple) were established. Thus, two backgrounds and two count rates are given for Channels 2 and 4. The necessity for, and the problems associated with, this procedure can be appreciated by examining the data.

The following pages, included with the data received from SUI, should be adequate to define the manner in which the data were processed and the entries in the data sheets. It is to be understood that each data sheet corresponds to one passage of the satellite through the shell. Following each data sheet, in most cases, is a graph of the count rate of Channel 3 versus time.

A few typical data sheets are included (Tables B.1 and B.2). The full set of data sheets may be found in a supplement to this report.

SYMBOLS[1]

Ω = geographic longitude, + east and − west

Λ = geographic latitude, + north and − south

h = altitude above geoid

Λ 1000 = geographic latitude of the intersection of the magnetic line of force (centered dipole approximation) through the position of peak counting rate of Channel 3 with a sphere whose radius is 1,000 km greater than that of the earth.

t_E = elapsed time in hours after the event whose consequences are tabulated.

NOTES[1]

1. The tabular and graphical data should be inter-

[1] Taken from SUI Research Report 58-11.

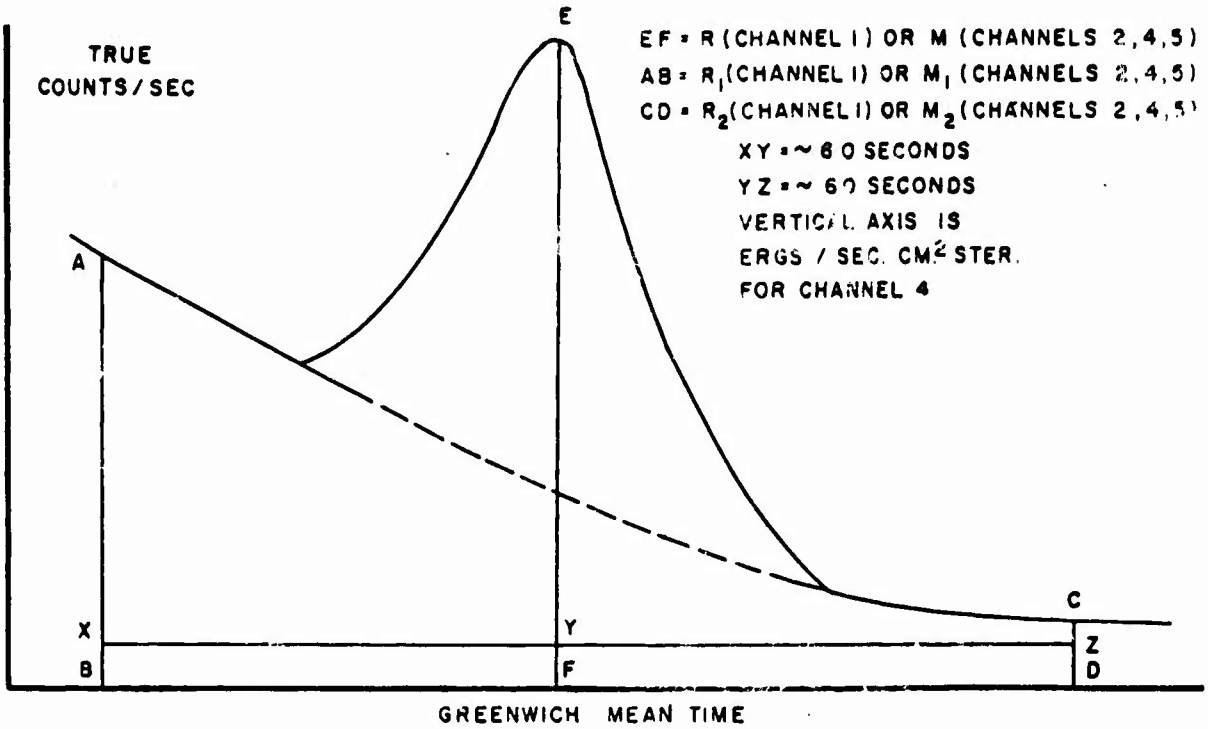

Figure B.1 Explanation of symbols, Channels 1, 2, 4 and 5.

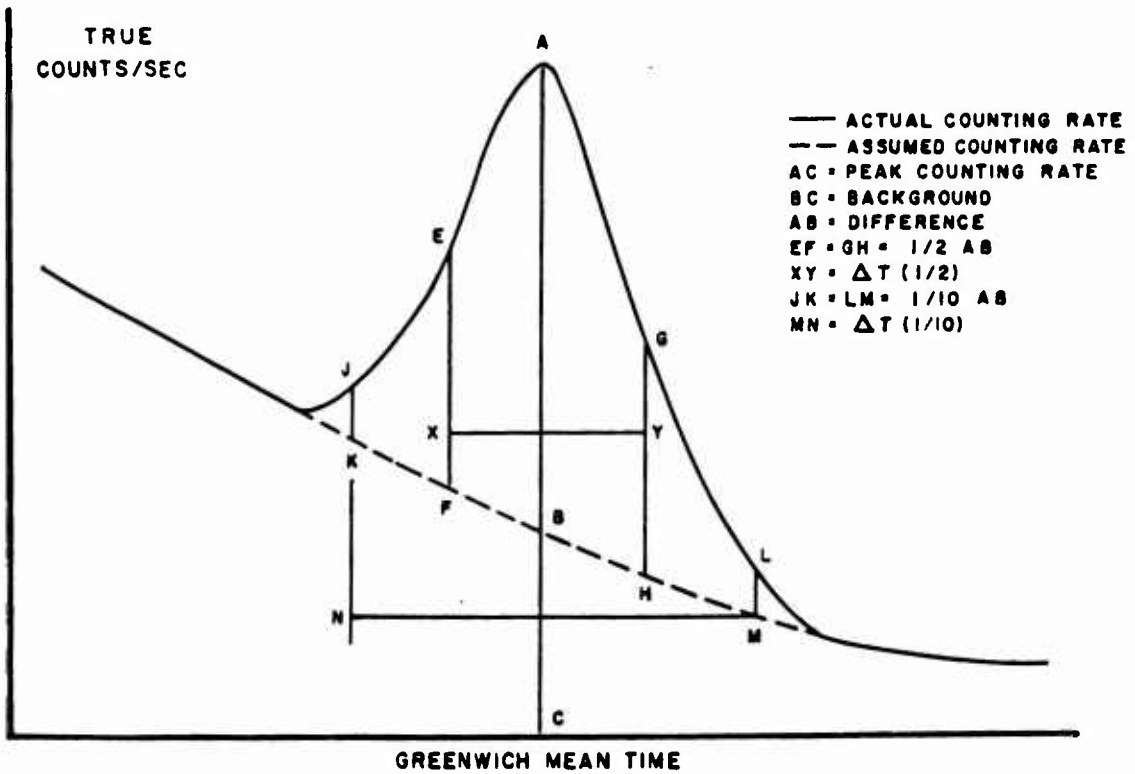

Figure B.2 Explanation of symbols, Channel 3.

TABLE B.1 DATA SHEET, 0607:50 27 AUGUST 1958

27 August 1958, 0607:50.± 2; Long Ω, −96° 41′ 30″; Lat Λ, +22° 51′; Alt h (km), 1,398; Λ 1000, 25.45; t_E, 3.67 hr.

Channel 1		Channel 3	
Time of Peak	0607:44.5	Peak Counting Rate	8,630
Peak Counting Rate	426.70	Background	730
R_1	148	Difference	7,900 ± 500
R_2	6.7	Δt ($\frac{1}{2}$)	32. ± 2
$R - \left(\frac{R_1 + R_2}{2}\right)$	349.35	Δt ($\frac{1}{10}$)	43. ± 4
		Peak Intensity Time	0607:50 ± 2

Channel 2		Channel 4	
Time of Max	0607:48.9	Time of Max	0607:49
Max Counting Rate	52,690	Max ergs/sec-cm^2-ster	6.08
Max_1	20,760	Max_1	1.69
Max_2	660	Max_2	1.69
$M - \left(\frac{M_1 + M_2}{2}\right)$	41,980	$M - \left(\frac{M_1 + M_2}{2}\right)$	4.39
Time of Min	0607:57.7	Time of Min	0607:54
Min Counting Rate	7,761	Min ergs/sec-cm^2-ster	0.98
Min_1	885	Min_1	0.234
Min_2	81.1	Min_2	0.328
$M - \left(\frac{M_1 + M_2}{2}\right)$	7,278	$M - \left(\frac{M_1 + M_2}{2}\right)$	0.70

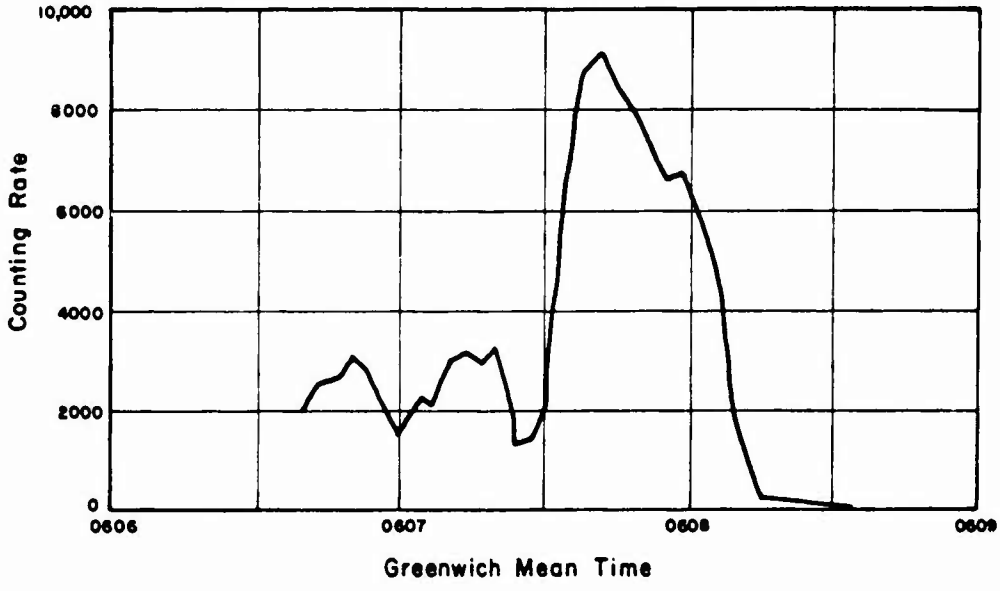

Figure B.3 True count rate versus Greenwich Mean Time, Channel 3, 27 August 1958.

TABLE B.2 DATA SHEET, 0356:42 28 AUGUST 1958

28 August 1958, 0356:42 ± 1; Long Ω, −72° 54′; Lat Λ, +17° 54′; Alt h (km), 1,538; Λ 1000, 21.3; t_E, 25.48 hr.

Channel 1		Channel 3	
Time of Peak	0356:36.5	Peak Counting Rate	4,000
Peak Counting Rate	272	Background	450
R_1	405	Difference	3,550 ± 200
R_2	71.5	Δt ($\frac{1}{2}$)	34. ± 3
$R - \left(\frac{R_1 + R_2}{2}\right)$	33.75	Δt ($\frac{1}{10}$)	63. ± 5
		Peak Intensity Time	0356:42 ± 1

Channel 2		Channel 4	
Time of Max	0356:39.1	Time of Max	0356:38.9
Max Counting Rate	11,330	Max ergs/sec-cm^2-ster	1.944
Max_1	5,027	Max_1	1.63
Max_2	2,356	Max_2	0.768
$M - \left(\frac{M_1 + M_2}{2}\right)$	7,638	$M - \left(\frac{M_1 + M_2}{2}\right)$	0.745
Time of Min	0356:43.9	Time of Min	0356:44.2
Min Counting Rate	1,858 (Ch 2)	Min ergs/sec-cm^2-ster	0.485
Min_1	480 (Ch 2)	Min_1	0.325
Min_2	53.3 (Ch 5)	Min_2	0.298
$M - \left(\frac{M_1 + M_2}{2}\right)$	1,591	$M - \left(\frac{M_1 + M_2}{2}\right)$	0.173

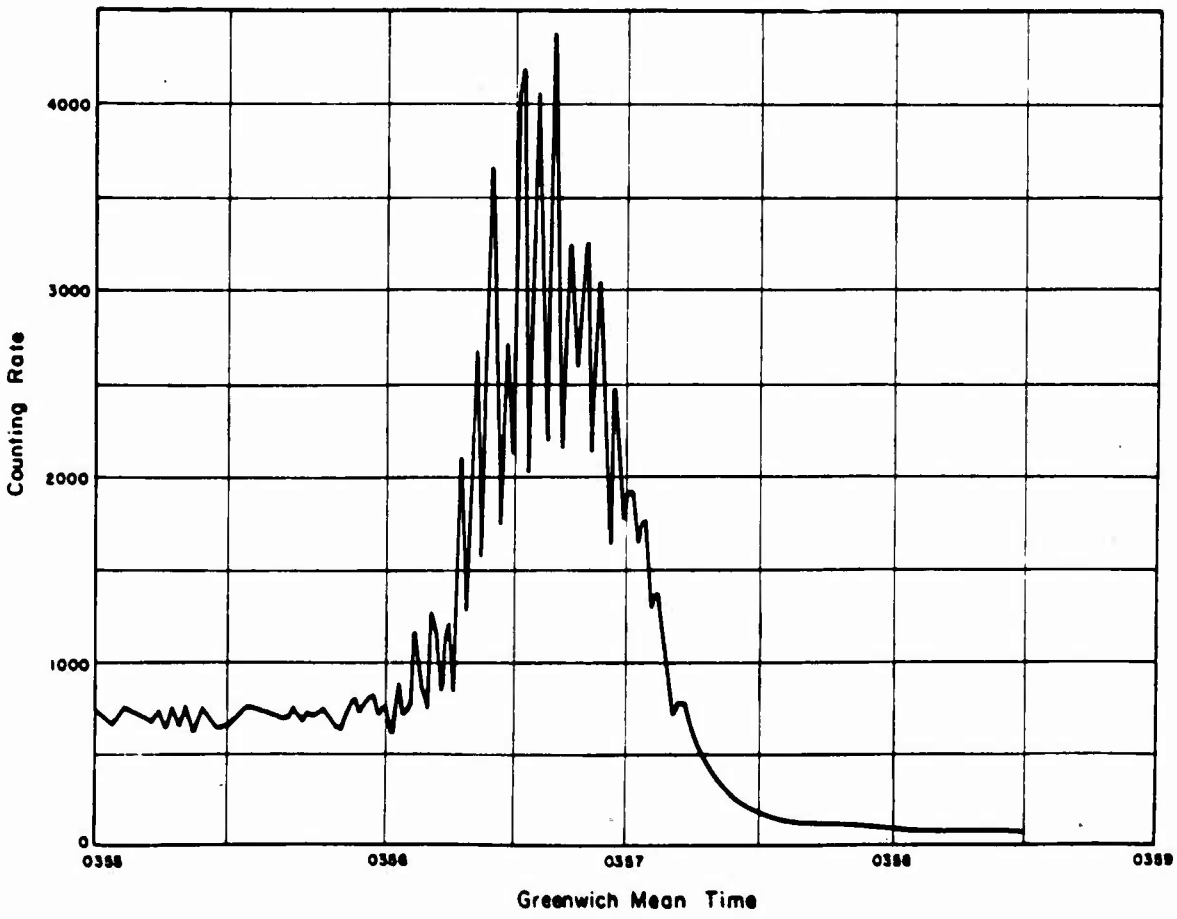

Figure B.4 True count rate versus Greenwich Mean Time, Channel 3, 28 August 1958.

preted in accordance with the detailed properties of the apparatus as described in Section 3.

2. All rates of Channels 1, 2, and 3 are the true rates of the respective detectors in counts per second.

3. Outputs of Channel 4 are in absolute units, ergs per second per square centimeter per steradian, assuming that all radiation entered the crystal through the entrance port (See Section 3 for discussion).

REFERENCES

1. N. C. Christofilos; "On the Possibility of Establishing a Plasma Shield of Relativistic Electrons in the Exosphere of the Earth as a Defense against Ballistic Missiles"; Document COPD-58-2, 10 January 1958; Secret Restricted Data.

2. J. A. Van Allen and others; "Observation of High Intensity Radiation by Satellites 1958 Alpha and Gamma"; SUI 58-5; and "Some Preliminary Reports of Experiments in Satellites 1958 Alpha and Gamma"; IGY Satellite Report Series No. 3, pp 73-92; National Academy of Sciences, Washington, D. C. (1958).

3. J. A. Van Allen, C. E. McIlwain and G. H. Ludwig; "Radiation Observations with Satellite 1958 Epsilon" (Satellite 1958 Epsilon is Explorer IV); SUI-58-10; Unclassified. This material is given in Chapter 3 and Appendix A of this report.

4. J. A. Van Allen and L. A. Frank; "Survey of Radiation Around the Earth to a Radial Distance of 107,400 Kilometers"; SUI Report No. 59-2, January 1959; State University of Iowa, Iowa City, Iowa; Unclassified.

5. "Explorer IV—1958 Epsilon Orbital Data Series"; Army Ballistic Missile Agency and Smithsonian Astrophysical Observatory, Issues 1-4.

6. A. E. Chudakov; "Photon Study on the Third Sputnik"; Rocket and Satellite Symposium, 5th Reunion of Comite Special Annee Geophysique Internationale, Moscow, 30 July to 9 August 1958.

7. S. F. Singer, Phys. Rev. Ltr. 1, 171-173 and 181-183 (1958).

8. L. Spitzer, Jr.; "Physics of Fully Ionized Gases"; Interscience Publishers, New York, N. Y. (1956); Unclassified.

9. W. H. Bostick; Scientific American 197, 87 (1957).

10. J. A. Welch, Jr. and W. A. Whitaker; "Theory of Geomagnetically Trapped Electrons from an Artificial Source"; April 29, 1959; Air Force Special Weapons Center, Air Research and Development Command, Kirtland Air Force Base, New Mexico; Unclassified.

11. J. A. Welch, Jr.; "Calculations on High Altitude Weapon Effects (U)"; Document AFSWC-TN-58-6, August 1958; Air Force Special Weapons Center, Kirtland Air Force Base, New Mexico; Secret Restricted Data.

12. "Relativistic Electrons Trapped in Earth's Magnetic Field"; Study Group Proceedings, UCRL, 10-21 February 1958, Document CXXVIII-70, 3A, 28 February 1958; University of California Radiation Laboratory, Livermore, California; Secret Restricted Data.

13. N. C. Christofilos; "Trapping and Lifetime of Charged Particles in the Geomagnetic Field"; UCRL-5407, 28 November 1958; University of California Radiation Laboratory, Livermore, California; Unclassified.

14. "Report of Second Working Group at LRL, Livermore, February 1959"; IDA-ARPA Document R-59-1, June 1959; Secret Restricted Data.

15. M. N. Rosenbluth and C. L. Longmire, Annals of Physics, I, 120-140 (1957).

16. L. Allen, Jr. and others; "Project Jason Measurement of Trapped Electrons from a Nuclear Device by Sounding Rockets"; April 19, 1959; Air Force Special Weapons Center, Air Research and Development Command, Kirtland Air Force Base, New Mexico; Unclassified.

17. J.A. Van Allen, C.E. McIlwain and G.H. Ludwig; "Satellite Observations of Radiation Artificially Injected into the Geomagnetic Field"; SUI, April 1959, State University of Iowa, Iowa City, Iowa; Unclassified.

18. V. Vouk, Nature 162, 330 (1948).

19. J.A. Van Allen; Paper presented at joint meeting of National Academy of Sciences and American Physical Society on 1 May 1958.

20. S.B. Treiman; Phys. Rev. 91, 957 (1953).

21. L.H. Meredith, M.B. Gottlieb and J.A. Van Allen; Phys. Rev. 97, 201-205 (1955).

22. J.A. Van Allen; Proc. Nat'l Academy of Sciences 43, 57-62 (1957).

23. J.A. Van Allen, Chapter 21, pp 188-193; and Willard H. Bennett, Chapter 22, pp 194-197, of Scientific Uses of Earth Satellites; University of Michigan Press, 1956; University of Michigan, Ann Arbor, Michigan.

24. Y. Aono and K. Kawakami; "Report of Ionosphere Research in Japan"; Vol. XIII, pp 28-36 (1958).

25. K.A. Anderson, Phys. Rev. Ltr. 1, 335-337 (1958) and Phys. Rev. 111, 1397-1405 (1958).

26. S.N. Vernov, Fifth General Assembly of CSAGI in Moscow, 20 July to 9 August 1958.

27. P.B. Kellog, Nuovo Cimento, in press.

28. S.K. Mitra; "The Upper Atmosphere"; p. 407, Royal Asiatic Society of Bengal, 1947.

29. H. Alfven; "Cosmical Electrodynamics"; Oxford University Press, London, 1950; Unclassified.